Referee response to "Sensitivity of spatial aerosol particle distributions to the boundary conditions in the PALM model system 6.0" by Mona Kurppa et al.

We thank both referees for their valuable comments and suggestions. Please find our detailed point-by-point responses below (in black).

The changes made to the manuscript are visualised in the attached file "manuscript_see_differences.pdf". Page and line numbers given in this response refer to that document.

P = page

L = line number

Anonymous Referee #1:

The study applies the LES model PALM in an urban setup in order to model air quality parameters in a street canyon of a major road and its surrounding in Helsinki. The model is evaluated against stationary and mobile observations. Furthermore, the authors examine different ways of providing boundary conditions for their LES simulations. The evaluation of the different simulations is conducted by applying a number of different statistical measures. This detailed evaluation is scientifically sound. However, the complexity of several different statistical measures in addition to the different simulations makes it difficult to write the analysis in an understandable way, which would make it easy for the reader to follow the analysis and results. I highly recommend to revise sections 4.2 and 4.3 in terms of writing. In these sections, the authors often jump between one measure or simulation and the other. For some of the paragraphs and sentences it was not clear to which simulation or time period they were referring to. Overall, I don't have concerns about the scientific relevance and the quality of the applied analysis. Therefore, the manuscript can be accepted for publication after minor revision.

Thank you for this comment regarding the clarity and readability. The Results section has now separated into three separate sections: 4. Comparison of the modelled and observed boundary conditions, 5. Evaluation of the air quality modelling results and 6. Sensitivity analysis. Furthermore, discussion about the meaning of the results has been moved from the section Discussion and conclusions to the respective results sections (see the comments of the Reviewer #2 and especially the major point 1). The changes have been marked in blue in the manuscript with track changes.

Specific comments

p.3, l.8-9: What do the authors mean with "but not necessarily stable performance"? If you apply boundary conditions from other model runs, you often use a (mostly coarser) larger scale model run. Such a continuous run would usually enable continuous boundary data.

The statement also seems to be in contrast to p.6, l.28-29 (“which allows realistic [...] boundary conditions”).

With this phrase we wanted to point out that NWP models do not perform equally well in all weather conditions. To make this idea more clear, the phrase has been modified as follows:

"... which provide a good spatial coverage but not necessarily stable performance." --> "... which provide a good spatial coverage but not necessarily stable performance **in all prevailing weather conditions**.” (P3 L9)

p.6., l.29: Do the authors mean that the forcing mesoscale flow does not provide enough turbulence, which would take time and distance to be generated on the higher resolution LES domain? I suggest to explain this with one or two more sentences to the benefit of the readers.

Yes, this is correct. The following sentences were added:

"*To reduce the time and distance for the mesoscale flow field to adjust to the LES modelling domain, a synthetic turbulence generator within PALM can be applied.*" --> "**As the mesoscale data do not contain resolved-scale turbulence, turbulence must first be developed within the PALM domain.** To reduce the time and distance for the mesoscale flow field to adjust **and turbulence to develop** within the LES modelling domain, a synthetic turbulence generator within PALM can be applied.” (P6 L30-32)

p.8, l.2-4: Are only the mast observations used as observation-based driving data? I think, the description of how observational data serve as boundary conditions could be extended.

The following sentences were added:

"Meteorological observations from the SMEAR~III station at z = 31 m are downloaded using the SmartSMEAR tool (Junninen et al., 2009).” (P8 L1-2)

"When applying the SMEAR III data, constant values are used for the entire vertical profile." (P8 L8-9)

p.8, l.31-32: Can the authors provide the size distribution parameters of the Hietikko et al. (2018) size distribution in the manuscript?

A figure on the aerosol size distribution has now been added to the Supplement (P7, Fig. S4). It includes the aerosol size distribution measured by Hietikko et al. (2018) and the one applied for the traffic-combustion-related aerosol emission in this study.

p.9, l.9: There is no number given for EF_{PM} in the manuscript. Can it be included in the manuscript? Furthermore, do EF_{PM} and $EF_{PM2.5}$ refer to the same quantity? In case not, I think it would help the reader to follow the calculation if numbers for both are given.

EF_{PM} has now been included in Table 3. Furthermore, on $EF_{PM2.5}$ has been replaced by EF_{PM} on P9 L1.

p.10, l.14-15: Would it be possible to run including variable roughness length, e.g. derived from the building structure or density? If so, would you expect a strong impact on the air flow? If it can be expected that a variable roughness length may affect the results substantially, I suggest to include this consideration in the discussion section.

In PALM, the Monin-Obukhov similarity theory (MOST) is applied as the wall model between the surface and the first grid level where scalars and horizontal velocity components are defined. This requires providing the roughness length, which characterises the roughness elements not resolved by the computational grid. As these simulations apply a high grid resolution (1-9 m), the roughness length describes mainly the surface material, while the impact of building structure and packing density on the flow are explicitly resolved.

p.11, l.14-15: In the figures the observations above 200 m show lower temperature and higher dew point temperature than the model.

Thank you for pointing out this typo. The sentences have been modified as follows:

"*The observed and modelled profiles of air (T) and dew-point temperature (T_D) correspond qualitatively well (Figs. 2c and S4 in the Supplement), but the observations higher values of T and T_D than MEPS above z = 200 m, especially at 8-9 am. Hence, MEPS predicts a stronger and shallower temperature inversion, which would lead to weaker vertical mixing.*" --> "The observed and modelled profiles of air (T) and dew-point temperature (T_D) correspond qualitatively well (Figs. 2c and S4 in the Supplement), but the observations show **lower (higher)** values of **T (T_D)** than MEPS above z = 200 m, especially at 8-9 am. MEPS **also** predicts a stronger and shallower **surface** temperature inversion, which would lead to weaker vertical mixing." (P11 L16-19)

p.11, l.28-30: For 21:00-24:00, there are two ADCHEM peaks, whereas the smaller one is at~50 nm(?) and the second at 100 nm, which is matching the observations.

The previous Figure S5 showed the size distributions in UTC time. Hence, the one matching the summer evening simulation would be 18:00-21:00.

We have now added the measured and modelled (ADCHEM) aerosol number size distributions for the specific modelling times to the Supplement (Fig. S6, S9 and S12). Fig. S9 for the evening simulation shows that the modelled PSD peaks at around 87 nm and the measured at 70 nm. These have now been corrected to the manuscript as well (P12 L1).

Figures S5, S10: Related to comment above. If this isn't a huge effort, I think it would be helpful to summarize the modelled PNSDs matching the investigation periods, i.e. 7:00-10:00 and 20:00-22:00, instead of the currently given time windows. Same is for winter period shown in Fig. S10.

Thank you for the comment. Background PSDs are now provided only for the specific modelling periods (see Fig. S6, S9 and S12).

p.12, l.3-4, Figure S10: The observed peak seems to be clearly at smaller sizes than the modelled one during 9:00-12:00. Again, providing the PNSD comparison for 7:00-10:00 would be helpful. Perhaps the authors could put these in the paper, and leave the diurnal evolution as it is in the supplement?

See the comments above. Note that the previous background PSD figures were provided in UTC time, not the local time which is UTC+3.

p.13, l.1-2: Can the authors please explain in little more detail the meaning of these acceptance criteria and why the have chosen these thresholds? That is, what error /deviation is accepted if the criteria is fulfilled. This is done exemplary later in the text for NMBF and NMAEF, however, I think it would be helpful already here in a more general manner.

The acceptance criteria are based on Hanna and Chang (2012) and Yu et al. (2010). For more details, the reader is suggested to look for these publications (see Table 5 caption).

p.16, l.4: In Table S3, I find NMBF for the side street in the summer morning first hour of -2.45 and -4.58 for EEPS and ELPI, respectively, which is different from the numbers reported in the text. Can the authors check again if the numbers in the text are correct and if so, please explain how these were calculated based on NMBF?

The values in the text are correct. From Yu et al. 2006, p. 29:

"For example, B_{NMBF} can be interpreted as follows: if B_{NMBF} is positive, the model overestimates the observations by a factor of B_{NMBF}+1; e.g. for B_{NMBF} = 1.2, the model overestimates the observations by a factor of 2.2. If B_{NMBF} is negative, the model underestimates the observations by a factor of 1−B_{NMBF}; for example, B_{NMBF} = −1.2 indicates that the model underestimates the observations by a factor of 2.2."

p.16, l.11: Related to the comment above, the numbers 3.68-4.36 differ from NMBF in the tables S8 and S9.

See the response above.

p.18, l.1: Overestimated by $M_{MET}M_{PSD}$ or $O_{MET}O_{PSD}$? Are the numbers 2.7 and 4.2 supposed to be found in Table 6 or not shown?

By $M_{MET}M_{PSD}$. This has now been clarified in the phrase:

"Also in the winter morning (Table S13), $M_{MET}M_{PSD}$ performs slightly better than $O_{MET}O_{PSD}$ modelling OC and $PM_{2.5}$ in the right order of magnitude, but the other chemical components are overestimated by a factor of around 2.7–4.2." --> "Also in the winter morning (Table S13), $M_{MET}M_{PSD}$ performs slightly better than $O_{MET}O_{PSD}$ in modelling OC and $PM_{2.5}$ in the right order of magnitude, but $M_{MET}M_{PSD}$ still overestimates the mass concentrations of the other chemical components by a factor of around 2.7–6.5." (P22 L4-7)

The phrase refers to Table S13. To improve readability, references to the correct tables have now been added (P22 L5).

p.18, l.1-2: What do the authors mean with the last sentence of this section? I think this thought needs more explanation in the text.

Thank you for the comment. The sentence has been improved as follows:

"Whether $M_{MET}M_{PSD}$ or $O_{MET}O_{PSD}$ performs better corresponds to the results on the vertical dispersion of LDSA." --> Comparing modelled values with point observations in a street canyon is very sensitive to the correct wind direction because perpendicular wind component leads to accumulation of pollutants to the leeward side of the street canyon. As the vertical dispersion of LDSA was also shown sensitive to the wind direction, the results on the performance of modelling the correct chemical composition corresponds to those on the vertical dispersion of LDSA (see Section 4.2.2)." (P22 L7-11)

p.21, l.8: Slower than what? It is not clear to what other observation or model result the wind speed of $O_{MET}O_{PSD}$ is compared to.

Thank you for pointing out this. "than in $O_{WD,mast}O_{PSD}$ was added." (P23 L25-26)

p. 24, l.24-26: Can the authors please explain this thought and its conclusion?

Stronger wind speeds generate more turbulence, which enhances ventilation and dispersion of pollutants upwards from the street level. Stronger atmospheric stability, instead, suppresses turbulence and ventilation of pollutants, leading to higher street-level concentrations.

In the summer evening simulation, MEPS data shows higher wind speeds (--> more turbulence and enhanced ventilation), but also stronger stratification (--> weaker turbulence and weaker ventilation) than the observation at the Kivenlahti mast. Hence, the impact of stronger wind speed and stronger stratification can balance each other, which could explain similar results in *$M_{MET}M_{PSD}$ and $O_{MET}O_{PSD}$*.

Other comments

p.1, l.10: I suggest to change “factor of two” to “fraction of data within a factor of two”, or similar.

“fraction of data within a ” was added for clarity (P1 L10).

p.1, l.12-13: One “and” too much in the enumeration.

There is a comma missing that separates the two sentences: The horizontal distribution is most sensitive to the wind speed and atmospheric stratification, and vertical distribution (is sensitive) to the wind direction. A comma was added (P1 L13).

p.2, l.7: What do the authors mean with “being at the same level”? I assume the authors refer to the height, i.e. in~1.5 m above ground? However, the pollutants are not only in this height, as the sentence might suggest.

We changed "level" to "height" (P2 L7). As it is stated in the phrase, traffic exhaust and road dust are emitted around the same height (i.e., 1 m above ground) where urban dwellers inhale outdoor air.

p.2, l.34 – p.3, l.1: Does this sentence refer to the study by Kuurpa et al. 2019? If so,the link to the sentence before is not clear.

A citation to Kurppa et al. (2019) was added for clarity (P2 L34)

p.3, l.16-17: I think, better English would be “can model boundary conditions cause” ->“can be / is caused by model boundary conditions”.

Thank you for the comment. The phrase was modified as follows:

"Hence, it is still unclear how much uncertainties in aerosol particle concentrations and size distributions can model boundary conditions cause." --> "Hence, it is still unclear how much uncertainty in aerosol particle concentrations and size distributions is caused by model boundary conditions.” (P3 L16-17)

p.3., l.21-23: Perhaps try to split this rather long sentence holding so much information into two or more sentences to improve readability.

Thank you for the comment. This long phrase was modified as follows:

"The campaign focused on the spatial variability of aerosol particle number, surface area and mass both in horizontal and vertical as well as aerosol size distributions and chemical composition with a high temporal and spatial resolution measured using a mobile laboratory and a drone." ---> "The campaign focused on the spatial variability of aerosol particle number, surface area and mass both in horizontal and vertical as well as aerosol size distributions and chemical composition. The observations were carried out with a high temporal and spatial resolution using a mobile laboratory and a drone.” (P3 L21-23)

p.7, Table 2: I did not do the maths, but just see that two numbers deviate. Below the table it says “591 m”, however Lz is given as 606 m in the table. Which is the correct one?

Thank you for noticing this typo. The value 606 m is the correct one and the table footnote has been corrected (P7).

p.8, l.28 & 29: Should it be “total mass emission factors” and “number emission factors”, at least this is what EF usually stands for. Emission factor is also used in the following.

You are correct. The word "factor" has been added accordingly:

"Aerosol particle emission inventories are typically provided as total mass emission **factors** $EF_{PM2.5}$. In SALSA, these would need to be translated to number emission **factors** EF_N, assuming some size distribution for the emitted aerosol particles." (P9 L1-2)

p.8, l.30: “sensitivity” -> “sensitive”.

Thanks! This has now been corrected. (P9 L3)

p.12, Figure 2; Figure S6; Figure S8: Missing “)” after “m s^{-1}”.

Thank you for noticing these! Missing brackets have been added accordingly.

p.14, Figure 3: Is the tick mark in the yellow color at 2 x 10^5 cm^{-3}?

Yes, this is correct. A tick label at 2 x 10^5 cm^{-3} has been added.

Figure 4, 7 and 8: I suggest to change in the caption “The grey ...” to “The grey area...”, or similar.

"The grey indicates" has been modified to "The grey **area** indicates" in these figure captions.

p.16, l.12: Is “overperform” the right word? To my non-native speaker knowledge it means something like "better than expected“? In a quick search, I only find it in a financial context.

For clarity, the word "overperform" is no longer used in the manuscript. The phrases containing "overperform" have been modified as follows:

"In the winter morning, $M_{MET}M_{PSD}$ fulfills the acceptance criteria during the first hour, except for NMAEF, and overperforms $O_{MET}O_{PSD}$,..." --> "In the winter morning, $M_{MET}M_{PSD}$ fulfills the acceptance criteria during the first hour, except for NMAEF, and performs better than $O_{MET}O_{PSD}$..." (P16 L6-7).

"In the winter morning, $M_{MET}M_{PSD}$ overperforms along the main street..." --> "In the winter morning, $M_{MET}M_{PSD}$ produces better results than $O_{MET}O_{PSD}$ along the main street." (P19 L 8)

"In the summer evening, $M_{MET}M_{PSD}$ overperforms $O_{MET}O_{PSD}$ and correctly reproduces..." --> "In the summer evening, *$M_{MET}M_{PSD}$* corresponds better to observations than $O_{MET}O_{PSD}$ and correctly reproduces..." (P22 L3-4)

p.17, l.3 & 4: The abbreviations ACSM and MAAP should be given with their long name here.

Both ACSM and MAAP have now been written out in the text (see P20 L1-2).

p.17, l.9: The statement refers to Figures S12 and S13, not “S11-12”.

Thank you for noticing this typo. It has been corrected accordingly (P20 L10).

p.17, l.11: Nitrate has a typo superscript “1”.

This typo has now been corrected.

p.17, l.12: NH4+, as named in Table 6 is ammonium not ammonia. Furthermore, similar to the other substances the chemical formula for ammonium should be given in brackets in the text.

Thank you for noticing this typo. It has been corrected on P22 L2. Furthermore, NH_3 was also falsely named as ammonium instead of ammonia on P6 L13.

p.17, l.12-13: Again, I don't understand the meaning of "overperform" here. Do the authors mean something like "performs better than $O_{MET}O_{PSD}$"?

See the comment above. The word "overperform" is no longer used in the manuscript for clarity.

p.17, Figure 6: Really unimportant detail... Nevertheless, the color for "Stationary" changed compared to Figure 5? I think it is easier for the reader if it would not.

It is important to make the manuscript as easy as possible to follow. The same colour has now been used for "Stationary" in Figs. 6 and 7.

p.18, l.7: I suggest to add "see Fig. 4" somewhere in this brackets.

The phrase has now been modified as follows (P22 L16 – P23 L1-4).

"Regarding all variables used in the evaluation, only minor differences due to using modelled or measured PSD as a boundary condition are observed between $M_{MET}M_{PSD}$ and $M_{MET}O_{PSD}$ (e.g., FB = −0.02 and FB = 0.01, and NMSE = 1.17 and NMSE = 1.15 for the horizontal distribution of N tot , respectively)." --> "Regarding all variables used in the evaluation, only minor differences due to using modelled or measured PSD as a boundary condition are observed between $M_{MET}M_{PSD}$ and $M_{MET}O_{PSD}$. For instance for the horizontal distribution of N_{tot} (e.g., FB = −0.02 and FB = 0.01, and NMSE = 1.17 and NMSE = 1.15 for the horizontal distribution of N_{tot}, respectively (see Fig. 4). "

p.21, Table 6: Can the authors color code the numbers as done for Table S12 and S13?

We must check this with the Editorial Support whether it is possible to use colour-coded fonts in the main text.

p.21, Table 6; Table S12, Table S13: I suggest to change "Performance in the modelling" to "Performance of the modelled" or "Model performance for" in the table captions.

"Performance in the modelling" has been changed to "Performance of the modelled" in the captions of Table 6 (P22), and Tables S12 and S13 (P21 in the supplement).

p.22, l.1: It should be mentioned in the beginning of this paragraph that you now focus on the performance for LDSA.

The phrase was modified as follows:

"At the supersite (Figs. 11a,c and 7), $O_{MET}O_{PSD}$ agrees better than $M_{MET}M_{PSD}$ with the observations (e.g., FB = 0.13 and FB = 0.59, and NMSE = 0.21 and NMSE = 4.78, respectively, during the first hour) and hence modifying the MEPS wind direction to correspond the observed one at Kivenlahti increases the performance (Fig. 7)." --> "The observed vertical profile of LDSA at the supersite on the summer morning corresponds better to the modelled by $O_{MET}O_{PSD}$ and $O_{WD,mast}O_{PSD}$ than $M_{MET}M_{PSD}$ (Fig. 7). Hence,

modifying the MEPS wind direction to correspond the observed one at Kivenlahti increases the model performance." (P23 L9-14)

p.22, l.2: I suggest to add “of the summer morning” after “during the first hour”.

"on the summer morning" was added to the phrase on P24 L9 (see the comment above).

p.22, l.6: I think instead of “Where” it should be “Whereas”.

This is correct. This has been corrected accordingly (P25 L2).

p.22, l.6: Does “lower” refer to "lower than $M_{MET}M_{PSD}$"? If so, it should be mentioned here.

This is corrected. "than $M_{MET}M_{PSD}$" has been added (P25 L2).

p.23, Figure 11: It should be $O_{WD,mast}O_{PSD}$ and $O_{WD,SMEAR}O_{PSD}$ in the legend.

This has now been corrected (P25).

p.23, l.2-3: It should be mentioned that it is now refered to the difference to $M_{MET}M_{PSD}$ and not the observations.

"compared to $M_{MET}M_{PSD}$" has been added to the phrase (P25 L8).

Supplement p.1: The seems to be something wrong with the section counting. S1 is missing, also S3.2 and S3.3.

The section counting follows the one of the main text. Hence, some sections which do not include any supplementary material, are missing from the counting.

Anonymous Referee #2:

The manuscript (MS) deals with evaluating a new model system that couples an aerosol dynamics module (SALSA2.0) with a LES model system (PALM 6.0) for high-resolution urban air quality modeling. The main objective is to validate the horizontal and vertical distributions of aerosols in terms of particle number concentrations, size distributions and chemical compositions. In particular, authors investigate the model sensitivity to meteorological boundary conditions and aerosol background concentrations.

The authors simulated three periods in summer and winter with different meteorological conditions and compared them with the measurements conducted using a mobile laboratory and a drone in an urban neighborhood in Helsinki, Finland. The results highlight the high sensitivity of urban LES modeling to meteorological boundary conditions and the aerosol background concentrations.

The methods and assumptions are scientifically sound and well explained in the MS. The outcomes have important implications for future studies urban air quality modeling using LES. I consider the objectives of the MS interesting for the community and within the scopes of the journal. However, the presentation need improvements. Therefore, I recommend the MS for publication after minor revision. My major points are:

1- In the result section, there are extensive and detailed explanations (sometimes too wordy) about the plots but no discussion. There are few sentences in section 5 but it is not enough. The authors should move the discussions to section 4 and expand them. It is important to explain “what” we see in the plots. Nevertheless, more important than that is to know “why”.

Thank you for this valuable comment. The Results section has now separated into three separate sections: 4. Comparison of the modelled and observed boundary conditions, 5. Evaluation of the air quality modelling results and 6. Sensitivity analysis. Furthermore, discussion about the meaning of the results has been moved from the section Discussion and conclusions to the respective results sections. The changes have been marked in blue in the manuscript with track changes.

2- The model somehow struggles with the mixing state of the atmosphere. I want to see direct quantitative measure of turbulence (e.g., TKE) at least between different runs. The vertical profile of the potential temperature or the Richardson number could be helpful too. Most importantly, the discrepancies are attributed to the mixing state in the simulations and observations. Thus, a direct measure of the atmospheric mixing state would be essential.

The vertical profiles of TKE for the child domain have been now included for comparison (PXX Fig. X). Discussion about this figure has been added in the following locations:

"This likely stems from the underestimation of the wind speeds above 217 m in $O_{MET}O_{PSD}$ (Fig. 2a), leading to lower mechanical turbulence production and mixing (Fig. 5a on the turbulent kinetic energy (TKE)). “ (P15 L1-3)

"This is surprising considering the clearly stronger winds in MEPS at z < 200 m than what is observed on the Kivenlahti mast. Yet, MEPS predicts a more stable stratification, which leads to nearly equal TKE values (Fig. 5b). This can justify why the difference in the spatial variability of aerosol particle concentrations between $M_{ME}OM_{PSD}$ and $O_{MET}O_{PSD}$ is not that large.” (P16 L2-5)

"Contrary to the summer evening, MEPS predicts clearly lower wind speeds in the winter morning, which would lead to weaker mixing, but at the same time the observed temperature inversion on the Kivenlahti mast is stronger than the modelled by MEPS especially during the first hours. Hence, the stronger stability and suppression of turbulence (Fig. 5c) can explain the higher concentrations in $O_{MET}O_{PSD}$. “ (P16 L8-11)

3- Several statistics are used in the MS but it is not clear what they represent. In the current form, they are rather confusing and make it hard to grasp the key message. For the horizontal distribution, I recommend SAL method.

The statistical measures applied in this study are mostly well-known and frequently applied, except for NMBF and NMAEF which have been explained in more detail. However, we agree that the Results section could be improved. We have now added more discussion and explanations to Section 5.1 and Table 5. The modified text has been marked in the manuscript (P13 L11-16).

Thank you also for proposing the usage of SAL. We calculated the statistics, but we think that the added value is not notable. SAL has been created for evaluation model performance in modelling precipitation areas. Hence, this method could be valuable when modelling the dispersion of individual pollutant puffs. More reasoning:

- Here, L (location) is always small because the concentration fields are bounded by the buildings.
- A (amplitude) is already measured by NMSE and NMAEF.
- Since the evaluation is done at resolution of 5 m using both spatially and temporally averaged concentration fields, it can be misleading to analyse S. For example, strong gradients in the modelling can be greatly smoothed by the averaging.

4- I am a bit confused with the role of the aerosol dynamics and chemistry. It seems that the simulations differ in boundary conditions only. But the PSD and composition differ too. So is there a feedback from the atmospheric state to aerosol dynamics and chemistry? With the chemical boundary conditions fixed, these differences stem from the processes within the child domain only. Is that right? What are the individual roles of aerosol dynamics, chemistry and meteorology? It would be helpful to elaborate on this.

Thank you for the comment.

In this study, we wanted to focus on the impact of the boundary conditions on the simulated concentrations, as this information is essential for the model users. Also, a detailed analysis on the gaseous species has been left out and will likely be provided in a future study. This was done to avoid making the manuscript too wide.

The individual roles of different aerosol dynamic processes have been investigated in Kurppa et al. (2019).

Yes, the differences in concentrations stem from the chemical and physical processes of air pollutants only within the innermost (child) domain.

Other comments:

P1L8: do you mean “are driven” instead of “are drawn”? This occurs several times in the MS.

We use "are drawn from" on purpose. For clarity, we have replaced it with "are taken from" (see P1 L8 and P7 L6).

P4L25: please explain in detail why you choose these dates. I assume it is based on the diurnal and seasonal variations in the mixing state of the atmosphere. What about the urban heat island?

Dates were chosen so that the weather conditions clearly differ, but also based on the observation data quality and coverage.

P6L19: wouldn’t this be part of the reason why OC is well captured but not sulfate and Nitrate? What about the winter period?

The transport of organic vapours from the chemistry module to SALSA and back is still under development and hence the impact of e.g. VOC on aerosol particle growth is not yet considered in (P28 L 23-24). We have now added the following phrase to discuss this linkage between the chemistry module and SALSA:

"However, the transfer of different organic vapours from the chemistry module to SALSA is still under development." (P6 L20-21)

P6L23: “at the same time”?

Thank you for noticing this typo. It has now been corrected to "at the same time" (P6 L24).

P6L23: “a high enough resolution is needed” is too generic. Please add a range.

We added "in the order of ~1 m" for the range (P6 L24).

Table2: the innermost domain has 1 m resolution. But later the results are aggregate a 5 m grid for comparisons. Then what is the point of this expensive simulation?

The mobile observation data are aggregated to a resolution of 5 m for two reasons: 1) the GPS signal has an accuracy in the order of 5 m and 2) the number of observation points is limited and therefore in a 1 m x 1 m grid one grid point could represent only one measurement instance.

Applying this resolution (5 m) for the model is not fine enough for resolving the flow in street canyons (Xie and Castro, 2006).

P9L22-26: this text is repetition of table 4.

Thank you for the comment. We still think that it is the clearest to explain the simulation names in the text as well as list them in a table.

P10L20: The boundaries of the innermost domain are fixed for the chemicals. This means that the air masses come and go without bringing or taking any pollutants. Does this make sense in the resolution you are dealing with?

In the time scales considered here (1-2 hours), we can assume that the background concentrations remain rather the same. The aerosol and chemistry modules are run only within the innermost domain to limit the computational costs, as these modules make the simulations 10-20 times more expensive.

P11L5: Most of the figures cited here are in the supplementary material. This is not helpful for the reader. I understand that the MS should not be lengthy. But perhaps with some reorganization

As you mentioned, the manuscript becomes easily very lengthy. We have carefully decided the figures we think are the most relevant for transforming the message and supporting the conclusions.

Figure 2: Adding the potential temperature to this plot would be helpful.

We decided to keep only absolute temperature in the figure. However, TKE figure has been added (P16 Fig. 5).

Figure 3: add name tags to each row and column so that the reader can navigate more easily.

Name tags for each row (measured or modelled) and column (times) have been added (P14 Fig. 3).

Figure 4: I have problem understanding this type of figure. Perhaps because the purpose of each parameter is not well explained? What about SAL method?

We have now explained the different statistical measures in more detail. See the comment about SAL above.

Figure 5: It is difficult to have a solid conclusion here. Higher LDSA is (or should be) associated with higher number concentration. The model always fails to capture the profile in the morning hours. What are the individual contributions of MET and PSD?

Fig. 5 illustrates the vertical profiles of LDSA at the supersite. The main conclusion is that the vertical profile is very sensitive to the wind direction.

The individual contribution of MET and PSD is shown in Fig. 11. The influence of background PSD is mainly seen above the building height (z > 30 m), while within the street canyon, wind speed and direction strongly modify the vertical dispersion.

P17L1-10: same as the previous comment.

Are you referring to the subsection 4.2.4 Aerosol chemical composition? The conclusion has been emphasised in Section 7:

"In general, the chemical composition is acceptably reproduced except for NH^+_4, which is highly overestimated at all times. Yet, the performance is not always systematic with the horizontal and vertical distributions." (P26 L22).

P19L7-8: this is an odd sentence.

Reading the phrase now afterwards, we totally agree. The phrase has been modified as follows: "*The difference in the modelled PSD between $M_{MET}M_{PSD}$ and $M_{MET}O_{PSD}$ is smaller than when the wind speed and/or direction are different ($O_{WD,mast}O_{PSD}$ and $O_{WD,SMEAR}O_{PSD}$, Fig. S12 in the Supplement).*" --> "The wind speed and/or direction influence the modelled PSD more than the background PSD (see Fig. S12 in the Supplement)." (P23 L14-16)

Figure 9: It might be that the coagulation (aerosol dynamics) is not fast enough. Is this a reason why fine particles are overestimated? This can be tested by aerosol dynamics on/off.

Actually, the smallest particles are underestimated at the background location. Instead, the concentration of the smallest particles are correctly simulated above the streets with traffic.

As shown in Kurppa et al. (2019), coagulation influences mainly sub-10 nm particles and their concentrations are reduced by 10% or less in a street canyon.

Figure 10 and Table S2: SAL might be a better method to compare these plots.

Thank you for the comment. We still think that SAL might not be the best methods for air quality modelling within street canyons.

P24L26: replace “huge” with “large”.

The phrase has been removed when modifying the discussion section.

Sensitivity of spatial aerosol particle distributions to the boundary conditions in the PALM model system 6.0

Mona Kurppa[1], Pontus Roldin[2], Jani Strömberg[1], Anna Balling[1], Sasu Karttunen[1], Heino Kuuluvainen[3], Jarkko V. Niemi[4], Liisa Pirjola[5], Topi Rönkkö[3], Hilkka Timonen[6], Antti Hellsten[6], and Leena Järvi[1,7]

[1]Institute for Atmospheric and Earth System Research, Faculty of Science, University of Helsinki, Helsinki
[2]Division of Nuclear Physics, Lund University, Lund, Sweden
[3]Aerosol Physics Laboratory, Physics Unit, Tampere University, Tampere, Finland
[4]Helsinki Region Environmental Services Authority (HSY), Helsinki, Finland
[5]Department of Automotive and Mechanical Engineering, Metropolia University of Applied Sciences, Vantaa, Finland
[6]Atmospheric Composition Research, Finnish Meteorological Institute, Helsinki, Finland
[7]Helsinki Institute of Sustainability Science, University of Helsinki, Helsinki

Correspondence: Mona Kurppa (mona.kurppa@helsinki.fi), Leena Järvi (leena.jarvi@helsinki.fi)

Abstract.

High-resolution modelling is needed to understand urban air quality and pollutant dispersion in detail. Recently, the PALM model system 6.0, which is based on the large-eddy simulation (LES), was extended with a detailed aerosol module SALSA2.0 to enable studying the complex interactions between the turbulent flow field and aerosol dynamic processes. This study represents an extensive evaluation of the modelling system against the horizontal and vertical distributions of aerosol particles measured using a mobile laboratory and a drone in an urban neighbourhood in Helsinki, Finland. Specific emphasis is on the model sensitivity of aerosol particle concentrations, size distributions and chemical compositions to boundary conditions of meteorological variables and aerosol background concentrations. The meteorological boundary conditions are taken~~drawn~~ from both a numerical weather prediction model and observations, which occasionally differ strongly. Yet, the model shows good agreement with measurements (fractional bias < 0.67, normalised mean-square error < 6, fraction of data within a factor of two > 0.3, normalised mean bias factor < 0.25 and normalised mean absolute error factor < 0.35) in respect of both horizontal and vertical distribution of aerosol particles, their size distribution and chemical composition. The horizontal distribution is most sensitive to the wind speed and atmospheric stratification, and vertical distribution to the wind direction. The aerosol number size distribution is mainly governed by the flow field along the main street with high traffic rates and in its surroundings by the background concentrations. The results emphasize the importance of correct meteorological and aerosol background boundary conditions, in addition to accurate emission estimates and detailed model physics, in quantitative high-resolution air pollution modelling and future urban LES studies.

1 Introduction

Exposure to outdoor air pollution is a major global threat resulting up to 0.8 million premature deaths in Europe (Lelieveld et al., 2019) and 3 million worldwide (Lelieveld et al., 2015; WHO, 2016) every year. Specifically aerosol particles can be extremely harmful, and based on a recent study by Burnett et al. (2018) outdoor fine particulate air pollution ($PM_{2.5}$) solely could have caused up to 8.9 million deaths worldwide in 2015. As over half of the global population lives in cities (55 % according to UN, 2019), urban air quality is of major importance. In addition to high population densities, urban areas are characterized by major air pollutant sources, namely traffic exhaust and road dust, being at the same height~~level~~ where urban dwellers inhale outdoor air. The dispersion of these traffic-related pollutants is not, however, straightforward as buildings, trees and other obstacles modify the flow within the urban canopy and hence also pollutant dispersion (Tominaga and Stathopoulos, 2013) as well as the environment for aerosol dynamic processes and chemical reactions to occur.

As a consequence of the complex interactions between the urban morphology, meteorology, local emissions and air pollutant dynamics and chemistry, air quality is highly variable both in time and space, and strong concentration gradients are observed in urban areas. However, measurements from a single monitoring station nearest to the individual's residence, hospital, or primary health care clinic have commonly been applied in air pollution exposure studies (Andersen et al., 2012; Adam et al., 2015), which can lead to notable errors. Moreover, both the size and chemical composition of aerosol particles are of major importance when it comes to their health impacts (Kampa and Castanas, 2008; Kelly and Fussell, 2012). For instance, particle deposition in lungs depends strongly on the inhaled particle size (Hussain et al., 2011), and thus the negative health effects of aerosol particles have been found to correlate more strongly with the surface area of particles than their number or mass (Brown et al., 2001; Oberdörster et al., 2005).

Computational fluid dynamics (CFD) models have been successfully applied in studying the air flow and dispersion of air pollutants in urban areas. Mainly models based on either Reynolds-averaged Navier Stokes (RANS, e.g., Baik et al., 2009; Kwak et al., 2015; Santiago et al., 2020) or large-eddy simulation (LES, e.g., García-Sánchez et al., 2018; Letzel et al., 2012; Salim et al., 2011) have been utilised. While being computationally more expensive than RANS, LES has been shown to perform better in resolving instantaneous turbulence structures in a complex urban environment (García-Sánchez et al., 2018; Salim et al., 2011). Further, air pollutant concentrations can be significantly modified by their chemical and physical processes (Kurppa et al., 2019; Nikolova et al., 2016; Zhong et al., 2020), especially as the residence time of air pollutants is increased in a complex urban environment (Gronemeier and Sühring, 2019; Ramponi et al., 2015). Therefore a detailed module describing the characteristics of air pollutants and their dynamics is needed to enable modelling aerosol particles of different size, chemical composition and harmfulness. To date, only a few LES models include a module for treating aerosol particles with a specific size distribution and chemical composition and their dynamic processes (Kurppa et al., 2019; Steffens et al., 2013; Zhong et al., 2020).

The sectional aerosol module SALSA (Kokkola et al., 2008) was recently implemented to the PALM model system (Kurppa et al., 2019) to consider the impact of aerosol dynamic processes on aerosol concentrations and size distributions, and to study the relative importance of pollutant dispersion and aerosol dynamic processes. A model evaluation by Kurppa et al. (2019) in

central Cambridge, UK, showed the model to be capable of reproducing the vertical distributions of aerosol size distribution in a simple street canyon. However, due to the lack of observations, the capability of the model to reproduce the horizontal distributions of aerosol particles has not been studied yet. Also the meteorological conditions were limited to one single day and the examined street canyon had no vegetation.

Still, even if the air pollutant processes would be modelled accurately, correct boundary conditions for the meteorological variables and air pollutant concentrations are vital for realistic air quality simulations. Boundary conditions can be drawn from observations, which however are typically point measurements that lack spatial representatives and also are prone to measurement errors. Another alternative is to use model data, which provide a good spatial coverage but not necessarily stable performance in all prevailing weather conditions. Previously, CFD models have been successfully coupled with mesoscale models to study the impact of larger scale atmospheric features on microscale interactions (e.g., Baik et al., 2009; Heinze et al., 2017; Liu et al., 2012; Michioka et al., 2013; Wyszogrodzki et al., 2012) as well as to consider realistic air pollutant background concentrations (Kwak et al., 2015). Recently, Santiago et al. (2020) investigated the sensitivity of RANS-based urban PM_{10} (particulate matter with aerodynamic diameter < 10 µm) simulations on the meteorological boundary conditions and showed the model performance to be improved when replacing the wind direction (WD) predicted by the WRF model with the observed WD. However, Santiago et al. (2020) only modelled passive PM_{10} without taking into account chemical or physical transformation of aerosol particles. Hence, it is still unclear how much uncertainty~~ies~~ in aerosol particle concentrations and size distributions is caused by~~an~~ model boundary conditions ~~cause~~.

To further assess the performance of SALSA2.0 in the PALM model system 6.0 in simulating the spatial distribution of aerosol particle concentrations in an urban area and to examine the importance of meteorological and aerosol background boundary conditions, we will use observations made during an extensive measurement campaign in an urban neighbourhood in Helsinki, Finland, in summer and winter 2017. The campaign focused on the spatial variability of aerosol particle number, surface area and mass both in horizontal and vertical as well as aerosol size distributions and chemical composition. The observations were carried out with a high temporal and spatial resolution ~~measured~~ using a mobile laboratory and a drone. The model is evaluate~~dion is done~~ at three observation periods with different prevailing meteorological conditions.

2 Measurements

2.1 Measurement campaign

The model evaluation and sensitivity study is conducted around an Helsinki Region Environmental Services Authority (HSY) air quality monitoring site, hereafter referred as the "supersite", in Helsinki, Finland (60°11'47"N, 24°57'07"E). The site is located 3 km north-northeast from the Helsinki city centre, and it is characterised as an urban street-canyon kerbside station with a traffic rate of around 28,000 on a workday, of which 12 % are heavy duty vehicles (City of Helsinki, 2018). The street canyon is 42 m wide and the mean building height is around 19 m on the southwestern and 16 m on the northeastern side of the street (see Fig. 1 in Kuuluvainen et al., 2018) resulting in a height to width ratio of 0.42. The supersite consists of a container

Table 1. Instrumentation of the mobile laboratory Sniffer. Abbreviations: PSD = aerosol particle number size distribution, N_{tot} = total aerosol particle number concentration and PM_1 = mass of particulate matter with aerodynamic diameter < 1 µm.

Measured component	Instrument
PSD (5.6–560 nm)	Engine exhaust particle sizer (EEPS, model 3090, TSI)
PSD (7 nm–10 µm)	Electrical low-pressure impactor (ELPI, Dekati Ltd)
N_{tot} (> 2.5 nm)	Butanol condensation particle counter (CPC, model 3776, TSI)
Black carbon (in PM_1)	Aethalometer (Model AE33, Magee Scientific)

(length 8.0 m, width 1.7 m and height 2.7 m) equipped with standard air quality measurement devices measuring from 4 m above ground level.

To get information about the spatial variability of air pollutants around the supersite, a two-week measurement campaign was conducted in summer (6–16 Jun) and winter (28 Nov–11 Dec) 2017. During both campaigns the horizontal distribution of air pollutants in the neighbourhood was monitored on non-rainy days using a mobile laboratory and additionally during two intensive observation periods the vertical profiles of aerosol particles were measured using a drone.

The mobile laboratory Sniffer (Pirjola et al., 2004) measured the horizontal distribution of trace gases and aerosol particle concentrations and size distribution. The measurements were done in one to two hour slots with a 1-s temporal resolution during the morning and afternoon rush hours, around noon and in the late evening. During each observation period, Sniffer was driving along a main street (Mäkelänkatu) and a side street as well as standing at the supersite, opposite the supersite and on a field 185 m from the main street (hereafter "background"). The instrumentation of Sniffer is given in Table 1 and the measurement locations in Fig. S1 in the Supplement. The main inlet was situated above the windshield at 2.4 m and a global positioning system (model GPS V, Garmin) recorded the van speed and position. For a detailed description on Sniffer, see Enroth et al. (2016); Pirjola et al. (2016).

During the intensive observation periods, a multi-rotor drone (X8, VideoDrone Finland Ltd) carried an electrical particle sensor (Partector, Naneos GmbH) to measure the vertical distribution of the alveolar lung-deposited surface area (LDSA) of aerosol particles, which describes the total aerosol surface area penetrating to the deepest parts of lungs (see e.g., Kuula et al., 2020, and references within). The measurement were done on both sides of the street canyon when the Sniffer was simultaneously driving. The drone was flown ten times up-and-down between $z = 2-50$ m during one 30-minute measurement interval, after which measurements were repeated on the other side. Each intensive observation period started by measuring LDSA at the supersite and ended on the other side. Measurements were started at 3 m from the building wall and the horizontal location was kept constant with a GPS sensor of the drone. Additionally, LDSA was measured at the supersite by a Pegasor AQ Urban sensor (Pegasor Ltd.) and on the other side by a DiSCmini (Testo Ltd.) or with another Partector at 1 m and in winter also at 14 m. For the details of the instrumentation, see Kuuluvainen et al. (2018).

The sensitivity of the results to the PALM model boundary conditions is examined during the following three periods: 9 Jun morning (07:16–09:15) and evening (20:26–21:14), and 12 Dec morning (07:20–09:14).

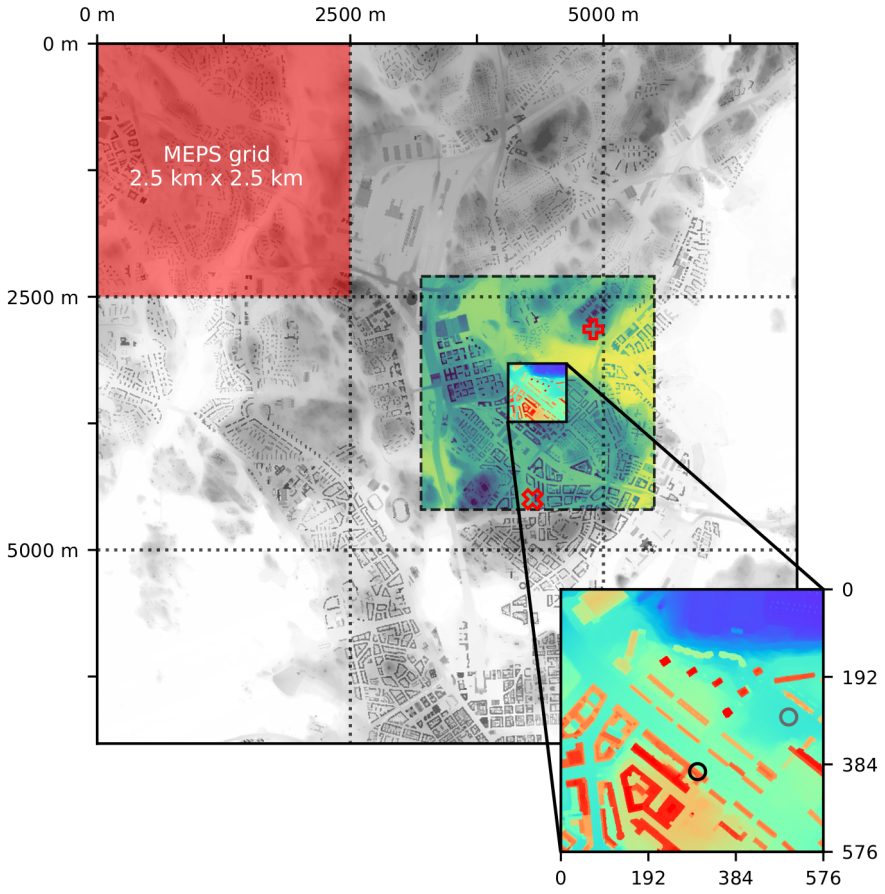

Figure 1. The modelling domain: root in grey, parent in viridis (dashed line) and child in rainbow (solid line). The grid size of the MEPS data is illustrated with a red area and dotted lines. The background air quality monitoring sites are marked with a red empty plus (SMEAR III) and a red empty cross (Kallio). In the zoomed figure over the child domain, the supersite is marked with a black circle and the background measurement point of Sniffer with a grey circle.

2.2 Additional measurements

In addition to the Sniffer and drone measurements, we use stationary aerosol observations from the supersite and two urban background monitoring sites: Kallio site operated by HSY and SMEAR III (Station for Measuring Ecosystem Atmospheric relations, Järvi et al., 2009) around 1.0 km southwest and 0.8 km northeast from the supersite, respectively (Fig. 1). See Table S1 for the instrumentation. In addition to aerosol observations, meteorological data (wind speed, wind direction, air temperature) from the SMEAR III measurement tower ($z = 31$ m) and Kivenlahti meteorological measurement mast 17.4 km west from the supersite (Wood et al., 2013) are used in the study.

3 Simulations

3.1 Model description

This study applies the PALM model system, version 6.0 (revision 4416) (Maronga et al., 2015, 2020), which features an LES core for atmospheric and oceanic boundary layer flows. PALM solves the non-hydrostatic, filtered, incompressible Navier-Stokes equations of wind (u, v, and w) and scalar variables (sub-grid-scale turbulent kinetic energy e, potential temperature θ, and specific humidity q) in Boussinesq-approximated form. PALM is especially suitable for complex urban areas, owing to its features such as a Cartesian topography scheme and a plant canopy module, which are applied here to include the aerodynamic impact of both solid buildings and permeable vegetation on the flow. Furthermore, so called PALM-4U (short for PALM for urban applications) components have recently been implemented to PALM (Maronga et al., 2020), including the aerosol module SALSA, the online chemistry module, and the self- and offline nesting features, which are all applied in this study.

SALSA (Kokkola et al., 2008; Kurppa et al., 2019) describes an aerosol size distribution by a number of size bins (10 by default) and each bin can be composed of different chemical components. Chemical components included are sulfuric acid (H_2SO_4), organic carbon (OC), black carbon (BC), nitric acid (HNO_3), ammoni~~aum~~ (NH_3), sea salt, dust, and water (H_2O). SALSA contains the following aerosol dynamic processes: coagulation, nucleation, dry deposition on solid surfaces and resolved-scale vegetation, and condensation and dissolutional growth by gaseous H_2SO_4, HNO_3, NH_3, and semi- and non-volatile organics (SVOC and NVOC). The gaseous compounds can be transferred to SALSA from the online chemistry module, which is based on Kinetic Pre-Processor (KPP, Damian et al., 2002) version 2.2.3 and an adapted version of the KP^4 pre-processing tool (Jöckel et al., 2010). The implementation is flexible, allowing the user to choose the chemical mechanism and components being considered. In this study, a simplified mechanism describing photochemical smog is applied (see Supplement, Section S3.2). Photolysis is parametrised based on Saunders et al. (2003). However, the transfer of different organic vapours from the chemistry module to SALSA is still under development.

To capture the dominant turbulent eddies of the atmospheric boundary layer (ABL) in LES, the horizontal extent of the modelling domain should span over several ABL heights, see e.g. (Fishpool et al., 2009; Chung and McKeon, 2010; Auvinen et al., 2020). At the same time, to resolve most of the kinetic energy within street canyons, a high enough grid resolution (in the order of ~ 1 m) is needed (Xie and Castro, 2006). Furthermore, uncertainty arising from the lateral boundary conditions usually decreases with increasing horizontal dimensions. To fulfill these contradicting requirements, a self-nesting feature has been included in PALM (Hellsten et al., 2017; Maronga et al., 2020). In self-nesting, one or several child domains are nested within a parent domain and the child obtains its boundary conditions from its parent. Furthermore, PALM incorporates an automated mesoscale offline nesting with a mesoscale operational weather prediction model, which allows realistic, non-cyclic and non-stationary boundary conditions for the flow. As the mesoscale data do not contain resolved-scale turbulence, turbulence must first be developed within the PALM domain. To reduce the time and distance for the mesoscale flow field to adjust and turbulence to develop within~~to~~ the LES modelling domain, a synthetic turbulence generator within PALM can be applied.

Table 2. Dimensions (L), number of grid points (N) and grid resolutions (Δ) of the model domains in x-, y- and z-directions.

Domain	$L_x \times L_y \times L_z$ (m^3)	$N_x \times N_y \times N_z$	Δ_x, Δ_y, Δ_z (m)
Root	$6,912 \times 6,912 \times 606$	$768 \times 768 \times 80$	9.0, 9.0, 6.0*
Parent	$2,304 \times 2,304 \times 288$	$768 \times 768 \times 96$	3.0, 3.0, 3.0
Child	$576 \times 576 \times 144$	$576 \times 576 \times 144$	1.0, 1.0, 1.0

*: Δ_z is stretched with a a factor 1.03 above $z = 300$ m resulting in a total domain height of 606~~591~~ m.

3.2 Model domain and morphological data

The model simulations are conducted over a root domain of 6.9 km $\times$ 6.9 km, within which two smaller domains, parent and child, are nested progressively (Fig. 1). The dimensions (L_x, L_y, L_z), number of grid points (N_x, N_y, N_z) and grid resolutions (Δ_x, Δ_y, Δ_z) of each domain are given in Table 2. In this study, the focus is on the child domain which matches with the area of the spatial aerosol measurements around the supersite.

Information on the building and vegetation height and land surface elevation are taken~~drawn~~ from high-resolution raster maps for Helsinki (Auvinen and Aarnio, 2019). The manipulation of the domain input files is done using the Python library P4UL (Auvinen and Karttunen, 2019). Only vegetation higher than $z_{\text{v,min}} = 4.0$ m are included in the simulations. Due to the lack of observational data on the leaf area density (LAD) of vegetation, a constant LAD value is applied for all tree crowns above $z_{\text{v,min}}$. In summer, LAD $= 1.2$ m^2 m^{-3} for broad-leaf trees (Abhijith et al., 2017), while in winter LAD is decreased to 20 % of the summertime value.

3.3 Meteorological boundary conditions

We apply both modelled and observed data as meteorological boundary conditions, which are set dynamic, i.e., they change with time.

As modelled data, numerical weather prediction data from MetCoOp Ensemble Prediction System (MEPS, Bengtsson et al., 2017; Müller et al., 2017) are applied. MEPS data were downloaded from the data archive (Norwegian Meteorological Institute, b) using the File Interpolation, Manipulation and EXtraction (Fimex) library (Norwegian Meteorological Institute, a). MEPS has a horizontal resolution of 2.5 km (see Fig. 1), 65 vertical levels and ten ensemble members. It is ran four times daily with a three-hourly cycling for data assimilation (3D-VAR). The lateral boundary data are from the European Centre of Medium-Range Forecasts (ECMWF) high resolution (HRES) atmospheric model. In this study, the MEPS control run, i.e., the ensemble member 0 with unperturbed initial and lateral boundary conditions, is used.

Data from the Kivenlahti mast are downloaded from FMI Open Data service (Finnish Meteorological Institute) as 10-minute-averaged. On the mast, meteorological observations are conducted at three to eight measurement levels between $z = 2-327$ m. Despite being located 17.4 km from the supersite, the closest observations of the vertical profile of basic meteorological

variables are conducted at Kivenlahti. Meteorological observations from the SMEAR III station at $z = 31$ m are downloaded using the SmartSMEAR tool (Junninen et al., 2009).

The initial conditions and dynamic meteorological boundary data are provided to PALM in a so-called dynamic driver. Of the MEPS data, the dynamic driver was created by the following procedure. First, the sigma-coordinates were translated to pressure coordinates and further to height coordinates applying the hypsometric equation. Then u, v, w, θ and water vapour mixing ratio q_v were interpolated from the MEPS grid to the PALM grid: first in horizontal over a two-dimensional grid using the cubic spline method and then in vertical using the linear interpolation. The Kivenlahti mast observations, instead, were linearly interpolated in vertical until the highest observation level, after which a constant value was used. When applying the SMEAR III data, constant values are used for the entire vertical profile. The dynamic driver created from the observational data does not include any horizontal variation.

A mesoscale interface, INIFOR, has been developed to transform mesoscale modelling data into PALM-readable boundary data. However, it is currently only available for COSMO-DE/D2 datasets, which do not cover Finland.

3.4 Air pollutant background concentrations

Similar to the meteorological boundary conditions (Section 3.3), both modelled and observed air quality data are used as background concentrations in the simulations. As in the previous model evaluation study (Kurppa et al., 2019), the modelled background aerosol particle number and trace gas concentrations are produced with the trajectory model for Aerosol Dynamics, gas and particle phase CHEMistry and radiative transfer (ADCHEM, Roldin et al., 2011b, a, 2019). ADCHEM is operated as a one-dimensional column trajectory model along HYSPLIT (Stein et al., 2015) air mass trajectories, starting seven days backwards in time (see Fig. S2 and S3 in the Supplement). The gas and aerosol particle compositions and size distributions are simulated along the back trajectories arriving to the coordinates of the supersite. For the emission inventories and parametrisations applied, see Section S3.4 in the Supplement. Detailed descriptions of the aerosol and cloud microphysics, new particle formation and gas-phase chemistry mechanisms in ADCHEM are provided by Roldin et al. (2019) and references therein.

To investigate the impact of the background aerosol size distribution (PSD) and concentration on the model simulations, PSD measurements from SMEAR III (see Section 2) are applied as an alternative for the modelled values. For simplicity, ADCHEM data are always used for the chemical composition of aerosol particles and gaseous concentrations.

For each PALM simulation, the concentrations are averaged over the simulation time and these temporally constant vertical profiles are then introduced to the simulation domain by a decycling method, in which background concentrations are fixed at the lateral boundaries.

3.5 Air pollutant emissions

In this study, air pollutant emissions only from traffic combustion are included, as traffic is the main pollutant source within the modelling domain (Helsinki Region Environmental Services Authority). Traffic-lane maps separating different road categories, i.e., main streets, collector roads and residential streets, have been generated by combining lane and street type information from the Map Service (City of Helsinki). The lane width is 3.5 m. Emissions are introduced as dynamic surface fluxes.

Table 3. Unit emission factors for traffic combustion (s = solid and g = gaseous) on 9 Jun between 7:00–8:00 in units $\times 10^{-5}$ g m^{-1} vehicle^{-1}. Abbreviations: PM = total mass of particulate matter, BC = black carbon, OC = organic carbon, NO = nitrous oxide, NO_2 = nitrous dioxide, OCSV = semi-volatile organic carbon, RH = alkanes, H_2SO_4 = sulphuric acid, N_2O = nitrous oxide and NH_3 = ammonia.

PM	BC(s)	OC(s)	NO(g)	NO_2(g)	OCSV(g)	RH(g)	H_2SO_4(g)	N_2O(g)	NH_3(g)	Fuel
1.4	1.0	0.3	49.4	13.9	0.039	1.5	0.01	1.0	3.5	9.8×10^3

Aerosol particle emission inventories are typically provided as total mass emission factors EF_{PM} ~~$EF_{PM_{2.5}}$~~. In SALSA, these would need to be translated to number emission factors EF_N, assuming some size distribution for the emitted aerosol particles. However, converting aerosol mass to number is highly sensitive~~ity~~ to the assumed size distribution. Therefore in this study we choose to apply a number emission factor $EF_N = 4.22 \times 10^{15}$ kg$_{fuel}^{-1}$ based on fuel consumption and a number size distribution estimated by Hietikko et al. (2018) at the supersite in May 2017 (see Fig. S4 in the Supplement).

For gaseous compounds, mass composition of aerosol particles and fuel, unit emission factors $EF_{[compound]}$ (Table 3) are calculated using emission inventory by the European Environmental Agency for 2017 (Ntziachristos et al., 2016) and specifically the Tier 3 method, which applies information on the mileage per vehicle category and technology, and driving speed. However, since no information on the cumulative mileage for different Euro classes was available, $EF_{NH_3(g)}$ and $EF_{N_2O(g)}$ are based on the Tier 1 method (see Ntziachristos et al., 2016, Eq. 28). Furthermore, the following estimates were applied: $EF_{SVOC(g)} = 0.01 EF_{NMOG}$ (Zhao et al., 2017, Fig. 2), $EF_{RH(g)} = 0.4 EF_{NMOG}$ (Huang et al., 2015, Fig. 4), where NMOG stands for non-methane organic gases and RH(g) for alkanes, and $EF_{H_2SO_4(g)} = 0.1\ EF_{SO_2}$ (Arnold et al., 2006, 2012; Miyakawa et al., 2007). Emitted aerosol particles smaller than 15 nm in diameter are assumed to be composed of 75 % OC and 25 % H_2SO_4, whereas larger particles contain 72 % BC, 21 % OC and 7 % H_2SO_4 as estimated from EF_{PM}, EF_{BC} and EF_{OC}.

The hourly vehicle fleet compositions for the neighbourhood are obtained from the Helsinki Region Environmental Services Authority (HSY and Urban Environment Division of the City of Helsinki, personal communications, 1 Oct, 2018), the mileage for each vehicle technology from the ALIISA model (VTT, 2018) and the fuel sulphur content from the LIPASTO database (VTT, 2017). The traffic rates in the neighborhood are estimated by normalising the mean traffic volumes per each street (Urban Environment Division of the City of Helsinki, Helsinki Region Environmental Services Authority and Helsinki Region Municipalities, 2018) with traffic counts from an online traffic monitoring station located in the northwestern corner of the child domain (City of Helsinki, personal communications, 3 Mar, 2018). Traffic volumes for both southward and northward traffic are measured separately.

Table 4. Simulation abbreviations. WD = wind direction and PSD = aerosol particle number size distribution.

Simulation	Background meteorology	Background PSD
$\mathrm{M_{MET}M_{PSD}}$	Modelled by MEPS	Modelled by ADCHEM
$\mathrm{O_{MET}O_{PSD}}$	Observed at Kivenlahti	Observed at SMEAR III
$\mathrm{M_{MET}O_{PSD}}$	Modelled by MEPS	Observed at SMEAR III
$\mathrm{O_{WD,mast}O_{PSD}}$	Modelled, but WD from Kivenlahti	Observed at SMEAR III
$\mathrm{O_{WD,SMEAR}O_{PSD}}$	Modelled, but WD from SMEAR III	Observed at SMEAR III

3.6 Model set-up

The length of the morning simulations on 9 Jun and 12 Dec are two hours, and evening simulation on 9 Jun only one hour. Simulation times correspond to the observation periods.

For all simulation times, two simulations using either modelled (M) or observed (O) boundary conditions for the flow and background aerosol particle number size distribution (PSD) are conducted. The first set-up, hereafter $\mathrm{M_{MET}M_{PSD}}$, applies the modelled meteorological (MET) boundary conditions from the MEPS data and the modelled PSD from the ADCHEM model. The second set-up, hereafter $\mathrm{O_{MET}O_{PSD}}$, applies the observed meteorological data from the Kivenlahti mast and the observed PSD from SMEAR III. Furthermore, two types of sensitivity tests are conducted for the summer morning. Firstly, model sensitivity on the background PSD is studied running a simulation with the modelled meteorological boundary conditions and observed background PSD ($\mathrm{M_{MET}O_{PSD}}$). Secondly, the influence of wind direction (WD) on pollutant dispersion is investigated by replacing WD in the MEPS data by WD measured on the Kivenlahti mast ($\mathrm{O_{WD,mast}O_{PSD}}$) or at the SMEAR III station ($\mathrm{O_{WD,SMEAR}O_{PSD}}$). As $\mathrm{WD_{SMEAR\ III}}$ is only measured at $z = 31\ \mathrm{m}$, the wind direction at the model boundaries in $\mathrm{O_{WD,SMEAR}O_{PSD}}$ is set constant with height. In total nine different simulations have been conducted.

The aerosol and chemistry modules are run only within the child domain to limit computational costs. In all simulations, the aerosol processes of condensation and dissolutional growth, coagulation, dry deposition and sedimentation are included and calculated every 1.0 s. The aerosol particle size distribution is described by 10 size bins, of which three are within the first subrange between 2.5–15 nm and seven within the second subrange 15 nm–1 $\mu\mathrm{m}$. Aerosol particles are assumed to be internally mixed and hygroscopic, and can contain $\mathrm{H_2SO_4}$, OC, BC, $\mathrm{HNO_3}$, and/or $\mathrm{NH_3}$. The chemical reactions are calculated at every time step of the PALM model.

The advection of both momentum variables and scalars is based on the fifth-order advection scheme by Wicker and Skamarock (2002) together with a third-order Runge-Kutta time-stepping scheme (Williamson, 1980). The pressure term in the prognostic equations for momentum is calculated using the iterative multigrid scheme (Hackbusch, 1985). The roughness height is $z_0 = 0.05\ \mathrm{m}$ (Letzel et al., 2012) and the drag coefficient applied for the trees $C_D = 0.3$.

Simulations were first run only for the root domain for 1 h, called here the precursor run, after which the final simulations were started. The final simulations including also the nested parent and child domains were initialised using the final state

of the precursor run. Offline nesting is used as forcing for the root domain and the parent and child are nested within using one-way self nesting. As SALSA and chemistry are run only within the child domain, for them the nesting is not applied and the boundary conditions of air pollutants are set at the child boundaries. The data output was collected starting after the first 15 minutes of the final simulation. Simulations were performed on the Centre for Scientific Computing (CSC) Puhti supercluster. Using in total 394 Intel Xeon processor cores, each simulation required 39–80 h of computing time.

4 Comparison of the modelled and observed boundary conditions

~~Section 4 presentsdescribes the differences in the modelled and observed boundary conditions. After that, Section 5 focuses on the performance of the simulations applying only modelled ($M_{MET}M_{PSD}$) or only observed ($O_{MET}O_{PSD}$) boundary conditions. Finally, Section 6 investigates the impact of background PSD and wind direction on the model performance.~~

The summer morning on 9 Jun is characterized by very calm northerly-north-westerly winds with the horizontal wind speed $U \approx 1.0 - 1.5\ \mathrm{m\,s^{-1}}$ at $z = 30\ \mathrm{m}$ and mainly $U < 2.5\ \mathrm{m\,s^{-1}}$ within the lowest $200\ \mathrm{m}$ on the Kivenlahti mast (Fig. 2a-b). The MEPS data show more westerly winds, with $-90° < \Delta\mathrm{WD} < -45°$ compared to the Kivenlahti observations, except at 9 am when the modelled and observed WD agree. Furthermore, the observed U are up to $0.5\ \mathrm{m\,s^{-1}}$ lower within the lowest $100\ \mathrm{m}$ during the first two hours and up to $1.0\ \mathrm{m\,s^{-1}}$ higher during the last two hours when compared to the MEPS data. As the highest measurement level for U on the Kivenlahti mast is $z = 217\ \mathrm{m}$, the interpolated profile used as the boundary condition in $O_{MET}O_{PSD}$ underestimates U above $217\ \mathrm{m}$ at 7 am. The observed and modelled profiles of air (T) and dew-point temperature (T_D) correspond qualitatively well (Figs. 2c and S54 in the Supplement), but the observations show lower (higher) values of T (~~and~~ T_D) than MEPS above $z = 200\ \mathrm{m}$, especially at 8–9 am. ~~Hence,~~ MEPS also predicts a stronger and shallower surface temperature inversion, which would lead to weaker vertical mixing. Observations at SMEAR III generally follow those on the Kivenlahti mast, expect that T is roughly $2\ °\mathrm{C}$ higher at SMEAR III compared to the Kivenlahti mast and WD typically falls between the MEPS data and Kivenlahti observations. The difference in WD can be explained by flow distortion at SMEAR III due to the adjacent buildings to the north of the measurement site (Nordbo et al., 2012). The observed background aerosol particle number concentrations at SMEAR III are around 80 % lower and the modelled PSD shows a smaller peak diameter of $D = 40\ \mathrm{nm}$~~$D = 28\ \mathrm{nm}$~~ instead of $D = 50\ \mathrm{nm}$ in the SMEAR III observations (Fig. S65). Furthermore, the observations show a secondary peak at $D = 14\ \mathrm{nm}$, which is not captured by ADCHEM.

By the evening, the observed U on the Kivenlahti mast had increased to $2.0 - 2.5\ \mathrm{m\,s^{-1}}$ at $z = 30\ \mathrm{m}$ (Fig. S76a) and the wind turned to south-west (Fig. S76b). The modelled and observed WD agree well ($\Delta\mathrm{WD} < 20°$), whereas clear discrepancy is shown for U. The MEPS predicts a low-level jet with the maximum U at $z = 100\ \mathrm{m}$ and shows up to $3\ \mathrm{m\,s^{-1}}$ higher values compared to the Kivenlahti observations at 8–9 pm. This low-level jet results in a strong wind shear and mechanical turbulence production. Instead above, U is overestimated in the interpolated Kivenlahti data at 9–10 pm. The profiles of T_D agree relatively well (Fig. S87), whereas MEPS predicts clearly lower T, with a difference up to $-5\ °\mathrm{C}$ close to the ground (Fig. S76c). The SMEAR III observations agree with those from the Kivenlahti mast. The modelled and observed background

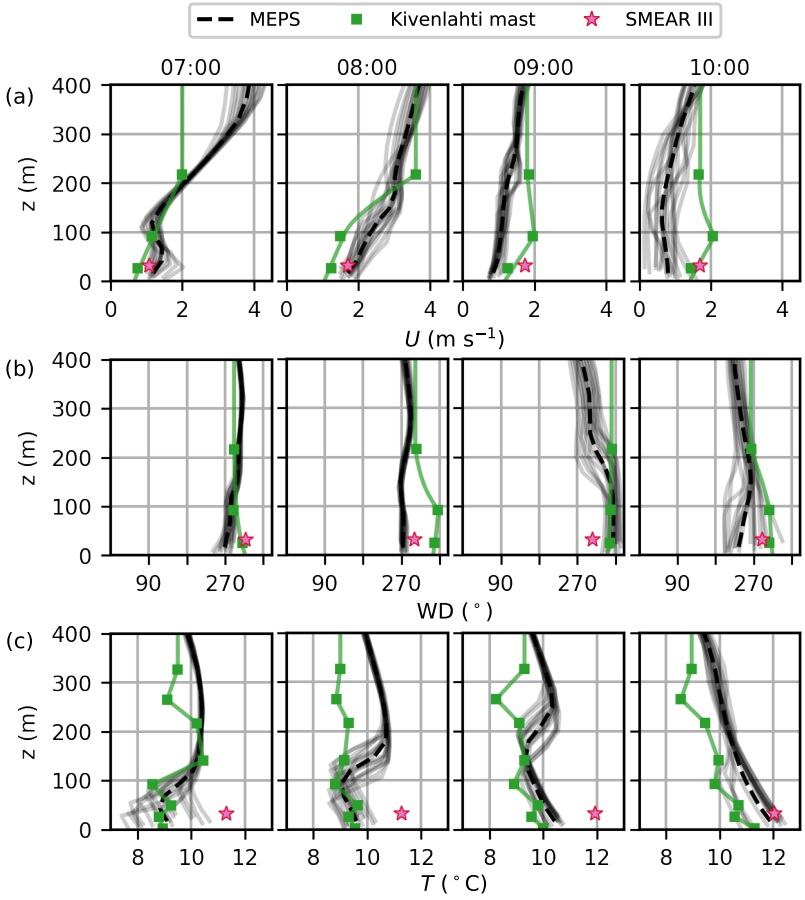

Figure 2. Horizontal a) wind speed U ($\mathrm{m\,s^{-1}}$), b) wind direction WD (°) and c) air temperature T (°C) on 9 Jun at local time (UTC+3). The modelled profiles at each MEPS grid point are shown by grey solid lines and their mean by a black dashed line. The observation from the Kivenlahti mast are shown by green solid squares and the interpolated profiles used as boundary conditions by a green solid line. Stars show the SMEAR III observations.

PSD agree in shape, but the peak is observed at $D = 70$ nm ~~$D = 79$ nm~~ compared to $D = 87$ nm ~~$D = 100$ nm~~ in ADCHEM and observed total number concentration is around 35 % lower (Fig. S9~~5~~).

In the winter morning on 7 Dec, easterly flow was observed and the wind was turning to south-east with both height and time (Fig. S8a-b). Winds were stronger than in the summer morning, around $2\ \mathrm{m\,s^{-1}}$ at $z = 30$ m. The observed and modelled WD agree, but MEPS predicts up to $3\ \mathrm{m\,s^{-1}}$ lower U above the canopy. An inversion layer above ground is captured both in MEPS and observations (Fig. S8c), yet it is stronger in the observations especially during the first hours. As a contrast to T, MEPS predicts down to -3 °C lower T_D compared to the Kivenlahti observations at 9 am (Fig. S11~~9~~). Similar to the summer morning, the observations on the Kivenlahti mast and SMEAR III are in agreement. Both the modelled and observed PSD peak at $D = 30$ nm, but the observed total number concentrations are around 60 % higher (Fig. S12~~10~~).

Table 5. The performance measures and acceptance criteria applied in the evaluation: fractional bias (FB), normalised mean squared error (NMSE), factor of two (FAC2), normalised mean bias factor (NMBF) and normalised mean absolute error factor (NMAEF). For more details on the acceptance criteria, see Hanna and Chang (2012) and Yu et al. (2006).

|FB|	NMSE	FAC2	|NMBF|	NMAEF
<0.67[1] The model under- or overestimates, respectively, by a factor of < 2	<6[1] Random scatter is < 2.4 times the mean	>0.3[1] Fraction of modelled values within the factor of 2 of the observed is more than 30%	<0.25[2] The model over- or underestimates by a factor of < 1.25	<0.35[2] The absolute gross error is < 0.35 times the mean observation

1: Hanna and Chang (2012), 2: Yu et al. (2006)

5 Evaluation of the air quality modelling results

The model is evaluated against observations at the three different observations periods, and in both summer and winter morning the evaluation is done separately for both modelling hours. ~~The following performance measures are applied in the evaluation: fractional bias (FB), normalised mean squared error (NMSE), factor of two (FAC2) (Chang and Hanna, 2004), normalised mean bias factor (NMBF) and normalised mean absolute error factor (NMAEF) (Yu et al., 2006). See Appendix A for the definitions and Table 5 for the acceptance criteria. In summary, FB and NMBF measure systematic error (i.e., bias), NMSE and NMAEF the total errors and FAC2 the correct scales. Additionally, the statistical significance of the model error (i.e. the absolute difference between the observations and modelled values) is estimated with the Student's t-test for the horizontal distributions.~~

5.1 Performance measures

The following performance measures are applied in the evaluation: fractional bias (FB), normalised mean squared error (NMSE), factor of two (FAC2) (Chang and Hanna, 2004), normalised mean bias factor (NMBF) and normalised mean absolute error factor (NMAEF) (Yu et al., 2006). See Table 5 for the acceptance criteria and Appendix A for the equations. In short, FB and NMBF measure systematic error (i.e., bias), NMSE and NMAEF both systematic and random errors, and FAC2 the correct concentration scales. Additionally, the statistical significance of the model error (i.e. the absolute difference between the observations and modelled values) is estimated with the Student's t-test for the horizontal distributions of N_{tot}.

5.2 Horizontal distribution of total aerosol particle number concentration

In order to compare the data, both the mobile Sniffer measurements containing its geographical coordinates and the PALM data output have been horizontally aggregated to a 5 $\mathrm{m} \times$ 5 m grid, with a threshold of at least three measurement points per grid to calculate the median value. A comparison between the measured and modelled median total aerosol particle number

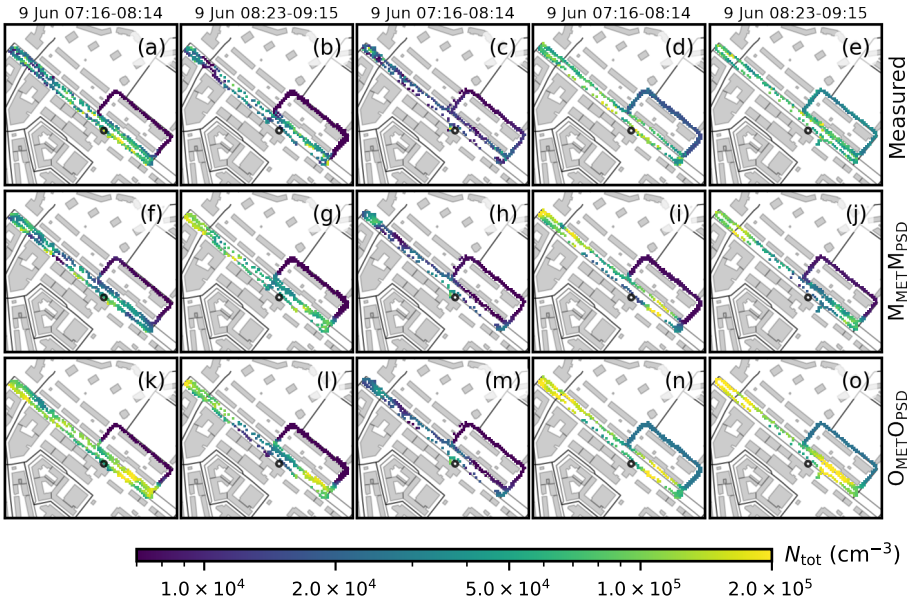

Figure 3. Measured (a-e) and modelled (f-o) median total aerosol number concentration (N_{tot}) along the Sniffer route for the summer morning (a,f,k for the first and b,g,l for the second hour), summer evening (c,h,m) and winter morning (d,i,n for the first and e,j,o for the second hour). The second row shows $\mathrm{M_{MET}M_{PSD}}$ and the third $\mathrm{O_{MET}O_{PSD}}$. Measurements are from $z = 2.4$ m and modelled values from $z = 2.5$ m. The supersite is marked with a black circle. ~~Note the different scale in different columns.~~

concentration (N_{tot}) values is illustrated in Fig. 3. In general, the model captures the large concentration gradient between the main street (in the middle from northwest to southeast) and the side street on the northeast side of the main street. However, the model overestimates N_{tot} at the north-western end of the Sniffer route at all simulation times, which is likely due to overestimation of the traffic emissions at an adjacent cross section. N_{tot} is well modelled also along the side street, except during the winter morning in $\mathrm{M_{MET}M_{PSD}}$ (Fig. 3d-e and 3i-j), when the model slightly underestimates N_{tot}. ~~Along the side street, the modelled N_{tot} is slightly higher than the observed in $\mathrm{M_{MET}M_{PSD}}$ during the first hour in the summer morning (Fig. 3f) and in $\mathrm{O_{MET}O_{PSD}}$ during the first hour in the winter morning (Fig. 3n).~~ The performance measures in simulating the horizontal distribution of N_{tot} and whether the acceptance criteria are fulfilled are shown in Fig. 4 ~~shows the performance measures in simulating the horizontal distribution of N_{tot}~~ for all simulation times ~~and whether the acceptance criteria are fulfilled~~. Overall, FB, NMSE and FAC2 show mostly acceptable model performance. ~~In general, NMBF and NMAEF are more strict measures.~~ However, NMBF often~~mostly~~ exceeds the acceptance criteria showing that the model tends to over- or underestimate the observations by 25 % or more. NMAEF never fulfills the criteria indicating that the absolute gross error between the observed and modelled values is always over 35 % larger than the mean observation. ~~However, the other measures show mostly acceptable model performance.~~

During the first hour in the summer morning, $\mathrm{M_{MET}M_{PSD}}$ performs better than $\mathrm{O_{MET}O_{PSD}}$ with respect to all performance measures. $\mathrm{O_{MET}O_{PSD}}$ clearly overestimates N_{tot} along the main street (Fig. 3k)~~.~~ despite a stronger temperature inversion

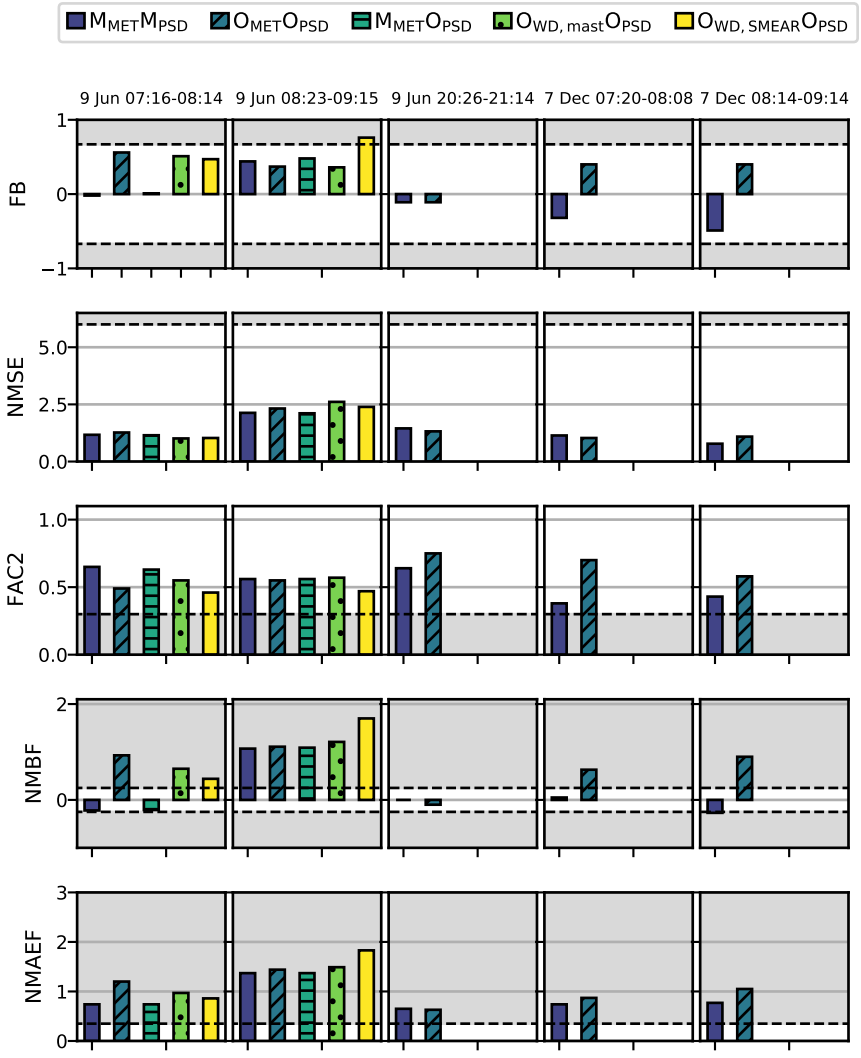

Figure 4. Model performance for the horizontal distribution of N_{tot} using the performance measures fractional bias (FB), normalised mean squared error (NMSE), factor of two (FAC2), normalised mean bias factor (NMBF) and normalised mean absolute error factor (NMAEF). The grey area indicates that the value exceeds the acceptance criteria given in Table 5. See Table 4 for the simulation names. Note that in the summer evening and winter morning, only two simulations have been conducted.

in the MEPS model data ($M_{MET}M_{PSD}$) compared to the Kivenlahti ($O_{MET}O_{PSD}$) observations (Fig. 2c). This likely stems from the underestimation of the wind speeds above 217 m in $O_{MET}O_{PSD}$ (Fig. 2a), which would lead to lower mechanical turbulence production and to lower mean turbulent kinetic energy (TKE) in $O_{MET}O_{PSD}$ (Fig. 5a). During the second hour, no large differences in N_{tot} are observed, as the wind speed and direction of the input data become more equal. ~~For the second hour the difference is small.~~

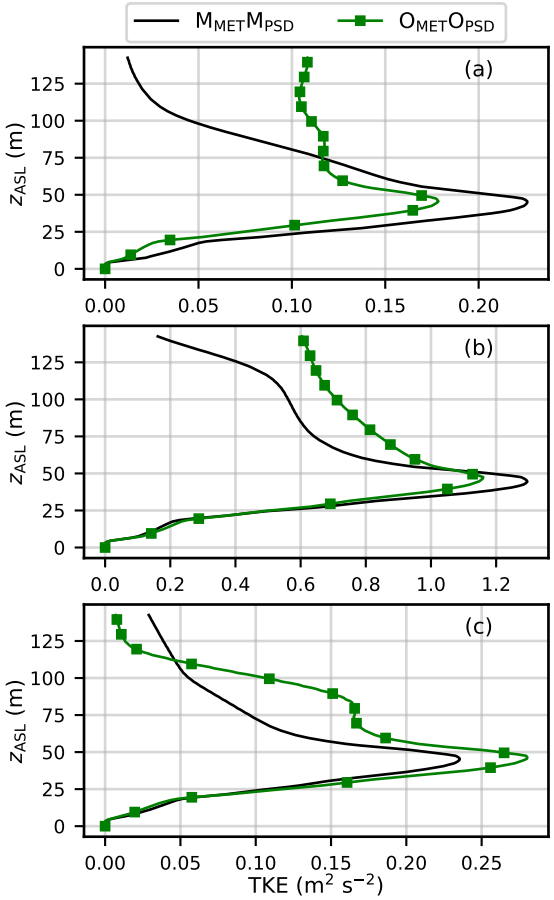

Figure 5. The vertical profile of the mean turbulent kinetic energy (TKE) over the entire child domain for the a) summer morning, b) summer evening and c) winter morning simulation. Each profile is temporally-averaged over the whole simulation.

Instead in the summer evening, $\mathrm{O_{MET}O_{PSD}}$ performs slightly better than $\mathrm{M_{MET}M_{PSD}}$ (e.g., FAC2 $= 0.75$ and FAC2 $= 0.67$, respectively), but both acquire good performance values and even NMBF is within the acceptance criteria. This is surprising considering the clearly stronger winds in MEPS at $z < 200$ m than what is observed on the Kivenlahti mast. Yet, MEPS predicts a more stable stratification, which leads to nearly equal TKE values (Fig. 5b). This can justify why the difference in the spatial variability of aerosol particle concentrations between $\mathrm{M_{MET}M_{PSD}}$ and $\mathrm{O_{MET}O_{PSD}}$ is not that large.

In the winter morning, $\mathrm{M_{MET}M_{PSD}}$ fulfills the acceptance criteria during the first hour, except for NMAEF, and ~~over~~performs better than $\mathrm{O_{MET}O_{PSD}}$. However~~,, but~~ during the second hour the difference is small. Interestingly, FAC2 is higher for $\mathrm{O_{MET}O_{PSD}}$ than $\mathrm{M_{MET}M_{PSD}}$ over the whole simulation. Contrary to the summer evening, MEPS predicts clearly lower wind speeds in the winter morning, which would lead to weaker mixing, but at the same time the observed temperature inversion on the Kivenlahti mast is stronger than the modelled by MEPS especially during the first hours. Hence, the stronger stability and suppression of turbulence (Fig. 5c) can explain the higher concentrations in $\mathrm{O_{MET}O_{PSD}}$. However, it should be noted that for the first hour

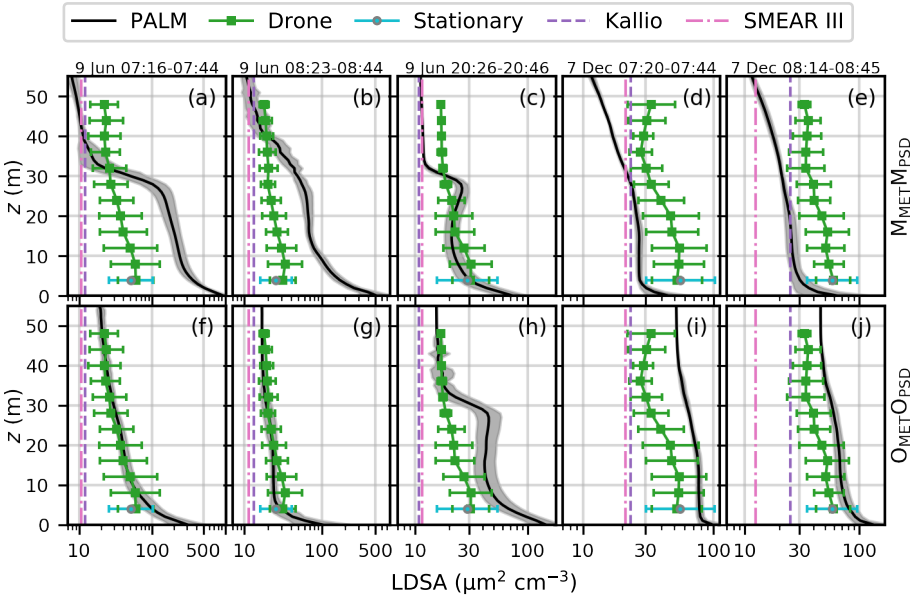

Figure 6. Measured (marker with error bar) and modelled (black line and grey shaded area) lung-deposited surface area (LDSA) of aerosol particles at the supersite for the summer morning (a,f for the first and b,g for the second hour), summer evening (c,h) and winter morning (d,i for the first and e,j for the second hour). The first row shows $\mathrm{M_{MET}M_{PSD}}$ and the second $\mathrm{O_{MET}O_{PSD}}$. The figure shows the geometric mean (measured: marker, modelled: solid line) and geometric standard deviation (measured: error bar, modelled: shaded area). Dashed lines show the geometric mean at the urban background monitoring sites in Kallio and SMEAR III.

the differences in the model absolute error between $\mathrm{M_{MET}M_{PSD}}$ and $\mathrm{O_{MET}O_{PSD}}$ are not significant and for the second hour Student's t-test cannot be performed (see Table S2 in the Supplement).

5.3 Vertical profile of the lung-deposited surface area

The modelled vertical profile of alveolar LDSA is evaluated against the observed one over a $5\ \mathrm{m} \times 5\ \mathrm{m}$ area next to the supersite on the northern side of the container (Fig. 6) and opposite the supersite on the other side of the main street (Fig. 7). In the summer morning, $\mathrm{M_{MET}M_{PSD}}$ performs well opposite the supersite (Figs. 7a-b and 9) especially during the first hour, but it clearly overestimates LDSA at the supersite (Figs. 6a-b and 8). On the contrary, $\mathrm{O_{MET}O_{PSD}}$ successfully reproduces the LDSA profile at the supersite (Figs. 6f-g) but not opposite it (Figs. 7f-g). This can be explained by the wind direction: according to the meteorological boundary condition analysis in Section 4, the wind direction predicted by MEPS is more westerly than the observed at Kivenlahti. Therefore, a canyon vortex forming in the main street canyon pushes pollutants upwind to the western side of the street in $\mathrm{M_{MET}M_{PSD}}$. On the other hand, the opposite is observed for $\mathrm{O_{MET}O_{PSD}}$ for which the wind direction is more from the north. In the summer evening, $\mathrm{M_{MET}M_{PSD}}$ fulfills all acceptance criteria, while $\mathrm{O_{MET}O_{PSD}}$ overestimates LDSA on both sides of the street canyon. This is contradictory to the horizontal distribution of N_{tot}, based on which $\mathrm{O_{MET}O_{PSD}}$ showed better performance. In the winter morning, $\mathrm{O_{MET}O_{PSD}}$ shows slightly better performance at the

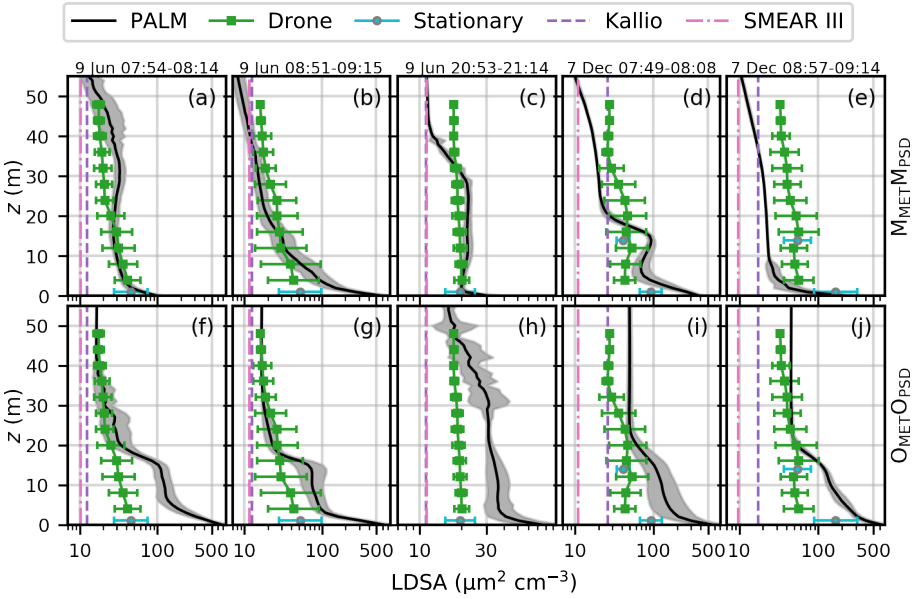

Figure 7. Measured (marker with error bar) and modelled (black line and grey shaded area) lung-deposited surface area (LDSA) of aerosol particles opposite the supersite for the summer morning (a,f for the first and b,g for the second hour), summer evening (c,h) and winter morning (d,i for the first and e,j for the second hour). The first row shows $M_{MET}M_{PSD}$ and the second $O_{MET}O_{PSD}$. The figure shows the geometric mean (measured: marker, modelled: solid line) and geometric standard deviation (measured: error bar, modelled: shaded area). Dashed lines show the geometric mean at the urban background monitoring sites in Kallio and SMEAR III.

supersite, whereas $M_{MET}M_{PSD}$ underestimates LDSA, but it also has a lower background concentration. Instead~~, while~~ opposite the supersite $O_{MET}O_{PSD}$ clearly overestimates LDSA below the building height. For the summer evening and winter morning, the differences in the shape of the vertical LDSA profiles are not as notable as in the summer morning, which can be explained by the good correspondence of the Kivenlahti wind direction observations with the MEPS data.

5.4 Aerosol size distribution

Fig. 10 illustrates the observed and modelled PSD for $M_{MET}M_{PSD}$ separately along the main and side street, at the supersite and opposite it, and in the background during the first hour of the summer morning 9 Jun. In addition to the Sniffer measurements with EEPS and ELPI, the modelled values are compared against DMPS measurements at the supersite and SMEAR III. The model successfully reproduces PSD along the main street and specifically at the supersite, for which FB, NMSE and FAC2 are within the acceptance criteria (see Table S3 in the Supplement). Also at the background, the Sniffer measurements agree with the model based on FB, NMSE and FAC2 even though the concentration of the smallest (the mean bin diameter $D_{mid} < 25$ nm) aerosol particles is underestimated. Instead along the side street, the modelled values are clearly lower than the observed and, for instance, based on NMBF the model underestimates the EEPS and ELPI observations by a factor of 3.45 and 5.48, respectively.

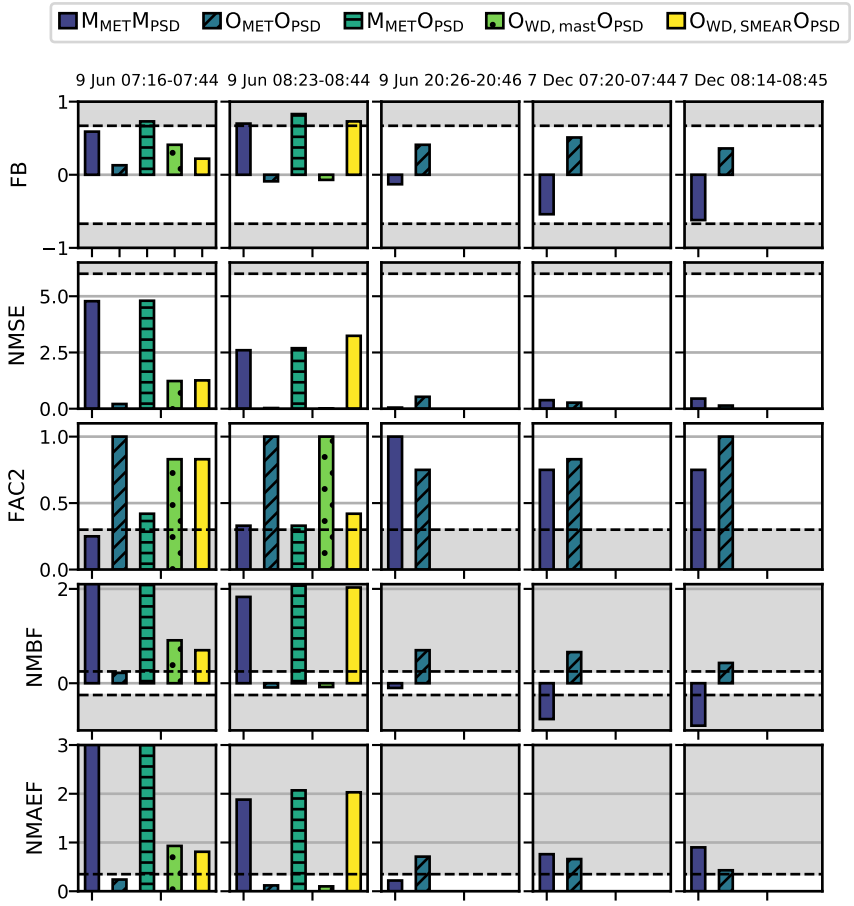

Figure 8. Model performance for the vertical distribution of LDSA at the supersite. The grey area indicates that the value exceeds the acceptance criteria given in Table 5. See Fig. 4 for details.

Comparing the two simulations with different boundary conditions, $M_{MET}M_{PSD}$ performs better along the main street and hence also at the supersite and opposite it during the first hour of the summer morning (Tables S3 and S4). However, during the second hour, the difference between $M_{MET}M_{PSD}$ and $O_{MET}O_{PSD}$ is minor, which was also observed for the horizontal distribution of N_{tot}. $O_{MET}O_{PSD}$, which uses the observed background PSD as boundary conditions, performs better along the side street and at the background. This is also observed in the summer evening (Tables S8 and S9) and winter morning (Tables S10 and S11). In the summer evening, both $M_{MET}M_{PSD}$ and $O_{MET}O_{PSD}$ perform equally well along the main street and equally bad at the supersite overestimating the EEPS measurements by a factor of 3.68–4.36 based on NMBF (Tables S8 and S9). In the winter morning, $M_{MET}M_{PSD}$ produces better results than $O_{MET}O_{PSD}$ ~~overperforms~~ along the main street. Instead, ~~while~~ at the supersite both $M_{MET}M_{PSD}$ and $O_{MET}O_{PSD}$ perform equally well and fulfil the acceptance criteria for FB, NMSE and FAC2 (Tables S10 and S11).

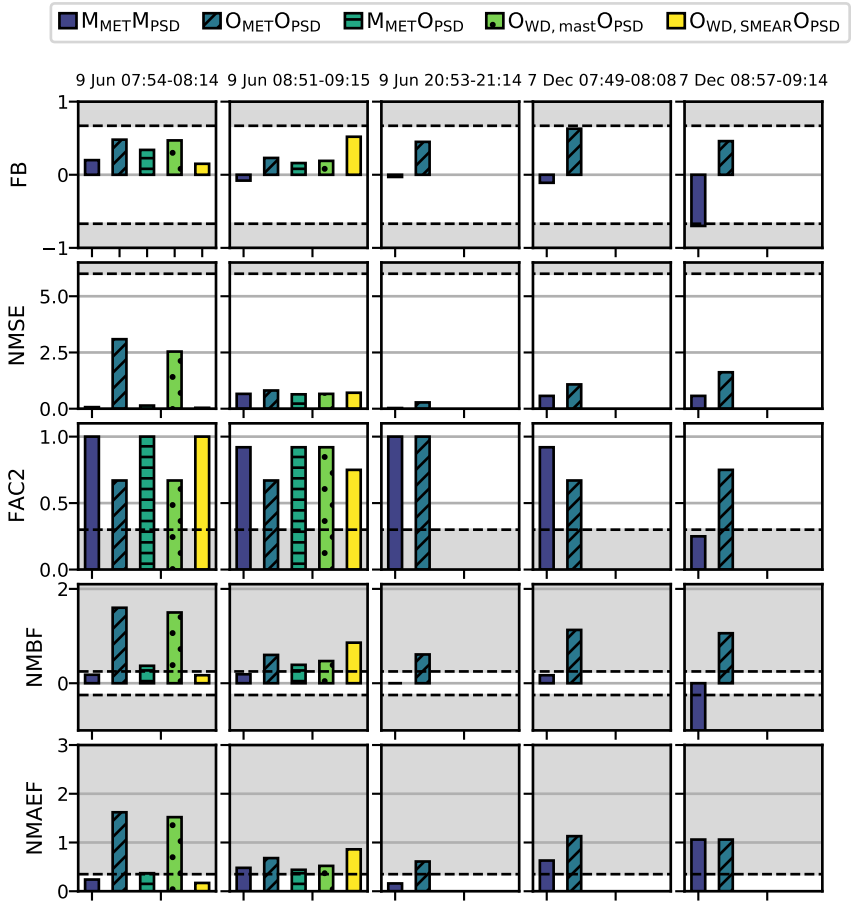

Figure 9. Model performance for the vertical distribution of LDSA opposite the supersite. The grey area indicates that the value exceeds the acceptance criteria given in Table 5. See Fig. 4 for details.

5.5 Aerosol chemical composition

The chemical composition of aerosols was measured at the supersite by an ACSM (Aerosol Chemical Speciation Monitor) and the black carbon (BC) concentration by a MAAP (Multi-Angle Absorption Photometer, see the Supplement, Table S1). Additionally Sniffer measured BC within PM_1. In general, the modelled and observed horizontal distribution of BC compare tolerably well based on the performance measures FB, NMSE and FAC2, while NMBF and NMAEF are not within the acceptance criteria (see Fig. S13~~11~~ in the Supplement). Overall, the performance is best for $M_{MET}M_{PSD}$ in the summer morning during the first hour. In the summer and winter morning, $O_{MET}O_{PSD}$ suffers from high positive bias and absolute error and $M_{MET}M_{PSD}$ in the winter morning from high absolute error. Instead in the summer evening, both simulations show NMSE and FAC2 within the acceptance criteria but still overestimate BC. Comparing to the measured chemical composition of aerosols at the supersite (Tables 6 and S12-13~~11-12~~) shows that the modelled concentration of organic carbon (OC) is in general in

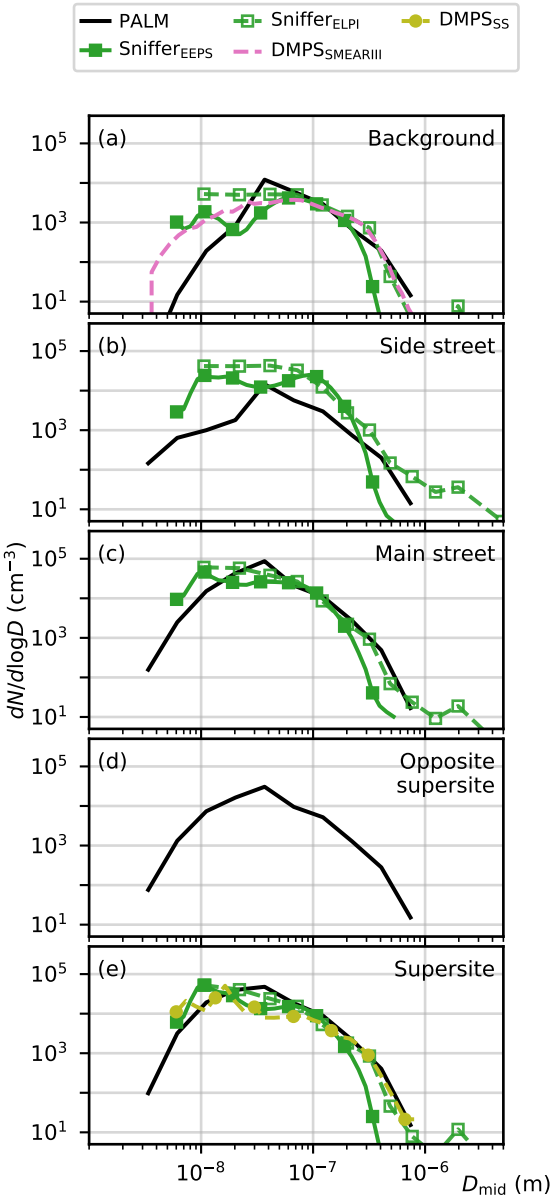

Figure 10. The mean aerosol number size distribution $dN/d\log D$ (cm^{-3}) at different parts of the domain at $z = 1.5$ m for $\mathrm{M_{MET}M_{PSD}}$ on 9 Jun morning at 07:16–08:14. Modelled values are shown with a black solid line and Sniffer measurements with green lines: solid with filled squares for EEPS and dotted with empty squares for ELPI. Stationary DMPS measurements are shown with a light-green solid line with circles (SS = supersite) and pink dotted line (SMEAR III). Note that for this observation period no stationary Sniffer measurements are available opposite the supersite.

Table 6. Performance of the modelled~~in the modelling~~ aerosol chemical composition at the supersite on 9 Jun morning between 07:16–09:15 am. See Fig. 4 for further description.

Simulation name	Variable	FB	NMSE	FAC2	NMBF	NMAEF
$M_{MET}M_{PSD}$	SO_4^-	0.73	1.65	0.50	1.60	1.60
	OC	0.42	0.75	0.50	0.75	0.97
	NO_3^-	0.15	0.04	1.00	0.16	0.16
	NH_4^+	1.60	26.44	0.00	18.05	18.05
	BC	1.39	15.07	0.00	10.02	10.02
	$PM_{2.5}$	1.20	6.65	0.33	5.10	5.10
$O_{MET}O_{PSD}$	SO_4^-	0.42	0.26	1.00	0.54	0.58
	OC	0.13	0.06	1.00	0.14	0.21
	NO_3^-	0.27	0.12	1.00	0.33	0.33
	NH_4^+	1.06	4.02	0.00	3.02	3.02
	BC	0.50	1.69	0.50	1.09	1.28
	$PM_{2.5}$	0.69	0.86	0.50	1.15	1.15

the right order of magnitude. Furthermore, in the summer morning (Table 6) especially the concentrations of sulphates (SO_4^-) and nitrates (NO_3^-), and also BC and $PM_{2.5}$ are correctly reproduced by $O_{MET}O_{PSD}$, while ammoniuma~~m~~ (NH_4^+) is highly overestimated especially by $M_{MET}M_{PSD}$ (NMBF $= 18.05$). In the summer evening (Table S12), $M_{MET}M_{PSD}$ corresponds better to observations than~~overperforms~~ $O_{MET}O_{PSD}$ and correctly reproduces SO_4^-, OC and $PM_{2.5}$, while overestimating the rest. Also in the winter morning (Table S13), $M_{MET}M_{PSD}$ performs slightly better than $O_{MET}O_{PSD}$ in modelling OC and $PM_{2.5}$ in the right order of magnitude, but $M_{MET}M_{PSD}$ still overestimates the mass concentrations of the other chemical components ~~are overestimated~~ by a factor of around 2.7–~~6.5~~4.2. Hence, the difference in the chemical composition is not systematic. Comparing modelled values with point observations in a street canyon is very sensitive to the correct wind direction because perpendicular wind component leads to accumulation of pollutants to the leeward side of the street canyon. As the vertical dispersion of LDSA was also shown sensitive to the wind direction, the results on the performance of modelling the correct chemical composition corresponds to those on the vertical dispersion of LDSA (see Section 5.3).~~Whether $M_{MET}M_{PSD}$ or $O_{MET}O_{PSD}$ performs better corresponds to the results on the vertical dispersion of LDSA.~~

6 Sensitivity analysis

6.1 Background aerosol size distribution

Sensitivity of the modelled aerosol concentrations to the background PSD is investigated by applying the modelled PSD ($M_{MET}M_{PSD}$) from ADCHEM and the observed PSD at SMEAR III ($M_{MET}O_{PSD}$) as the background PSD. Regarding all

variables used in the evaluation (N_{tot}, LDSA, PSD and aerosol chemical composition), only minor differences ~~due to using modelled or measured PSD as a boundary condition~~ are observed between $\mathrm{M_{MET}M_{PSD}}$ and $\mathrm{M_{MET}O_{PSD}}$. For instance, for the horizontal distribution of N_{tot}~~(e.g.~~, FB $= -0.02$ and FB $= 0.01$, and NMSE $= 1.17$ and NMSE $= 1.15$~~ for the horizontal distribution of N_{tot}~~, respectively (see Fig. 4). The difference in the horizontal distribution of N_{tot} (Fig. 11b) is mainly within -20–20 % with slightly higher (lower) concentrations in the southern (northern) part of the domain. This difference stems from roughly 80 % lower observed than modelled background N_{tot} and thus the air being advected from northwest is cleaner in $\mathrm{M_{MET}O_{PSD}}$ compared to $\mathrm{M_{MET}M_{PSD}}$.

Similar to the horizontal distribution, the vertical profile of LDSA for $\mathrm{M_{MET}O_{PSD}}$ does not differ from $\mathrm{M_{MET}M_{PSD}}$ within the street canyon (Fig. 12). Only a small decrease in model performance is observed opposite the supersite when applying the observed PSD as the boundary condition (e.g., FB is increased from 0.20 to 0.34 and NMSE from 0.07 to 0.14 during the first hour, Fig. 9). However, above $z > 30$ m, the difference gradually approaches 65–160 %, i.e., the relative difference in the background N_{tot} between the modelled ADCHEM values and SMEAR III observations.

With respect to PSD, $\mathrm{M_{MET}M_{PSD}}$ and $\mathrm{M_{MET}O_{PSD}}$ perform mostly equally good or bad, except for slightly better performance of $\mathrm{M_{MET}O_{PSD}}$ on the side street. The wind speed and/or direction influence the modelled PSD more than the background PSD (see~~The difference in the modelled PSD between $\mathrm{M_{MET}M_{PSD}}$ and $\mathrm{M_{MET}O_{PSD}}$ is smaller than when the wind speed and/or direction are different ($\mathrm{O_{WD,mast}O_{PSD}}$ and $\mathrm{O_{WD,SMEAR}O_{PSD}}$,~~ Fig. S1~~412~~ in the Supplement).

6.2 Background meteorological conditions

In Section 5, the simulation using the observed data as boundary conditions ($\mathrm{O_{MET}O_{PSD}}$) was shown to perform worse than when using the modelled MEPS data ($\mathrm{M_{MET}M_{PSD}}$) in the summer morning. As the observed wind speed at Kivenlahti and the one modelled by MEPS differ (see Section 4), we separately investigate the ~~influence of the incoming wind direction on the~~ model sensitivity to the incoming wind direction.

In general, $\mathrm{O_{MET}O_{PSD}}$ and $\mathrm{O_{WD,mast}O_{PSD}}$, for which the meteorological boundary conditions are taken from MEPS but the incoming wind direction is replaced with the one measured on the Kivenlahti mast~~ but the wind speed is the same~~, result in a similar pattern for the difference in the horizontal distribution of N_{tot} compared to $\mathrm{M_{MET}M_{PSD}}$ (Fig. 11a,c). However, the differences are larger for $\mathrm{O_{MET}O_{PSD}}$, for which the incoming upper-level wind speed is up to 2 $\mathrm{m\,s^{-1}}$ slower than in $\mathrm{O_{WD,mast}O_{PSD}}$ during the first hour (Fig. 2a). This results in the aerosol particles being transported more to the southwest side of the main street. As the wind is more from the north in $\mathrm{O_{MET}O_{PSD}}$ than in $\mathrm{O_{WD,mast}O_{PSD}}$, also the impact of wind direction on the street canyon vortex along the main street is observed by clearly lower (higher) N_{tot} on the southern (northern) side of the street canyon. The similar patterns of ΔN_{tot} for $\mathrm{O_{MET}O_{PSD}}$ and $\mathrm{O_{WD,mast}O_{PSD}}$ but the higher absolute values of ΔN_{tot} for $\mathrm{O_{MET}O_{PSD}}$ indicate that the horizontal distribution is strongly controlled by the wind direction, while the absolute values depend on the wind speed. Instead $\mathrm{O_{WD,SMEAR}O_{PSD}}$, for which the wind direction is from SMEAR III and does not vary with height, shows clearly higher concentrations (up to +150 %) along the main street but smaller differences in its surroundings (-40–80 %).

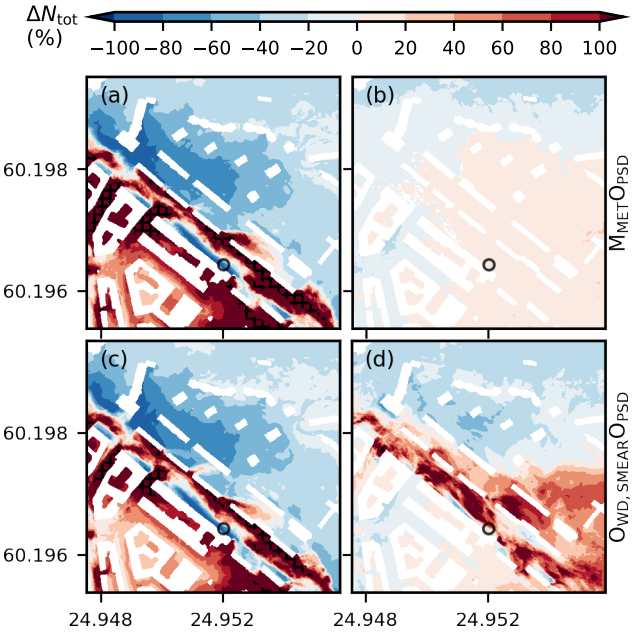

Figure 11. Relative difference in the total aerosol number concentration (ΔN_{tot}) at $z = 2.5$ m on 9 Jun morning between 07:16–09:15 am compared to $\mathrm{M_{MET}M_{PSD}}$ for a) $\mathrm{O_{MET}O_{PSD}}$, b) $\mathrm{M_{MET}O_{PSD}}$, c) $\mathrm{O_{WD,mast}O_{PSD}}$ and d) $\mathrm{O_{WD,SMEAR}O_{PSD}}$. Area with black crosses show $|\Delta N_{\mathrm{tot}}| > 150$ %. Buildings are shown with white and black circle denotes the location of the supersite. Note that ΔN_{tot} is shown here for the whole simulation and not separately for each hour.

Replacing the modelled wind direction with the one observed on the Kivenlahti mast ($\mathrm{O_{WD,mast}O_{PSD}}$) or SMEAR III ($\mathrm{O_{WD,SMEAR}O_{PSD}}$) improves the model performance for the horizontal distribution of N_{tot} during the first summer morning hour (Fig. 4). However, for the second hour $\mathrm{O_{WD,SMEAR}O_{PSD}}$ is shown to perform even worse than $\mathrm{O_{MET}O_{PSD}}$ based on a lower FAC2 and higher NMBF and NMAEF. During the first hour, $\mathrm{O_{WD,SMEAR}O_{PSD}}$ performs better than $\mathrm{O_{WD,mast}O_{PSD}}$ based on FB, NMBF and NMAEF, indicating that there is more bias in $\mathrm{O_{WD,mast}O_{PSD}}$, while during the second hour $\mathrm{O_{WD,SMEAR}O_{PSD}}$ performs better only based on NMSE. Presumably, wind has too much westerly component in $\mathrm{O_{WD,SMEAR}O_{PSD}}$ compared to the northerly winds in the MEPS and Kivenlahti data, which results in the traffic-emissions downstream being flushed along the main street.

The observed vertical profile of LDSA at the supersite on the summer morning corresponds better to the modelled by $\mathrm{O_{MET}O_{PSD}}$ and $\mathrm{O_{WD,mast}O_{PSD}}$ than $\mathrm{M_{MET}M_{PSD}}$ (Fig. 8). Hence, modifying the MEPS wind direction to correspond the observed one at Kivenlahti increases the model performance.~~At the supersite (Figs. 8 and 12a,c), $\mathrm{O_{MET}O_{PSD}}$ agrees better than $\mathrm{M_{MET}M_{PSD}}$ with the observations (e.g., FB = 0.13 and FB = 0.59, and NMSE = 0.21 and NMSE = 4.78, respectively, during the first hour) and hence modifying the MEPS wind direction to correspond the observed one at Kivenlahti increases the performance (Fig. 8).~~ During the second hour, $\mathrm{O_{WD,mast}O_{PSD}}$ performs even slightly better than $\mathrm{O_{MET}O_{PSD}}$ (e.g., FB = -0.07 and FB = -0.09, and NMSE = 0.01 and NMSE = 0.03). However, applying the wind direction from SMEAR III

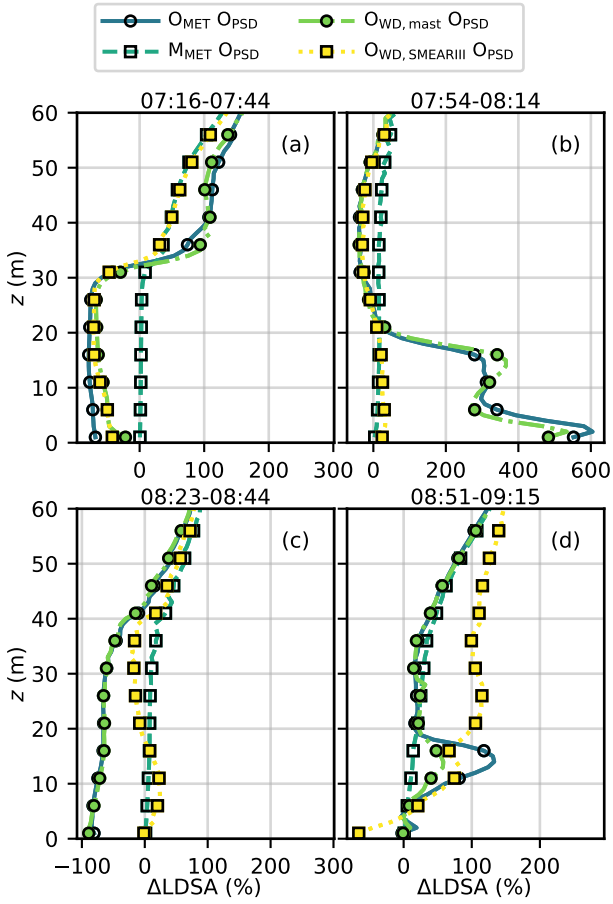

Figure 12. Relative difference in the lung-deposited surface area (ΔLDSA) of aerosol particles compared to $\mathrm{M_{MET}M_{PSD}}$ at the supersite (a,c) and opposite supersite (b,d) on 9 Jun morning. The figure shows the difference in the geometric mean for $\mathrm{O_{MET}O_{PSD}}$ (solid line with empty circles), $\mathrm{M_{MET}O_{PSD}}$ (dashed line with empty squares), $\mathrm{O_{WD,mast}O_{PSD}}$ (dash-dot line with filled squares) and $\mathrm{O_{WD,SMEAR}O_{PSD}}$ (dotted line with filled squares).

improves the model performance only for the first hour while during the second hour $\mathrm{O_{WD,SMEAR}O_{PSD}}$ performs worst. Whereas $\mathrm{O_{WD,mast}O_{PSD}}$ results in lower (higher) LDSA than $\mathrm{M_{MET}M_{PSD}}$ below (above) $z = 30 - 40$ m, ~~during the second hour~~ $\mathrm{O_{WD,SMEAR}O_{PSD}}$ shows higher values until the building height ($z = 19$ m) during the second hour, above~~after~~ which it gradually starts to follow the ΔLDSA for $\mathrm{O_{WD,mast}O_{PSD}}$. Opposite the supersite up to five-fold values compared to $\mathrm{M_{MET}M_{PSD}}$ are observed in $\mathrm{O_{MET}O_{PSD}}$ and $\mathrm{O_{WD,mast}O_{PSD}}$ within the first hour (Fig. 12b) and the model performance is clearly decreased when using the observed wind direction from Kivenlahti (e.g., FB is increased from 0.20 to 0.47 and FAC2 decreased from 1.00 to 0.67, Fig. 9). Instead, $\mathrm{O_{WD,SMEAR}O_{PSD}}$ performs better than $\mathrm{M_{MET}M_{PSD}}$. Within the second hour, ΔLDSA compared to $\mathrm{M_{MET}M_{PSD}}$ is mainly within ±50 % below the building height, but above $\mathrm{O_{WD,SMEAR}O_{PSD}}$ deviates from the other pro-

files showing two-fold values. All ΔLDSA profiles gradually approach ∼100 %, which results from using different PSD for $M_{MET}M_{PSD}$ and for rest of the simulations.

Similarly for the aerosol size distribution, changing the modelled wind direction by MEPS to the one measured at Kivenlahti improves model performance at the background and slightly decreases elsewhere during the first hour, whereas during the last hour PSD is modelled better along the side street and at the supersite (see Tables S3 and S6 in the Supplement). Applying the wind direction from SMEAR III generally does not improve model performance (Table S7). Along the main street, the difference in PSD is mainly governed by the emission, which is shown by the peak at $D_{mid} \approx 30$ nm in Fig. S1412 (in the Supplement), while at the background ΔN follows the difference in the boundary conditions for aerosol particles.

7 Discussion and conclusions

This study provides an extensive evaluation of the SALSA2.0 module in the PALM model system 6.0 on simulating the horizontal distribution of aerosol particle number concentrations (N_{tot}), size distributions and black carbon concentrations and the vertical distribution of surface area (LDSA) in a complex urban environment. In addition, the aerosol chemical composition in a single measurement location is examined. Simulations are conducted under three different meteorological conditions: two hours in a summer morning, one hour in a summer evening and two hours in a winter morning. The study also investigates the model sensitivity to the boundary conditions of meteorological variables and background aerosol concentrations during the different times.

Overall, the modelled aerosol concentrations compare well against observations. Indeed, the concentration fields are strongly influenced by the applied boundary conditions for the meteorological variables, while in this study the background PSD is shown less important. Especially the vertical profiles of LDSA are sensitive to the wind direction as it influences the formation and direction of the canyon vortex and thus the accumulation of pollutant to the leeward side of the street canyon. This also affects the model performance regarding the aerosol chemical composition, which is measured only at one point at the supersite. In general, the chemical composition is acceptably reproduced except for NH_4^+, which is highly overestimated at all times. Yet, the performance is not always systematic with the horizontal and vertical distributions. Furthermore, the horizontal distribution of N_{tot} is ruled by the prevailing wind speed and atmospheric stability, which both control the turbulent mixing and ventilation. It is speculated that the wind speed and stability counteract each other in the summer and winter morning, so that stronger stability can suppress TKE and turbulent mixing despite high wind speeds and consequent mechanical turbulence production, and vice versa.

~~In the summer morning, a stronger temperature inversion is present in the MEPS model data compared to the Kivenlahti observations. Still, N_{tot} along the main street is higher when measured boundary conditions ($O_{MET}O_{PSD}$) are used instead of the modelled ones ($M_{MET}M_{PSD}$) during the first hour. This likely stems from the underestimation of the wind speeds above 217 m in $O_{MET}O_{PSD}$, leading to lower mechanical turbulence production and mixing. During the second hour, no large differences in N_{tot} are observed, as the wind speed and direction of the input data become more equal. The 45–90° difference in the modelled and measured wind directions especially during the first hour results in pollutant accumulation and overestimation of LDSA at~~

~~the supersite (i.e., to the southwestern side of the main street canyon) in $\mathrm{M_{MET}M_{PSD}}$ and opposite the supersite in $\mathrm{O_{MET}O_{PSD}}$. This also leads to overestimation of especially nitrates and black carbon at the supersite in $\mathrm{M_{MET}M_{PSD}}$, whereas the chemical composition of aerosol particles is well reproduced in $\mathrm{O_{MET}O_{PSD}}$. However in terms of PSD, $\mathrm{M_{MET}M_{PSD}}$ in general performs better than $\mathrm{O_{MET}O_{PSD}}$ around the main street and at the supersite.~~

~~By the evening, MEPS shows only slightly more southerly but clearly stronger winds at $z < 200\ \mathrm{m}$ than what is observed on the Kivenlahti mast. To be precise, MEPS predicts a low-level jet with the maximum wind speed at $z = 100\ \mathrm{m}$. Still, both simulations perform nearly equally. Slightly higher N_{tot} and overestimation of near-surface LDSA in $\mathrm{O_{MET}O_{PSD}}$ can be explained by the difference in the wind speed. This is also reflected in the aerosol chemical composition at the supersite. MEPS predicts a more stable stratification, which might justify why the difference in the spatial variability of aerosol particle concentrations between $\mathrm{M_{MET}M_{PSD}}$ and $\mathrm{O_{MET}O_{PSD}}$ is not that large~~huge.~~

~~MEPS predicts clearly stronger wind speeds in the winter morning, but still the near-surface N_{tot} is mainly overestimated in $\mathrm{O_{MET}O_{PSD}}$ during the first simulation hour. The higher concentrations in $\mathrm{O_{MET}O_{PSD}}$ can be attributed to a stronger temperature inversion leading to less efficient mixing. During the second hour, the difference in performance is small. Similarly, opposite the supersite $\mathrm{O_{MET}O_{PSD}}$ clearly overestimates LDSA below the building height, but interestingly $\mathrm{O_{MET}O_{PSD}}$ performs better in modelling the vertical distribution of LDSA at the supersite. $\mathrm{M_{MET}M_{PSD}}$ slightly underestimates the concentrations at the supersite, but also the background concentration of LDSA is lower. Interestingly, the difference in the chemical composition is not systematic as $\mathrm{M_{MET}M_{PSD}}$ reproduces better the concentration of organics and $\mathrm{O_{MET}O_{PSD}}$ the concentration of nitrates and black carbon.~~

~~Modifying the boundary conditions from MEPS by applying the wind direction measured on the Kivenlahti mast ($\mathrm{O_{WD,mast}O_{PSD}}$) improves model performance in the summer morning, indicating that the wind predicted by MEPS is not correct. Especially the vertical profiles of LDSA are sensitive to the wind direction as it influences the formation and direction of the canyon vortex and thus the accumulation of pollutant to the leeward side of the street canyon. The similar patterns of ΔN_{tot} for $\mathrm{O_{MET}O_{PSD}}$ and $\mathrm{O_{WD,mast}O_{PSD}}$ but the higher absolute values of ΔN_{tot} for $\mathrm{O_{MET}O_{PSD}}$ indicate that the horizontal distribution is strongly controlled by the wind direction, while the absolute values depend on the wind speed. In contrast, applying the vertically constant wind direction from SMEAR III worsens the model performance within the second simulation hour. Presumably wind has too much westerly component compared to the northerly winds in the MEPS and Kivenlahti data, which results in the traffic-emissions downstream being flushed along the main street and also being accumulated near the ground. Contrary to the wind direction, the background PSD has only a small influence on the model performance. However, the shape of PSD influences also the magnitude of integrated aerosol measures, such as LDSA, and therefore, for example, the background LDSA is over three-fold in $\mathrm{M_{MET}M_{PSD}}$ compared to $\mathrm{O_{WD,mast}O_{PSD}}$ in the summer evening.~~

Consequently, meteorological boundary conditions are particularly important for quantitative urban air quality modelling using LES, and therefore the inlet meteorology should be evaluated prior to conducting CFD simulations (Santiago et al., 2020). However in our case, we are unable to thoroughly evaluate the modelled meteorology. In Santiago et al. (2020), the meteorological observations were made within the simulation domain, while in our case the closest measurements at SMEAR III are 800 m away from the supersite. Observations are available also from the Kivenlahti mast, which has several measurement

levels, but is located over 17 km away from the supersite and represents more semi-urban to rural area. Another problem with the Kivenlahti data is the lack of wind observations above 217 m in summer, which presumably leads to, for instance, underestimation of the incoming wind speed during the first simulation hour in the summer morning and around 9 pm in the summer evening. Consequently, neither observations are optimal for evaluating the modelled meteorology nor providing meteorological boundary conditions for the simulations.

Of the aerosol metrics applied, LDSA directly estimates the health effect of aerosol exposure. The mean modelled LDSA concentration at $z = 4$ m varies between 27–360 $\mu\mathrm{m}^2\,\mathrm{cm}^{-3}$ at the supersite and 20–250 $\mu\mathrm{m}^2\,\mathrm{cm}^{-3}$ opposite the supersite, with the overall lowest LDSA opposite the supersite in $\mathrm{M_{MET}M_{PSD}}$ in the summer evening and highest at the supersite in $\mathrm{M_{MET}M_{PSD}}$ in the summer morning. As mentioned above, the wind direction is shown determining for accumulation of pollutants near the ground. The difference in near-ground LDSA between the supersite and opposite the supersite is the most pronounced in $\mathrm{M_{MET}M_{PSD}}$ during the first hour of the summer morning (360 and 37 $\mu\mathrm{m}^2\,\mathrm{cm}^{-3}$, respectively). This large concentration gradient across the street illustrates the degree of error that can be made in the estimated outdoor-exposure level in epidemiological studies. Compared to urban background and traffic monitoring stations (see Kuula et al., 2020, and references within), a street canyon allows for strong accumulation leading to high instantaneous concentrations.

However, LDSA is often overestimated near the ground in our simulations. One limitation of this study and in general in urban LES is omitting vehicle-induced turbulence (VIT), which would enhance vertical pollutant transport and mixing near the surface and very likely decrease concentrations near ground. The research to include VIT in LES without extensive computational costs is on-going and currently no freely available VIT-model exists for LES. Neglecting the thermal turbulence in the simulations is another important limitation of our study. We acknowledge that omitting the influence of anthropogenic heat and heating by incoming solar radiation leads to overestimation of the vertical stability near the ground, which can partly explain the overestimation of the modelled surface concentrations. However, the spatial variability has been shown less dependent on a detailed heating distribution Nazarian et al. (2018) and therefore the horizontal distribution is mainly determined by the predominant inflow conditions. Lastly, condensation of the biogenic volatile organic compounds on aerosol particles and their consecutive growth are not considered in PALM.

Code and data availability. The PALM code is freely available under the GNU General Public License v3. The exact model source code (revision 4416) is available at https://doi.org/10.5281/zenodo.4005366~~https://palm.muk.uni-hannover.de/trac/browser?rev=4416 (last access: 10 Sept 2019)~~. MEPS model data is distributed under Norwegian license for public data (NLOD) and Creative Commons 4.0 BY Internasjonal at http://thredds.met.no/thredds/catalog.html by the Norwegian Meteorological Institute.

All measurement data applied in the evaluation can be downloaded from https://doi.org/10.5281/zenodo.3828508 (Kurppa et al., 2020) and the input and output data, performance measures and source code modifications from https://doi.org/10.5281/zenodo.3824351 (Kurppa, 2020a). The scripts applied in the data analysis and model evaluation are freely available at https://doi.org/10.5281/zenodo.3839462 (Kurppa, 2020b), and the files and scripts for creating the PALM input data at https://doi.org/10.5281/zenodo.3839684 (Kurppa and Strömberg, 2020).

Video supplement. TEXT

Appendix A: Performance measures

Performance measures calculated using the modelled M_i and observed O_i values. N = number of samples.

$$\mathrm{FB} = \frac{1}{N}\sum \frac{(M_i - O_i)}{0.5(M_i + O_i)} \tag{A1}$$

$$\mathrm{NMSE} = \frac{N\sum(M_i - O_i)^2}{\sum M_i \sum O_i} \tag{A2}$$

$\mathrm{FAC2}$ = fraction of data that satisfy

$$0.5 \leq \frac{M_i}{O_i} \leq 2.0 \tag{A3}$$

$$\mathrm{NMBF} = \frac{\sum(M_i - O_i)}{\sum O_i} \quad \text{, if } \overline{M} \geq \overline{O} \tag{A4}$$

$$= \frac{\sum(M_i - O_i)}{\sum M_i} \quad \text{, if } \overline{M} < \overline{O} \tag{A5}$$

$$\mathrm{NMAEF} = \frac{\sum|M_i - O_i|}{\sum O_i} \quad \text{, if } \overline{M} \geq \overline{O} \tag{A6}$$

$$= \frac{\sum|M_i - O_i|}{\sum M_i} \quad \text{, if } \overline{M} \geq \overline{O} \tag{A7}$$

Author contributions. LJ and MK designed the concept of the study. MK prepared and conducted the LES simulations with contributions from AH, and PR conducted the ADCHEM simulations. MK, JS and SK contributed to the pre-processing of the used input data sets. LJ, HK, TR, JN, LP and HT planned the measurement campaign and MK, HK, SK and HT conducted parts of the measurements. AB participated to the post-processing scripts of the Sniffer data. MK wrote the manuscript with contributions from all co-authors.

Competing interests. The authors declare that they have no conflict of interest.

Acknowledgements. The authors are very grateful to Aleksi Malinen and Sami Kulovuori from the Metropolia University of Applied Sciences for technical expertise and operation of Sniffer, and to Aeromon Oy and Helsinki Region Environmental Services Authority (HSY) for

collaboration in conducting the drone measurements. This study was financially supported by the Doctoral programme in Atmospheric Sciences (ATM-DP), Helsinki Metropolitan Region Urban Research Program, the Academy of Finland Centre of Excellence (no. 307331), Business Finland (Cityzer; Services for effective decision making and environmental resilience) and Project Smart urban solutions for air quality, disasters and city growth (SMURBS, no. 689443) funded by ERA-NET-COFUND project under ERA-PLANET.

References

Abhijith, K., Kumar, P., Gallagher, J., McNabola, A., Baldauf, R., Pilla, F., Broderick, B., Sabatino, S. D., and Pulvirenti, B.: Air pollution abatement performances of green infrastructure in open road and built-up street canyon environments – A review, Atmos. Environ., 162, 71–86, https://doi.org/10.1016/j.atmosenv.2017.05.014, 2017.

Adam, M., Schikowski, T., Carsin, A. E., Cai, Y., Jacquemin, B., Sanchez, M., Vierkötter, A., Marcon, A., Keidel, D., Sugiri, D., Al Kanani, Z., Nadif, R., Siroux, V., Hardy, R., Kuh, D., Rochat, T., Bridevaux, P.-O., Eeftens, M., Tsai, M.-Y., Villani, S., Phuleria, H. C., Birk, M., Cyrys, J., Cirach, M., de Nazelle, A., Nieuwenhuijsen, M. J., Forsberg, B., de Hoogh, K., Declerq, C., Bono, R., Piccioni, P., Quass, U., Heinrich, J., Jarvis, D., Pin, I., Beelen, R., Hoek, G., Brunekreef, B., Schindler, C., Sunyer, J., Krämer, U., Kauffmann, F., Hansell, A. L., Künzli, N., and Probst-Hensch, N.: Adult lung function and long-term air pollution exposure. ESCAPE: a multicentre cohort study and meta-analysis, Eur. Respir. J., 45, 38–50, https://doi.org/10.1183/09031936.00130014, 2015.

Andersen, Z. J., Bønnelykke, K., Hvidberg, M., Jensen, S. S., Ketzel, M., Loft, S., Sørensen, M., Tjønneland, A., Overvad, K., and Raaschou-Nielsen, O.: Long-term exposure to air pollution and asthma hospitalisations in older adults: a cohort study, Thorax, 67, 6–11, https://doi.org/10.1136/thoraxjnl-2011-200711, 2012.

Arnold, F., Pirjola, L., Aufmhoff, H., Schuck, T., Lähde, T., and Hämeri, K.: First gaseous sulfuric acid measurements in automobile exhaust: Implications for volatile nanoparticle formation, Atmos. Environ., 40, 7097–7105, https://doi.org/10.1016/j.atmosenv.2006.06.038, 2006.

Arnold, F., Pirjola, L., Rönkkö, T., Reichl, U., Schlager, H., Lähde, T., Heikkilä, J., and Keskinen, J.: First Online Measurements of Sulfuric Acid Gas in Modern Heavy-Duty Diesel Engine Exhaust: Implications for Nanoparticle Formation, Environ. Sci. Technol., 46, 11 227–11 234, https://doi.org/10.1021/es302432s, 2012.

Auvinen, M. and Aarnio, M.: RasterH3D, last access: 20 Jun 2019, https://github.com/mjsauvinen/RasterH3D, 2019.

Auvinen, M. and Karttunen, S.: P4UL Pre- and Post-Processing Python Library for Urban LES Simulations, last access: 28 Jun 2019, https://github.com/mjsauvinen/P4UL, 2019.

Auvinen, M., Boi, S., Hellsten, A., Tanhuanpää, T., and Järvi, L.: Study of realistic urban boundary layer turbulence with high-resolution large-eddy simulation, Atmosphere, 11, 201, https://doi.org/10.3390/atmos11020201, 2020.

Baik, J.-J., Park, S.-B., and Kim, J.-J.: Urban Flow and Dispersion Simulation Using a CFD Model Coupled to a Mesoscale Model, J. Appl. Meteorol. Climatol., 48, 1667–1681, https://doi.org/10.1175/2009JAMC2066.1, 2009.

Bengtsson, L., Andrae, U., Aspelien, T., Batrak, Y., Calvo, J., de Rooy, W., Gleeson, E., Hansen-Sass, B., Homleid, M., Hortal, M., Ivarsson, K.-I., Lenderink, G., Niemelä, S., Nielsen, K. P., Onvlee, J., Rontu, L., Samuelsson, P., Muñoz, D. S., Subias, A., Tijm, S., Toll, V., Yang, X., and Køltzow, M. Ø.: The HARMONIE-AROME Model Configuration in the ALADIN-HIRLAM NWP System, Mon. Weather Rev., 145, 1919–1935, https://doi.org/10.1175/MWR-D-16-0417.1, 2017.

Brown, D. M., Wilson, M. R., MacNee, W., Stone, V., and Donaldson, K.: Size-Dependent Proinflammatory Effects of Ultrafine Polystyrene Particles: A Role for Surface Area and Oxidative Stress in the Enhanced Activity of Ultrafines, Toxicol. Appl. Pharm., 175, 191–199, https://doi.org/10.1006/taap.2001.9240, 2001.

Burnett, R., Chen, H., Szyszkowicz, M., Fann, N., Hubbell, B., Pope, C. A., Apte, J. S., Brauer, M., Cohen, A., Weichenthal, S., Coggins, J., Di, Q., Brunekreef, B., Frostad, J., Lim, S. S., Kan, H., Walker, K. D., Thurston, G. D., Hayes, R. B., Lim, C. C., Turner, M. C., Jerrett, M., Krewski, D., Gapstur, S. M., Diver, W. R., Ostro, B., Goldberg, D., Crouse, D. L., Martin, R. V., Peters, P., Pinault, L., Tjepkema, M., van Donkelaar, A., Villeneuve, P. J., Miller, A. B., Yin, P., Zhou, M., Wang, L., Janssen, N. A. H., Marra, M., Atkinson, R. W., Tsang, H., Quoc Thach, T., Cannon, J. B., Allen, R. T., Hart, J. E., Laden, F., Cesaroni, G., Forastiere, F., Weinmayr, G., Jaensch, A., Nagel,

G., Concin, H., and Spadaro, J. V.: Global estimates of mortality associated with long-term exposure to outdoor fine particulate matter, P. Natl. Acad. Sci., 115, 9592–9597, https://doi.org/10.1073/pnas.1803222115, 2018.

Chang, J. C. and Hanna, S. R.: Air quality model performance evaluation, Meteorol. Atmos. Phys., 87, 167–196, 2004.

Chung, D. and McKeon, B. J.: Large-eddy simulation of large-scale structures in long channel flow, J. Fluid Mech., 661, 341–364, https://doi.org/10.1017/S0022112010002995, 2010.

City of Helsinki: Map Service, last access: 19 Dec 2018, kartta.hel.fi.

City of Helsinki: Traffic rates in Helsinki, map (in Finnish), last access: 19 May 2020, https://www.hel.fi/static/liitteet/kaupunkiymparisto/liikenne-ja-kartat/kadut/liikennetilastot/autoliikenne/Autoliikennekartta.pdf, 2018.

Damian, V., Sandu, A., Damian, M., Potra, F., and Carmichael, G. R.: The kinetic preprocessor KPP-a software environment for solving chemical kinetics, Comput. Chem. Eng., 26, 1567–1579, https://doi.org/10.1016/S0098-1354(02)00128-X, 2002.

Enroth, J., Saarikoski, S., Niemi, J., Kousa, A., Ježek, I., Močnik, G., Carbone, S., Kuuluvainen, H., Rönkkö, T., Hillamo, R., and Pirjola, L.: Chemical and physical characterization of traffic particles in four different highway environments in the Helsinki metropolitan area, Atmos. Chem. Phys., 16, 5497–5512, https://doi.org/10.5194/acp-16-5497-2016, 2016.

Finnish Meteorological Institute: Weather observations: Kivenlahti mast, last access: 18 Feb 2020, http://opendata.fmi.fi/wfs.

Fishpool, G. M., Lardeau, S., and Leschziner, M. A.: Persistent Non-Homogeneous Features in Periodic Channel-Flow Simulations, Flow Turbul. Combust., 83, 323–342, https://doi.org/10.1007/s10494-009-9209-z, 2009.

García-Sánchez, C., van Beeck, J., and Gorlé, C.: Predictive large eddy simulations for urban flows: Challenges and opportunities, Build. Environ., 139, 146–156, https://doi.org/10.1016/j.buildenv.2018.05.007, 2018.

Gronemeier, T. and Sühring, M.: On the Effects of Lateral Openings on Courtyard Ventilation and Pollution—A Large-Eddy Simulation Study, Atmosphere, 10, https://doi.org/10.3390/atmos10020063, 2019.

Hackbusch, W.: Multi-grid methods and applications (1st ed.), Springer-Verlag Berlin Heidelberg., 1985.

Hanna, S. and Chang, J.: Acceptance criteria for urban dispersion model evaluation, Meteorol. Atmos. Phys., 116, 133–146, https://doi.org/10.1007/s00703-011-0177-1, 2012.

Heinze, R., Moseley, C., Böske, L. N., Muppa, S. K., Maurer, V., Raasch, S., and Stevens, B.: Evaluation of large-eddy simulations forced with mesoscale model output for a multi-week period during a measurement campaign, Atmos. Chem. Phys., 17, 7083–7109, https://doi.org/10.5194/acp-17-7083-2017, 2017.

Hellsten, A., Ketelsen, K., Barmpas, F., Tsegas, G., Moussiopoulos, N., and Raasch, S.: Nested multi-scale system implemented in the PALM large-eddy simulation model, in: Air pollution modelling and its application XXV, edited by Klemens, M. and Kallos, G., pp. 287–292, Springer, 2017.

Helsinki Region Environmental Services Authority: Descriptions for the stationary monitoring stations (in Finnish), last access: 27 Apr 2020, https://www.hsy.fi/fi/asiantuntijalle/ilmansuojelu/mittausasematpks/Documents/Pysyvien%20mittausasemien%20kuvaukset.pdf.

Hietikko, R., Kuuluvainen, H., Harrison, R. M., Portin, H., Timonen, H., Niemi, J. V., and Rönkkö, T.: Diurnal variation of nanocluster aerosol concentrations and emission factors in a street canyon, Atmos. Environ., 189, 98–106, https://doi.org/10.1016/j.atmosenv.2018.06.031, 2018.

Huang, C., Wang, H. L., Li, L., Wang, Q., Lu, Q., de Gouw, J. A., Zhou, M., Jing, S. A., Lu, J., and Chen, C. H.: VOC species and emission inventory from vehicles and their SOA formation potentials estimation in Shanghai, China, Atmos. Chem. Phys., 15, 11 081–11 096, https://doi.org/10.5194/acp-15-11081-2015, 2015.

Hussain, M., Madl, P., and Khan, A.: Lung deposition predictions of airborne particles and the emergence of contemporary diseases, Part-I, Health, 2, 51–59, 2011.

Järvi, L., Hannuniemi, H., Hussein, T., Junninen, H., Aalto, P., Hillamo, R., Mäkelä, T., Keronen, P., Siivola, E., Vesala, T., and Kulmala, M.: The urban measurement station SMEAR III: Continuous monitoring of air pollution and surface-atmosphere interactions in Helsinki, Finland, Boreal Environ. Res., 14, 86–109, 2009.

Jöckel, P., Kerkweg, A., Pozzer, A., Sander, R., Tost, H., Riede, H., Baumgaertner, A., Gromov, S., and Kern, B.: Development cycle 2 of the Modular Earth Submodel System (MESSy2), Geosci. Model Dev., 3, 717–752, https://doi.org/10.5194/gmd-3-717-2010, 2010.

Junninen, H., Lauri, A., Keronen, P., Aalto, P., Hiltunen, V., Hari, P., and Kulmala, M.: Smart-SMEAR: on-line data exploration and visualization tool for SMEAR stations, Boreal Environment Research, pp. 447–457, 2009.

Kampa, M. and Castanas, E.: Human health effects of air pollution, Environ. Pollut., 151, 362–367, https://doi.org/10.1016/j.envpol.2007.06.012, proceedings of the 4th International Workshop on Biomonitoring of Atmospheric Pollution (With Emphasis on Trace Elements), 2008.

Kelly, F. J. and Fussell, J. C.: Size, source and chemical composition as determinants of toxicity attributable to ambient particulate matter, Atmos. Environ., 60, 504–526, https://doi.org/10.1016/j.atmosenv.2012.06.039, 2012.

Kokkola, H., Korhonen, H., Lehtinen, K. E. J., Makkonen, R., Asmi, A., Järvenoja, S., Anttila, T., Partanen, A. I., Kulmala, M., Järvinen, H., Laaksonen, A., and Kerminen, V. M.: SALSA - a Sectional Aerosol module for Large Scale Applications, Atmos. Chem. Phys., 8, 2469–2483, https://doi.org/10.5194/acp-8-2469-2008, 2008.

Kurppa, M.: Model input and output, performance measures and modifications in the source code for PALM simulations on Mäkelänkatu in Helsinki, Finland, https://doi.org/10.5281/zenodo.3824351, 2020a.

Kurppa, M.: Python scripts for evaluating PALM simulations against mobile air quality observations on Mäkelänkatu in Helsinki, Finland, https://doi.org/10.5281/zenodo.3839462, 2020b.

Kurppa, M. and Strömberg, J.: Input files and scripts for creating PALM simulation input files on Mäkelänkatu in Helsinki, Finland, https://doi.org/10.5281/zenodo.3839684, 2020.

Kurppa, M., Hellsten, A., Roldin, P., Kokkola, H., Tonttila, J., Auvinen, M., Kent, C., Kumar, P., Maronga, B., and Järvi, L.: Implementation of the sectional aerosol module SALSA2.0 into the PALM model system 6.0: model development and first evaluation, Geosci. Model Dev., 12, 1403–1422, https://doi.org/10.5194/gmd-12-1403-2019, 2019.

Kurppa, M., Balling, A., Karttunen, S., Kuuluvainen, H., Järvi, L., Niemi, J. V., Pirjola, L., Rönkkö, T., and Timonen, H.: Mobile and stationary air pollution measurements around an air quality monitoring site on Mäkelänkatu in Helsinki, Finland, https://doi.org/10.5281/zenodo.3828508, 2020.

Kuula, J., Kuuluvainen, H., Niemi, J. V., Saukko, E., Portin, H., Kousa, A., Aurela, M., Rönkkö, T., and Timonen, H.: Long-term sensor measurements of lung deposited surface area of particulate matter emitted from local vehicular and residential wood combustion sources, Aerosol Sci. Tech., 54, 190–202, https://doi.org/10.1080/02786826.2019.1668909, 2020.

Kuuluvainen, H., Poikkimäki, M., Järvinen, A., Kuula, J., Irjala, M., Maso, M. D., Keskinen, J., Timonen, H., Niemi, J. V., and Rönkkö, T.: Vertical profiles of lung deposited surface area concentration of particulate matter measured with a drone in a street canyon, Environ. Pollut., 241, 96–105, https://doi.org/10.1016/j.envpol.2018.04.100, 2018.

Kwak, K.-H., Baik, J.-J., Ryu, Y.-H., and Lee, S.-H.: Urban air quality simulation in a high-rise building area using a CFD model coupled with mesoscale meteorological and chemistry-transport models, Atmos. Environ., 100, 167–177, https://doi.org/10.1016/j.atmosenv.2014.10.059, 2015.

Lelieveld, J., Evans, J. S., Fnais, M., Giannadaki, D., and Pozzer, A.: The contribution of outdoor air pollution sources to premature mortality on a global scale, Nature, 525, 367–371, https://doi.org/10.1038/nature15371, 2015.

Lelieveld, J., Klingmüller, K., Pozzer, A., Pöschl, U., Fnais, M., Daiber, A., and Münzel, T.: Cardiovascular disease burden from ambient air pollution in Europe reassessed using novel hazard ratio functions, Eur. Heart J., 40, 1590–1596, https://doi.org/10.1093/eurheartj/ehz135, 2019.

Letzel, M. O., Helmke, C., Ng, E., An, X., Lai, A., and Raasch, S.: LES case study on pedestrian level ventilation in two neighbourhoods in Hong Kong, Meteorol. Z., 21, 575–589, https://doi.org/10.1127/0941-2948/2012/0356, 2012.

Liu, Y., Miao, S., Zhang, C., Cui, G., and Zhang, Z.: Study on micro-atmospheric environment by coupling large eddy simulation with mesoscale model, J. Wind Eng. Ind. Aerod., 107-108, 106–117, https://doi.org/10.1016/j.jweia.2012.03.033, 2012.

Maronga, B., Gryschka, M., Heinze, R., Hoffmann, F., Kanani-Sühring, F., Keck, M., Ketelsen, K., Letzel, M. O., Sühring, M., and Raasch, S.: The Parallelized Large-Eddy Simulation Model (PALM) version 4.0 for atmospheric and oceanic flows: model formulation, recent developments, and future perspectives, Geosci. Model Dev., 8, 2515–2551, https://doi.org/10.5194/gmd-8-2515-2015, 2015.

Maronga, B., Banzhaf, S., Burmeister, C., Esch, T., Forkel, R., Fröhlich, D., Fuka, V., Gehrke, K. F., Geletič, J., Giersch, S., Gronemeier, T., Groß, G., Heldens, W., Hellsten, A., Hoffmann, F., Inagaki, A., Kadasch, E., Kanani-Sühring, F., Ketelsen, K., Khan, B. A., Knigge, C., Knoop, H., Krč, P., Kurppa, M., Maamari, H., Matzarakis, A., Mauder, M., Pallasch, M., Pavlik, D., Pfafferott, J., Resler, J., Rissmann, S., Russo, E., Salim, M., Schrempf, M., Schwenkel, J., Seckmeyer, G., Schubert, S., Sühring, M., von Tils, R., Vollmer, L., Ward, S., Witha, B., Wurps, H., Zeidler, J., and Raasch, S.: Overview of the PALM model system 6.0, Geosci. Model Dev., 13, 1335–1372, https://doi.org/10.5194/gmd-13-1335-2020, 2020.

Michioka, T., Sato, A., and Sada, K.: Large-eddy simulation coupled to mesoscale meteorological model for gas dispersion in an urban district, Atmos. Environ., 75, 153–162, https://doi.org/10.1016/j.atmosenv.2013.04.017, 2013.

Miyakawa, T., Takegawa, N., and Kondo, Y.: Removal of sulfur dioxide and formation of sulfate aerosol in Tokyo, J. Geophys. Res.-Atmos., 112, https://doi.org/10.1029/2006JD007896, 2007.

Müller, M., Homleid, M., Ivarsson, K.-I., Køltzow, M. A. Ø., Lindskog, M., Midtbø, K. H., Andrae, U., Aspelien, T., Berggren, L., Bjørge, D., Dahlgren, P., Kristiansen, J., Randriamampianina, R., Ridal, M., and Vignes, O.: AROME-MetCoOp: A Nordic Convective-Scale Operational Weather Prediction Model, Weather Forecast., 32, 609–627, https://doi.org/10.1175/WAF-D-16-0099.1, 2017.

Nazarian, N., Martilli, A., and Kleissl, J.: Impacts of realistic urban heating, part I: spatial variability of mean flow, turbulent exchange and pollutant dispersion, Bound.-Lay. Meteorol., 166, 367–393, 2018.

Nikolova, I., MacKenzie, A. R., Cai, X., Alam, M. S., and Harrison, R. M.: Modelling component evaporation and composition change of traffic-induced ultrafine particles during travel from street canyon to urban background, Faraday Discuss., 189, 529–546, https://doi.org/10.1039/C5FD00164A, 2016.

Nordbo, A., Järvi, L., Haapanala, S., Moilanen, J., and Vesala, T.: Intra-City Variation in Urban Morphology and Turbulence Structure in Helsinki, Finland, Bound.-Lay. Meteorol., 146, 469–496, 2012.

Norwegian Meteorological Institute: File Interpolation, Manipulation and EXtraction library, last access: 12 June 2019, https://wiki.met.no/fimex/start, a.

Norwegian Meteorological Institute: MET Norway Thredds Service, last access: 12 June 2019, https://thredds.met.no/thredds/catalog.html, b.

Ntziachristos, L., Samaras, Z., Kouridis, C., Samaras, C., Hassel, D., Mellios, G., McCrae, I., Hickman, J., Zierock, K.-H., Keller, M., Rexeis, M., Andre, M., Winther, M., Pastramas, N., Gorissen, N., Boulter, P., Katsis, P., Joumard, R., Rijkeboer, R., Geivani-

dis, S., and Hausberger, S.: EMEP/EEA air pollutant emission inventory guidebook, PART B: 1.A.3.b.i-iv Road transport, last access: 18 Jun 2018, https://www.eea.europa.eu/publications/emep-eea-guidebook-2016/part-b-sectoral-guidance-chapters/1-energy/1-a-combustion/1-a-3-b-i/view, 2016.

Oberdörster, G., Oberdörster, E., and Oberdörster, J.: Nanotoxicology: An Emerging Discipline Evolving from Studies of Ultrafine Particles, Environ. Health Persp., 113, 823–839, https://doi.org/10.1289/ehp.7339, 2005.

Pirjola, L., Parviainen, H., Hussein, T., Valli, A., Hämeri, K., Aaalto, P., Virtanen, A., Keskinen, J., Pakkanen, T., Mäkelä, T., and Hillamo", R.: "Sniffer"—a novel tool for chasing vehicles and measuring traffic pollutants, Atmos. Environ., 38, 3625–3635, https://doi.org/10.1016/j.atmosenv.2004.03.047, 2004.

Pirjola, L., Dittrich, A., Niemi, J. V., Saarikoski, S., Timonen, H., Kuuluvainen, H., Järvinen, A., Kousa, A., Rönkkö, T., and Hillamo, R.: Physical and Chemical Characterization of Real-World Particle Number and Mass Emissions from City Buses in Finland, Environ. Sci. Tech., 50, 294–304, https://doi.org/10.1021/acs.est.5b04105, 2016.

Ramponi, R., Blocken, B., Laura, B., and Janssen, W. D.: CFD simulation of outdoor ventilation of generic urban configurations with different urban densities and equal and unequal street widths, Build. Environ., 92, 152–166, 2015.

Roldin, P., Swietlicki, E., Massling, A., Kristensson, A., Löndahl, J., Eriksson, A., Pagels, J., and Gustafsson, S.: Aerosol ageing in an urban plume – implication for climate, Atmos. Chem. Phys., 11, 5897–5915, https://doi.org/10.5194/acp-11-5897-2011, 2011a.

Roldin, P., Swietlicki, E., Schurgers, G., Arneth, A., Lehtinen, K. E. J., Boy, M., and Kulmala, M.: Development and evaluation of the aerosol dynamics and gas phase chemistry model ADCHEM, Atmos. Chem. Phys., 11, 5867–5896, https://doi.org/10.5194/acp-11-5867-2011, 2011b.

Roldin, P., Ehn, M., Kurtén, T., Olenius, T., Rissanen, M. P., Sarnela, N., Elm, J., Rantala, P., Hao, L., Hyttinen, N., et al.: The role of highly oxygenated organic molecules in the Boreal aerosol-cloud-climate system, Nat. Commun., 10, 1–15, 2019.

Salim, S. M., Buccolieri, R., Chan, A., and Sabatino, S. D.: Numerical simulation of atmospheric pollutant dispersion in an urban street canyon: Comparison between RANS and LES, J. Wind Eng. Ind. Aerod., 99, 103–113, https://doi.org/10.1016/j.jweia.2010.12.002, 2011.

Santiago, J., Sanchez, B., Quaassdorff, C., de la Paz, D., Martilli, A., Martín, F., Borge, R., Rivas, E., Gómez-Moreno, F., Díaz, E., et al.: Performance evaluation of a multiscale modelling system applied to particulate matter dispersion in a real traffic hot spot in Madrid (Spain), Atmos. Pollut. Res., 11, 141–155, 2020.

Saunders, S. M., Jenkin, M. E., Derwent, R. G., and Pilling, M. J.: Protocol for the development of the Master Chemical Mechanism, MCM v3 (Part A): tropospheric degradation of non-aromatic volatile organic compounds, Atmos. Chem. Phys., 3, 161–180, https://doi.org/10.5194/acp-3-161-2003, 2003.

Steffens, J. T., Heist, D. K., Perry, S. G., and Zhang, K. M.: Modeling the effects of a solid barrier on pollutant dispersion under various atmospheric stability conditions, Atmos. Environ., 69, 76–85, https://doi.org/10.1016/j.atmosenv.2012.11.051, 2013.

Stein, A. F., Draxler, R. R., Rolph, G. D., Stunder, B. J. B., Cohen, M. D., and Ngan, F.: NOAA's HYSPLIT Atmospheric Transport and Dispersion Modeling System, B. Am. Meteorol. Soc., 96, 2059–2077, https://doi.org/10.1175/BAMS-D-14-00110.1, 2015.

Tominaga, Y. and Stathopoulos, T.: CFD simulation of near-field pollutant dispersion in the urban environment: A review of current modeling techniques, Atmos. Environ., 79, 716–730, https://doi.org/10.1016/j.atmosenv.2013.07.028, 2013.

UN: World Urbanization Prospects: The 2018 Revision (ST/ESA/SER.A/420), 2019.

Urban Environment Division of the City of Helsinki, Helsinki Region Environmental Services Authority and Helsinki Region Municipalities: Traffic volumes in Helsinki 2017, map (in Finnish), last access: 18 Jun 2018, https://www.hel.fi/static/liitteet/kaupunkiymparisto/liikenne-ja-kartat/kadut/liikennetilastot/autoliikenne/Autoliikennekartta.pdf, 2018.

VTT: LIPASTO unit emissions -database: Fuel properties, last access: 30 Nov 2018, http://lipasto.vtt.fi/yksikkopaastot/tunnusluvut/tunnusluvuttiee.htm, 2017.

VTT: ALIISA model (in Finnish), last access: 30 Nov 2018, http://lipasto.vtt.fi/aliisa/suoritejakaumat.htm, 2018.

WHO: Ambient air pollution: A global assessment of exposure and burden of disease, 2016.

Wicker, L. and Skamarock, W.: Time-splitting methods for elastic models using forward time schemes, Mon. Weather Rev., 130, 2088–2097, 2002.

Williamson, J. H.: Low-Storage Runge-Kutta Schemes, J. Comput. Phys., 35, 48–56, https://doi.org/10.1016/0021-9991(80)90033-9, 1980.

Wood, C. R., Järvi, L., Kouznetsov, R. D., Nordbo, A., Joffre, S., Drebs, A., Vihma, T., Hirsikko, A., Suomi, I., Fortelius, C., O'Connor, E., Moiseev, D., Haapanala, S., Moilanen, J., Kangas, M., Karppinen, A., Vesala, T., and Kukkonen, J.: An Overview of the Urban Boundary Layer Atmosphere Network in Helsinki, B. Am. Meteorol. Soc., 94, 1675–1690, https://doi.org/10.1175/BAMS-D-12-00146.1, 2013.

Wyszogrodzki, A. A., Miao, S., and Chen, F.: Evaluation of the coupling between mesoscale-WRF and LES-EULAG models for simulating fine-scale urban dispersion, Atmos. Res., 118, 324–345, https://doi.org/10.1016/j.atmosres.2012.07.023, 2012.

Xie, Z.-T. and Castro, I. P.: LES and RANS for turbulent flow over arrays of wall-mounted obstacles, Flow Turbul. Combust., 76, 291–312, https://doi.org/10.1007/s10494-006-9018-6, 2006.

Yu, S., Eder, B., Dennis, R., Chu, S.-H., and Schwartz, S. E.: New unbiased symmetric metrics for evaluation of air quality models, Atmos. Sci. Lett., 7, 26–34, https://doi.org/10.1002/asl.125, 2006.

Zhao, Y., Saleh, R., Saliba, G., Presto, A. A., Gordon, T. D., Drozd, G. T., Goldstein, A. H., Donahue, N. M., and Robinson, A. L.: Reducing secondary organic aerosol formation from gasoline vehicle exhaust, P. Natl. Acad. Sci., 114, 6984–6989, https://doi.org/10.1073/pnas.1620911114, 2017.

Zhong, J., Nikolova, I., Cai, X., MacKenzie, A. R., Alam, M. S., Xu, R., Singh, A., and Harrison, R. M.: Traffic-induced multicomponent ultrafine particle microphysics in the WRF v3.6.1 large eddy simulation model: General behaviour from idealised scenarios at the neighbourhood-scale, Atmos. Environ., 223, 117 213, https://doi.org/10.1016/j.atmosenv.2019.117213, 2020.

Contents

S2 Measurements

Table S1. Instrumentation. Abbreviations: PSD = aerosol particle size distribution, BC = black carbon, $\mathrm{PM}_{2.5}$ = particulate matter with aerodynamic diameter < 2.5 µm, LDSA = lung-deposited surface area.

Site	Variable	Instrument
Supersite	PSD (size range 6–800 nm)	Differential mobility particle sizer (DMPS: A20 CPC, Airmodus & Vienna-type Differential Mobility Analyzer (DMA))
	Aerosol chemical composition ($\mathrm{SO_4^-}$, OC, $\mathrm{NO_3^-}$, $\mathrm{NH_4^+}$, 40–600 nm)	Aerosol Chemical Speciation Monitor (ACSM, Aerodyne Research)
	BC (< 1 µm)	Multi-angle Absorption Photometer (MAAP 5012, Thermo Scientific Inc.)
	$\mathrm{PM}_{2.5}$	Tapered element oscillating microbalance (TEOM 1405, Thermo Scientific Inc.)
SMEAR III	PSD (6–800 nm)	Differential mobility particle sizer (DMPS: A20 CPC, Airmodus & Vienna-type Differential Mobility Analyzer (DMA))
	LDSA	AQ Urban (Pegasor Oy)
	Wind speed and direction	3D ultrasonic anemometer (Metek USA-1, Metek GmbH)
	Air temperature	3D ultrasonic anemometer (Metek USA-1, Metek GmbH)
Kallio	LDSA	AQ Urban (Pegasor Oy)

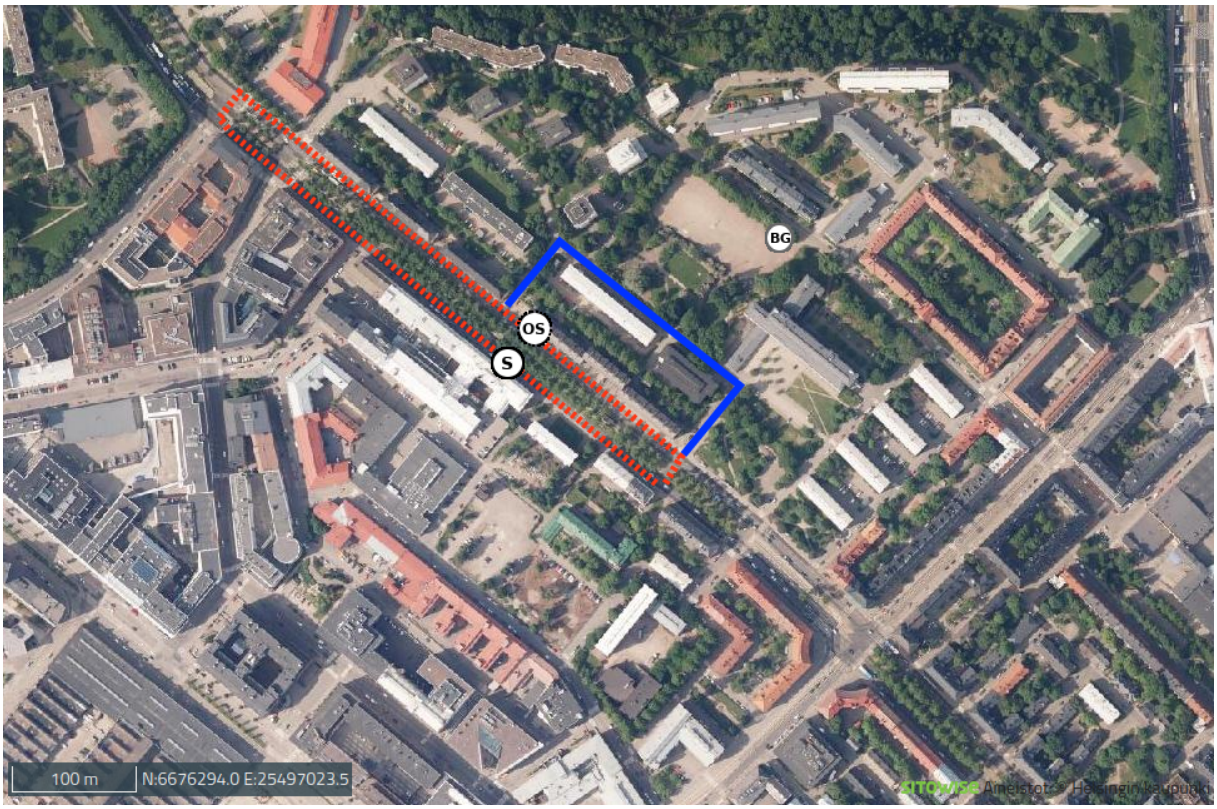

Figure S1. The Sniffer route: main street with a red dotted line and the side street with a blue solid line. Stationary measurement points: S = supersite, OS = opposite the supersite, BG = background. Map from https://kartta.hel.fi.

S3 Simulations

S3.1 Model description

The chemical mechanism `salsa+simple` found in the palm repository (https://palm.muk.uni-hannover.de/trac/browser/palm/trunk/UTIL/chemistry/gasphase_preproc/mechanisms/def_salsa%2Bsimple?rev=4416).

$$NO_2 + h\nu = NO + O_3 \quad \text{(R1)}$$

$$O_3 + H_2O = 2OH \quad \text{(R2)}$$

$$NO + O_3 = NO_2 \quad \text{(R3)}$$

$$RH + OH = RO_2 + H_2O \quad \text{(R4)}$$

$$RO_2 + NO = NO_2 + RCHO + HO_2 \quad \text{(R5)}$$

$$HO_2 + NO = NO_2 + OH \quad \text{(R6)}$$

$$NO_2 + OH = HNO_3 \quad \text{(R7)}$$

S3.4 Air pollutant background concentrations

The trace gas emissions along the ADCHEM trajectories are taken from the Copernicus Atmosphere Monitoring Service global and regional emissions (Granier et al., 2019). For the anthropogenic emissions of carbon monoxide (CO), non-methane volatile organic compounds (NMVOC), nitrous oxides ($\mathrm{NO_x}$), sulphur dioxide ($\mathrm{SO_2}$) and $\mathrm{NH_3}$ we use the CAMS-REG-v3.1 emission inventory for year 2015, which groups the air pollution emissions into 15 emission-type sectors. The spatial resolution is $0.05^\circ \times 0.1^\circ$. Over Finland the anthropogenic trace gas emissions are taken from an emission inventory provided by the Finnish Environment Institute (SYKE), which has been derived with the Finnish Regional Emission Scenario model FRES (Karvosenoja, 2008) and has a spatial resolution of $250\ \mathrm{m} \times 250\ \mathrm{m}$. From Finnish power plants and industry, emissions were provided as point sources. The anthropogenic primary particle emissions, apart those from road traffic, are estimated using the size-resolved primary particle emission inventory from Paasonen et al. (2016) with a spatial resolution of $0.5^\circ \times 0.5^\circ$. For the road traffic, primary particle emissions are estimated using the $\mathrm{NO_x}$ emissions from the road traffic and the temperature dependent road traffic exhaust emission factors derived from measurements in Helsinki (Ripamonti et al., 2013). In order to scale the road traffic exhaust particle emissions based on the $\mathrm{NO_x}$ emission factors an approximate $\mathrm{NO_x}$ emission factor of $1.0 \times 10^{-3}\ \mathrm{g\,vehicle^{-1}\,m^{-1}}$ was applied. This factor is estimated based on the $\mathrm{NO_x}$ vehicle emission factors reported at an urban street in Copenhagen ($0.93 \times 10^{-3}\ \mathrm{g\,vehicle^{-1}\,m^{-1}}$) and at a highway in Denmark ($1.4 \times 10^{-3}\ \mathrm{g\,vehicle^{-1}\,m^{-1}}$) (Wang et al., 2010). The characteristic size-resolved road traffic primary particle emission distribution is taken from Kristensson et al. (2004). Primary particle emissions from ships traffic is parameterized based on the $\mathrm{SO_2}$ emissions (Roldin et al., 2019). All anthropogenic emissions are corrected using monthly, weekly and hourly time profiles originally developed for the LOTOS-EUROS model (Schaap et al., 2008).

The size resolved marine sea-spray primary particle emissions are calculated using the parameterization from Mårtensson et al. (2003). The dimethyl sulphide emissions are considered using the daily CAMS-OCE global oceanic emissions with a spatial resolution of $0.5^\circ \times 0.5^\circ$ (Lana et al., 2011). Global soil $\mathrm{NO_x}$ emissions are taken from $0.5^\circ \times 0.5^\circ$ resolution, monthly emission files for year 2015 (Simpson et al., 2014). The biogenic VOC emissions are modelled using a one-dimensional version of MEGAN 2.04 (Model of Emissions of Gases and Aerosols from Nature Guenther et al., 2006), which has been implemented into ADCHEM (Roldin et al., 2019).

S3.4.1 9 Jun 2017

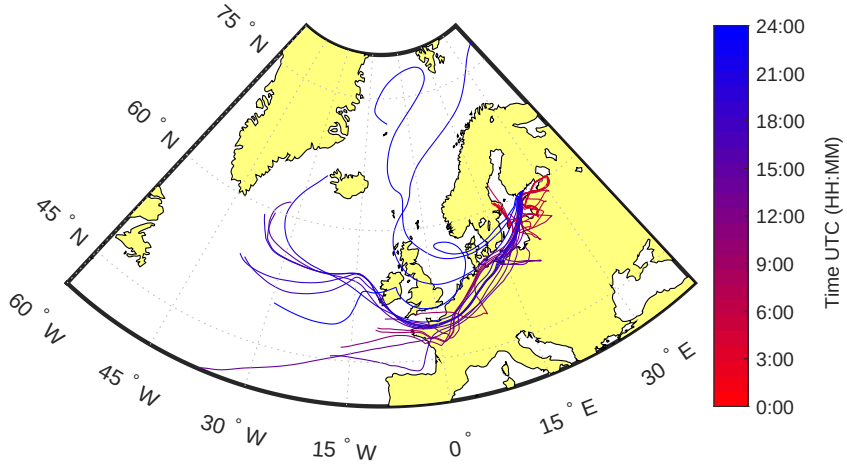

Figure S2. HYSPLIT seven-days-long back trajectories arriving to the supersite on 9 Jun 2017 from 00:00 UTC to 24:00 UTC

S3.4.2 12 Dec 2017

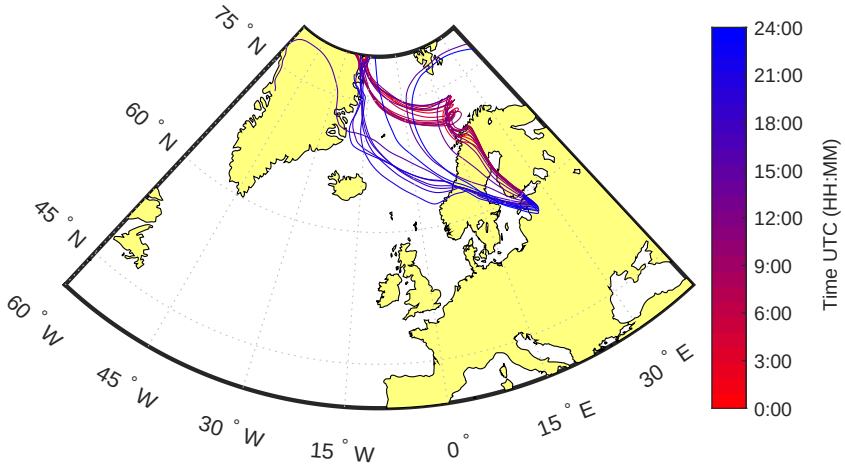

Figure S3. HYSPLIT seven-days-long back trajectories arriving to the supersite on 12 Dec 2017 from 00:00 UTC to 24:00 UTC

S3.5 Air pollutant emissions

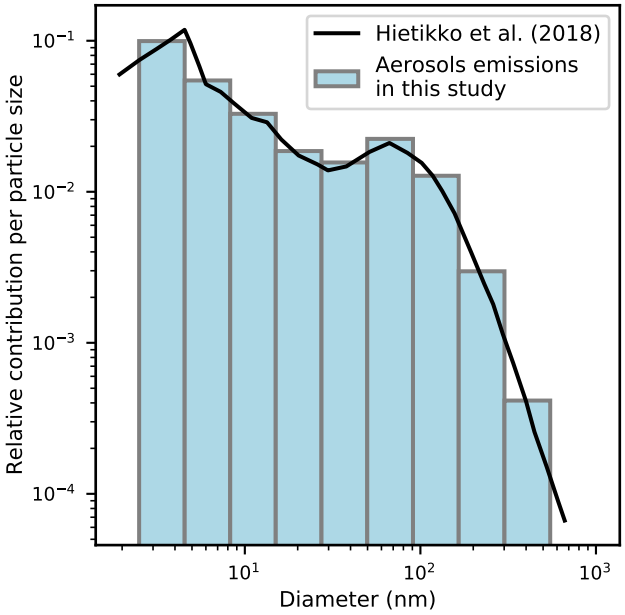

Figure S4. Relative contribution to the aerosol size distribution per particle size for Hietikko et al. (2018) and the traffic-combustion-related aerosol emission applied in this study.

S4 Comparison of the modelled and observed boundary conditions

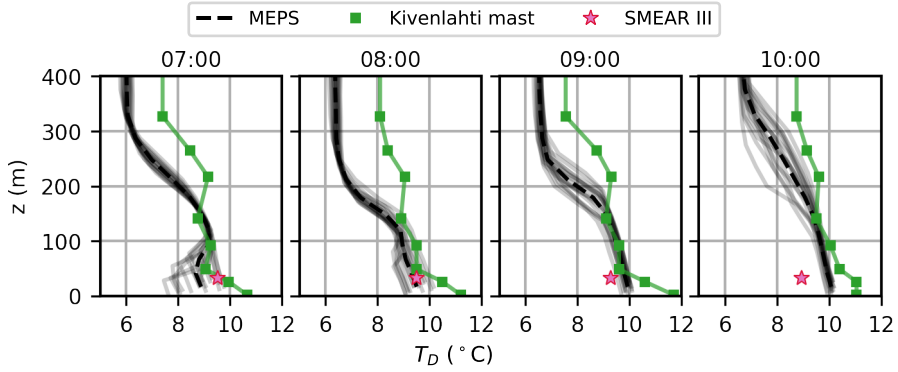

Figure S5. Dew-point temperature T_D (°C) on 9 Jun at local time (UTC+3). The modelled profiles at each MEPS grid point are shown by grey solid lines and their mean by a black dashed line. The observation from the Kivenlahti mast are shown by green solid squares and the interpolated profiles used as boundary conditions by a green solid line. Stars show the SMEAR III observations.

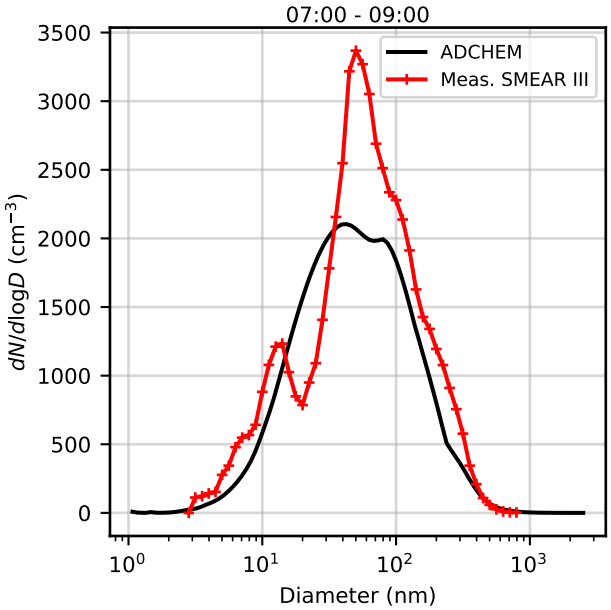

Figure S6. Mean modelled (black solid line) and measured aerosol size distribution at the SMEAR station (red line with crosses) on 9 Jun 2017 between 07:00-10:00 local time~~from 00:00 UTC to 24:00 UTC~~. Modelled values are from ADCHEM for a trajectory arriving in Helsinki (60°12'N, 24°57'E).

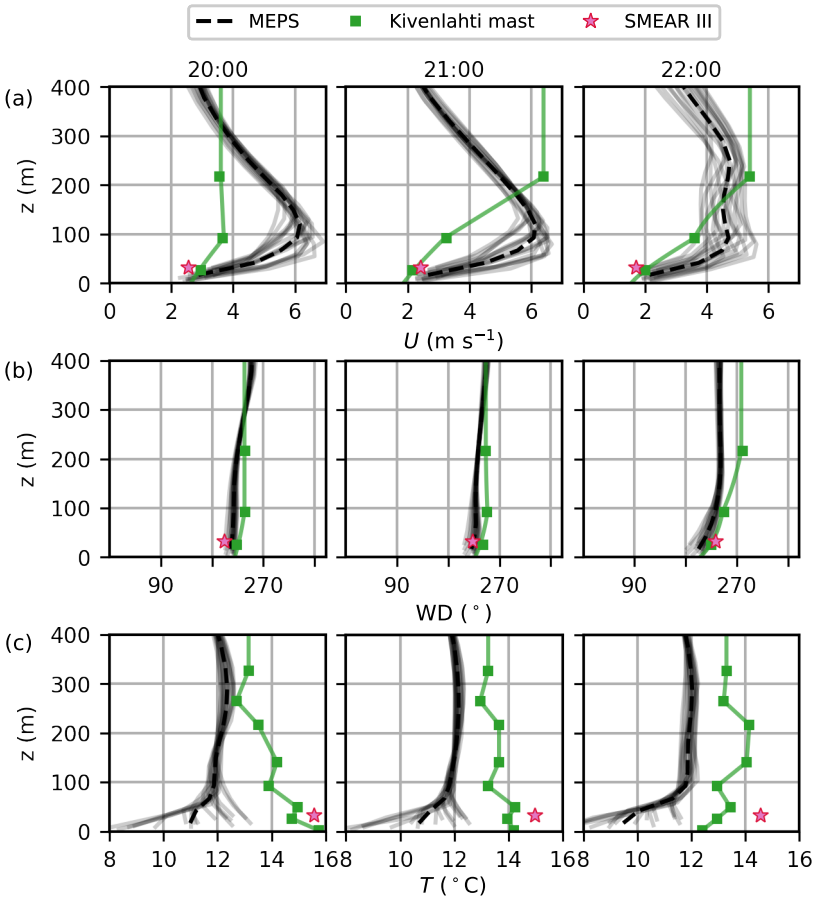

Figure S7. Horizontal a) wind speed U ($\mathrm{m\,s^{-1}}$, b) wind direction WD (°) and c) air temperature T °C) on 9 Jun at local time (UTC+3). See Fig. S5 caption for details.

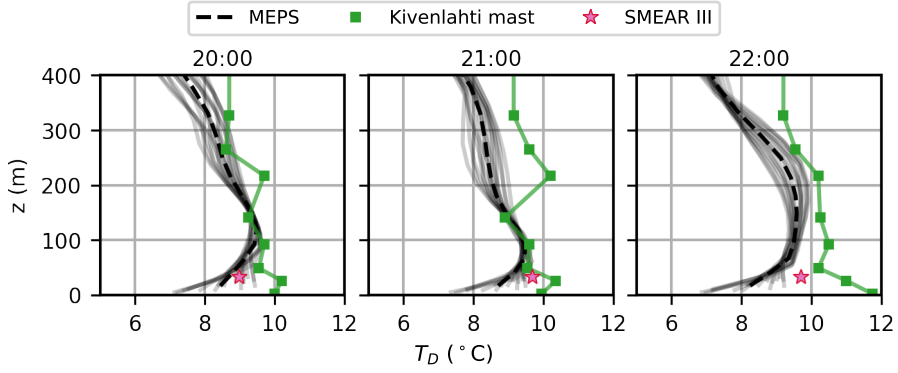

Figure S8. Dew-point temperature T_D (°C) on 9 Jun at local time (UTC+3). See Fig. S5 for details.

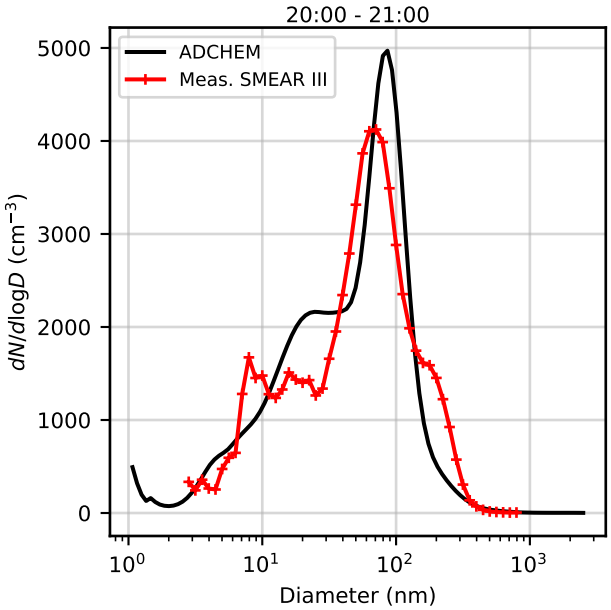

Figure S9. Mean modelled (black solid line) and measured aerosol size distribution at the SMEAR station (red line with crosses) on 9 Jun 2017 between 20:00-22:00 local time. Modelled values are from ADCHEM for a trajectory arriving in Helsinki (60°12'N, 24°57'E).

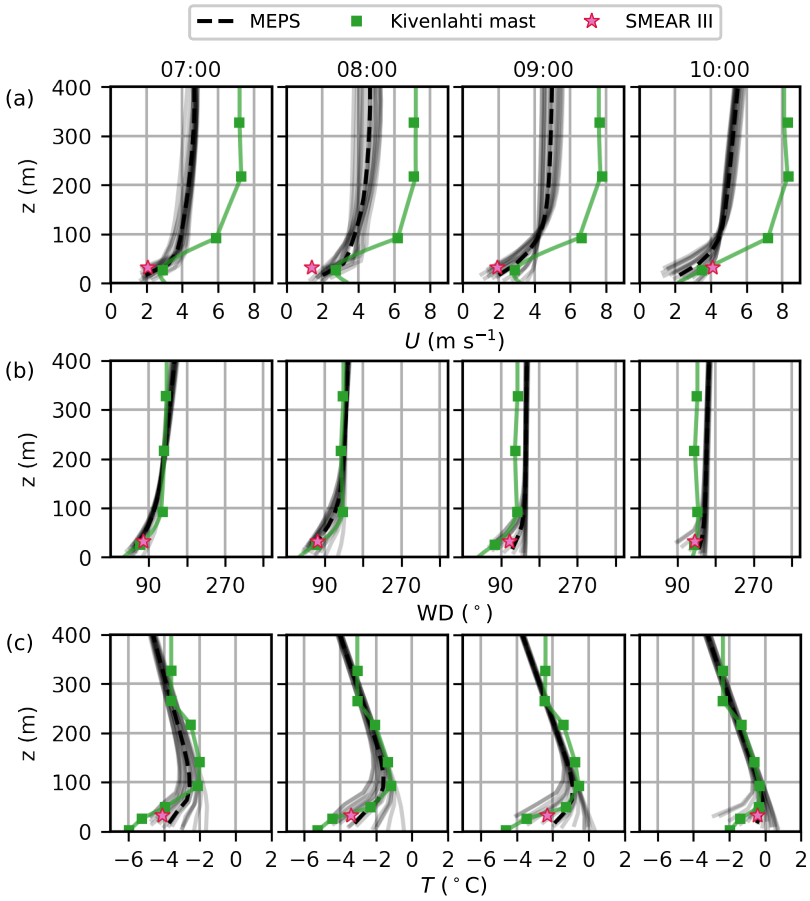

Figure S10. Horizontal a) wind speed U ($\mathrm{m\,s^{-1}}$, b) wind direction WD (°) and c) air temperature T °C) on 12 Dec at local time (UTC+3). See Fig. S5 caption for details.

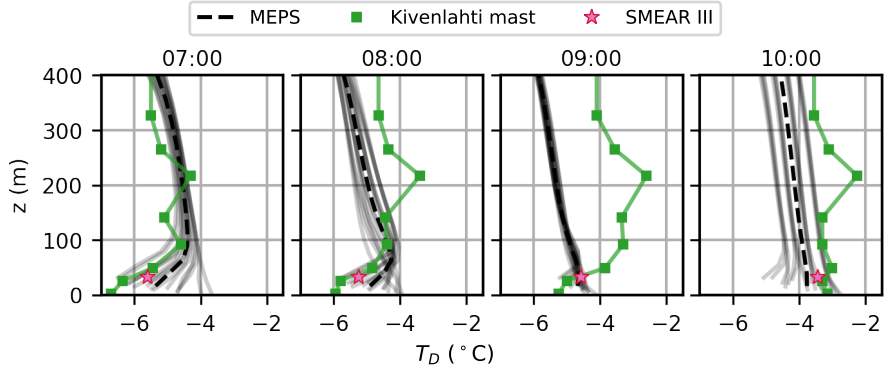

Figure S11. Dew-point temperature T_D (°C) on 12 Dec at local time (UTC+2). See Fig. S5 for details.

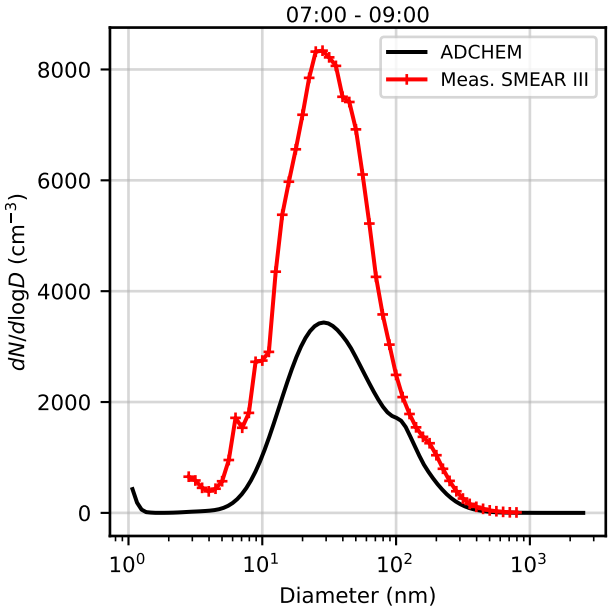

Figure S12. Mean modelled (black solid line) and measured aerosol size distribution at the SMEAR station (red line with crosses) on 12 Dec 2017 between 07:00-10:00 local time~~from 00:00 UTC to 24:00 UTC~~. Modelled values are from ADCHEM for a trajectory arriving in Helsinki (60°12'N, 24°57'E).

S5 Evaluation of the air quality modelling results

S5.2 Horizontal distribution of total aerosol particle number concentration

Table S2. Significance of differences in the model absolute error (i.e., the difference between the modelled and observed values) compared to $\mathrm{M_{MET}M_{PSD}}$ based on Student's t-test for the means of two independent samples.

Simulation time	Simulation name	Significantly different?	p-value
9 Jun, 07:16–08:14	$\mathrm{O_{MET}O_{PSD}}$	–*	–
	$\mathrm{M_{MET}O_{PSD}}$	–*	–
	$\mathrm{O_{WD,mast}O_{PSD}}$	–*	–
	$\mathrm{O_{WD,SMEAR}O_{PSD}}$	No	0.039
9 Jun, 08:23–09:15	$\mathrm{O_{MET}O_{PSD}}$	Yes	0.80
	$\mathrm{M_{MET}O_{PSD}}$	Yes	0.92
	$\mathrm{O_{WD,mast}O_{PSD}}$	Yes	0.39
	$\mathrm{O_{WD,SMEAR}O_{PSD}}$	–*	–
9 Jun, 20:26–21:14	$\mathrm{O_{MET}O_{PSD}}$	Yes	0.34
12 Dec, 07:20–08:08	$\mathrm{O_{MET}O_{PSD}}$	No	2×10^{-11}
12 Dec, 08:14–09:14	$\mathrm{O_{MET}O_{PSD}}$	–*	–

*: Variances are not homogeneous according to a Levene's test and a Student's t-test cannot be performed

Table S3. Model performance for the aerosol size distribution for $M_{MET}M_{PSD}$ on 9 Jun morning. Performance measures: fractional bias (FB), normalised mean squared error (NMSE), factor of two (FAC2), normalised mean bias factor (NMBF) and normalised mean absolute error factor (NMAEF). Colours indicate whether the value fits (blue) or not (red) within the criteria in Table 6.

Time	Measure	Instrument	Background	Side street	Main street	Opposite supersite	Supersite
07:20–08:08	FB	EEPS	0.04	-0.85	0.23	–	0.36
		ELPI	-0.26	-1.32	-0.05	–	0.20
	NMSE	EEPS	3.12	3.30	1.61	–	1.06
		ELPI	1.49	6.76	1.16	–	0.72
	FAC2	EEPS	0.50	0.12	0.50	–	0.50
		ELPI	0.38	0.00	0.75	–	0.62
	NMBF	EEPS	0.89	-2.45	0.40	–	0.27
		ELPI	0.06	-4.58	0.08	–	0.14
	NMAEF	EEPS	1.24	2.63	0.88	–	0.78
		ELPI	0.86	4.58	0.62	–	0.57
08:14–09:14	FB	EEPS	–	-0.75	0.44	0.15	0.78
		ELPI	–	-1.21	0.25	0.00	0.47
	NMSE	EEPS	–	2.44	11.09	4.91	15.64
		ELPI	–	4.23	7.05	3.82	9.16
	FAC2	EEPS	–	0.12	0.25	0.50	0.38
		ELPI	–	0.12	0.50	0.62	0.62
	NMBF	EEPS	–	-1.51	2.34	0.84	4.09
		ELPI	–	-2.99	1.33	0.42	2.33
	NMAEF	EEPS	–	2.04	2.76	1.34	4.15
		ELPI	–	2.99	1.91	1.24	2.60

S5.4 Aerosol size distribution

Table S4. Model performance for the aerosol size distribution for $O_{MET}O_{PSD}$ on 9 Jun morning. See Table S3 for further description.

Time	Measure	Instrument	Background	Side street	Main street	Opposite supersite	Supersite
07:20–08:08	FB	EEPS	0.07	-0.64	0.46	–	0.21
		ELPI	-0.42	-1.12	0.23	–	0.11
	NMSE	EEPS	0.19	2.25	10.32	–	5.44
		ELPI	0.86	3.44	7.74	–	4.66
	FAC2	EEPS	0.62	0.00	0.12	–	0.38
		ELPI	0.50	0.25	0.25	–	0.38
	NMBF	EEPS	0.07	-1.11	2.11	–	0.64
		ELPI	-0.68	-2.38	1.42	–	0.50
	NMAEF	EEPS	0.39	1.80	2.69	–	1.64
		ELPI	0.81	2.38	2.13	–	1.52
08:14–09:14	FB	EEPS	–	-0.68	0.45	0.57	0.13
		ELPI	–	-1.14	0.17	0.38	-0.27
	NMSE	EEPS	–	2.33	11.53	9.65	3.09
		ELPI	–	3.86	7.39	7.09	1.68
	FAC2	EEPS	–	0.12	0.25	0.12	0.50
		ELPI	–	0.25	0.38	0.38	0.62
	NMBF	EEPS	–	-1.33	2.42	2.50	0.65
		ELPI	–	-2.69	1.38	1.69	0.08
	NMAEF	EEPS	–	1.92	2.85	2.86	1.05
		ELPI	–	2.69	2.02	2.18	0.77

Table S5. Model performance for the aerosol size distribution for $M_{MET}O_{PSD}$ on 9 Jun morning. See Table S3 for further description.

Time	Measure	Instrument	Background	Side street	Main street	Opposite supersite	Supersite
07:20–08:08	FB	EEPS	0.27	-0.75	0.27	–	0.40
		ELPI	-0.12	-1.24	-0.10	–	0.16
	NMSE	EEPS	3.58	2.90	1.52	–	1.00
		ELPI	1.62	6.06	1.10	–	0.68
	FAC2	EEPS	0.50	0.12	0.50	–	0.38
		ELPI	0.38	0.12	0.62	–	0.62
	NMBF	EEPS	1.14	-2.16	0.40	–	0.28
		ELPI	0.20	-4.11	0.08	–	0.15
	NMAEF	EEPS	1.41	2.35	0.86	–	0.78
		ELPI	0.88	4.11	0.61	–	0.57
08:14–09:14	FB	EEPS	–	-0.67	0.46	0.20	0.81
		ELPI	–	-1.14	0.17	-0.04	0.41
	NMSE	EEPS	–	2.27	11.00	4.83	15.45
		ELPI	–	3.94	7.00	3.77	9.05
	FAC2	EEPS	–	0.12	0.25	0.38	0.12
		ELPI	–	0.25	0.38	0.50	0.38
	NMBF	EEPS	–	-1.37	2.35	0.87	4.15
		ELPI	–	-2.77	1.34	0.44	2.37
	NMAEF	EEPS	–	1.91	2.78	1.35	4.21
		ELPI	–	2.77	1.93	1.26	2.64

Table S6. Model performance for the aerosol size distribution for $O_{WD,mast}O_{PSD}$ on 9 Jun morning. See Table S3 for further description.

Time	Measure	Instrument	Background	Side street	Main street	Opposite supersite	Supersite
07:20–08:08	FB	EEPS	0.20	-0.73	0.44	–	0.27
		ELPI	-0.22	-1.21	0.19	–	0.18
	NMSE	EEPS	1.56	2.62	8.49	–	6.31
		ELPI	0.89	5.23	6.32	–	5.39
	FAC2	EEPS	0.50	0.12	0.25	–	0.38
		ELPI	0.50	0.25	0.38	–	0.38
	NMBF	EEPS	0.70	-1.86	1.78	–	0.88
		ELPI	-0.05	-3.59	1.17	–	0.72
	NMAEF	EEPS	0.96	2.17	2.35	–	1.82
		ELPI	0.71	3.59	1.82	–	1.68
08:14–09:14	FB	EEPS	–	-0.62	0.51	0.58	0.18
		ELPI	–	-1.07	0.21	0.33	-0.34
	NMSE	EEPS	–	2.31	10.85	6.77	1.41
		ELPI	–	2.89	6.88	4.90	0.87
	FAC2	EEPS	–	0.00	0.12	0.25	0.62
		ELPI	–	0.25	0.38	0.50	0.62
	NMBF	EEPS	–	-0.85	2.43	1.94	0.31
		ELPI	–	-1.93	1.39	1.26	-0.19
	NMAEF	EEPS	–	1.59	2.83	2.25	0.68
		ELPI	–	1.93	1.92	1.71	0.65

Table S7. Model performance for the aerosol size distribution for $O_{WD,SMEAR}O_{PSD}$ on 9 Jun morning. See Table S3 for further description.

Time	Measure	Instrument	Background	Side street	Main street	Opposite supersite	Supersite
07:20–08:08	FB	EEPS	0.21	-0.68	0.40	–	0.57
		ELPI	-0.14	-1.15	0.13	–	0.50
	NMSE	EEPS	4.24	2.29	6.44	–	12.04
		ELPI	1.97	4.31	4.76	–	10.53
	FAC2	EEPS	0.50	0.12	0.38	–	0.12
		ELPI	0.38	0.25	0.38	–	0.38
	NMBF	EEPS	1.27	-1.48	1.40	–	2.35
		ELPI	0.26	-2.98	0.87	–	2.08
	NMAEF	EEPS	1.56	1.94	1.95	–	3.08
		ELPI	1.00	2.98	1.50	–	2.73
08:14–09:14	FB	EEPS	–	-0.65	0.66	0.21	1.132
		ELPI	–	-1.12	0.35	-0.02	0.72
	NMSE	EEPS	–	2.19	13.25	5.08	34.93
		ELPI	–	3.73	8.46	3.99	21.75
	FAC2	EEPS	–	0.12	0.25	0.38	0.25
		ELPI	–	0.25	0.25	0.50	0.38
	NMBF	EEPS	–	-1.28	3.15	0.89	8.49
		ELPI	–	-2.62	1.89	0.45	5.21
	NMAEF	EEPS	–	1.85	3.47	1.44	8.50
		ELPI	–	2.62	2.24	1.32	5.35

Table S8. Model performance for the aerosol size distribution for $M_{MET}M_{PSD}$ on 9 Jun evening. See Table S3 for further description.

Time	Measure	Instrument	Background	Side street	Main street	Opposite supersite	Supersite
20:26–21:14	FB	EEPS	-0.70	-0.54	0.26	-0.10	1.02
		ELPI	-0.58	-0.75	-0.15	-0.16	1.20
	NMSE	EEPS	0.70	1.24	0.54	0.46	7.61
		ELPI	1.77	1.78	0.14	0.70	18.96
	FAC2	EEPS	0.50	0.38	0.62	0.38	0.25
		ELPI	0.38	0.38	0.88	0.38	0.12
	NMBF	EEPS	-0.60	-1.00	0.28	-0.17	3.63
		ELPI	-0.96	-1.38	-0.05	-0.11	8.89
	NMAEF	EEPS	0.85	1.11	0.54	0.62	3.69
		ELPI	1.24	1.46	0.27	0.60	8.89

Table S9. Model performance for the aerosol size distribution for $O_{MET}O_{PSD}$ on 9 Jun evening. See Table S3 for further description.

Time	Measure	Instrument	Background	Side street	Main street	Opposite supersite	Supersite
20:26–21:14	FB	EEPS	-0.15	-0.37	0.34	0.51	1.03
		ELPI	-0.25	-0.72	-0.21	0.26	1.01
	NMSE	EEPS	0.48	1.01	0.42	1.17	4.57
		ELPI	0.78	1.59	0.07	1.27	12.56
	FAC2	EEPS	0.50	0.50	0.75	0.50	0.25
		ELPI	0.75	0.50	0.88	0.62	0.25
	NMBF	EEPS	-0.01	-0.97	0.27	0.73	2.68
		ELPI	-0.24	-1.35	0.08	0.82	6.72
	NMAEF	EEPS	0.45	1.01	0.45	0.92	2.68
		ELPI	0.49	1.35	0.16	1.02	6.72

Table S10. Model performance for the aerosol size distribution for $M_{MET}M_{PSD}$ on 7 Dec morning. See Table S3 for further description.

Time	Measure	Instrument	Background	Side street	Main street	Opposite supersite	Supersite
07:20–08:08	FB	EEPS	-0.02	-0.65	0.27	–	-0.34
		ELPI	-0.02	-0.83	-0.02	–	-0.54
	NMSE	EEPS	0.64	2.71	3.08	–	1.70
		ELPI	1.56	3.38	4.58	–	1.41
	FAC2	EEPS	0.62	0.38	0.12	–	0.50
		ELPI	0.62	0.38	0.25	–	0.38
	NMBF	EEPS	0.17	-1.93	0.27	–	-1.04
		ELPI	0.53	-1.45	0.79	–	-0.33
	NMAEF	EEPS	0.58	1.95	1.23	–	1.28
		ELPI	0.82	1.91	1.51	–	0.93
08:14–09:14	FB	EEPS	-0.82	-0.64	0.03	-0.63	-0.28
		ELPI	-1.05	-0.87	-0.23	-1.02	-0.47
	NMSE	EEPS	1.93	2.70	5.21	8.61	3.13
		ELPI	2.49	3.96	7.78	8.42	3.37
	FAC2	EEPS	0.25	0.38	0.25	0.25	0.38
		ELPI	0.12	0.25	0.38	0.25	0.50
	NMBF	EEPS	-1.69	-1.67	0.36	-3.97	-0.86
		ELPI	-1.30	-1.26	0.97	-2.92	-0.22
	NMAEF	EEPS	1.70	1.68	1.51	3.98	1.64
		ELPI	1.82	2.01	1.98	3.11	1.25

Table S11. Model performance for the aerosol size distribution for $O_{MET}O_{PSD}$ on 7 Dec. See Table S3 for further description.

Time	Measure	Instrument	Background	Side street	Main street	Opposite supersite	Supersite
07:20–08:08	FB	EEPS	0.67	0.05	0.31	–	0.33
		ELPI	0.46	-0.23	0.04	–	0.12
	NMSE	EEPS	4.30	0.85	5.90	–	3.89
		ELPI	6.84	1.62	8.84	–	7.04
	FAC2	EEPS	0.38	0.50	0.00	–	0.25
		ELPI	0.50	0.62	0.25	–	0.50
	NMBF	EEPS	2.05	0.11	0.74	–	0.76
		ELPI	2.98	0.33	1.45	–	1.73
	NMAEF	EEPS	2.12	0.60	1.81	–	1.40
		ELPI	3.03	0.81	2.32	–	2.05
08:14–09:14	FB	EEPS	0.08	0.02	0.38	0.16	0.16
		ELPI	-0.42	-0.38	0.15	-0.12	-0.09
	NMSE	EEPS	0.42	0.15	10.69	4.06	1.38
		ELPI	0.38	0.48	16.27	6.92	1.84
	FAC2	EEPS	0.75	0.62	0.25	0.12	0.38
		ELPI	0.62	0.50	0.38	0.12	0.50
	NMBF	EEPS	0.04	-0.17	1.75	0.23	-0.06
		ELPI	0.20	-0.01	2.97	0.56	0.44
	NMAEF	EEPS	0.38	0.25	2.67	1.41	0.74
		ELPI	0.45	0.41	3.66	1.92	0.88

S5.5 Aerosol chemical composition

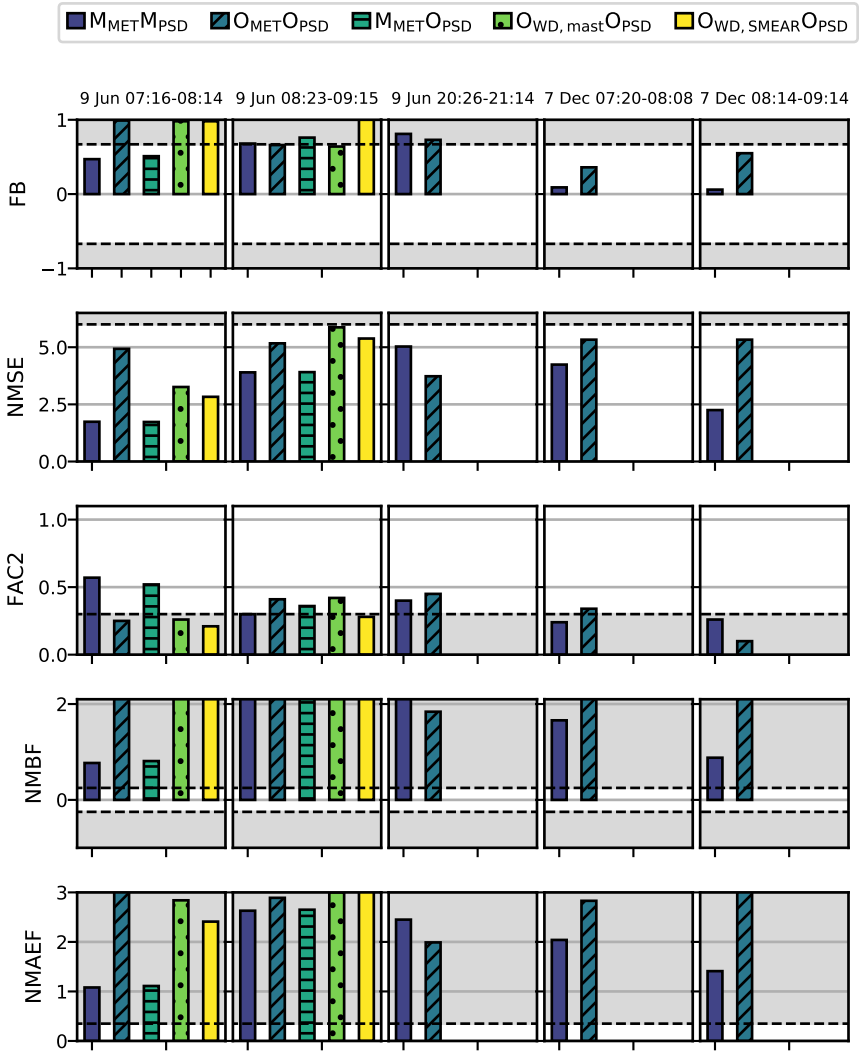

Figure S13. Model performance for the horizontal distribution of BC. See Table S3 for further description.

Table S12. Performance of the modelled~~in the modelling~~ aerosol chemical composition at the supersite on 9 Jun evening between 20:26–21:14. See Table S3 for further description.

Simulation name	Variable	FB	NMSE	FAC2	NMBF	NMAEF
$M_{MET}M_{PSD}$	SO_4^-	0.44	0.21	1.00	0.57	0.57
	OC	-0.29	0.11	1.00	-0.34	0.34
	NO_3^-	1.09	1.69	0.00	2.39	2.39
	NH_4^+	1.20	2.49	0.00	3.12	3.12
	BC	1.17	2.18	0.00	2.85	2.85
	$PM_{2.5}$	0.38	0.17	1.00	0.47	0.47
$O_{MET}O_{PSD}$	SO_4^-	0.81	0.78	0.00	1.36	1.36
	OC	0.13	0.02	1.00	0.13	0.13
	NO_3^-	1.27	2.73	0.00	3.51	3.51
	NH_4^+	1.58	6.79	0.00	7.55	7.55
	BC	1.48	4.89	0.00	5.70	5.70
	$PM_{2.5}$	0.83	0.85	0.00	1.42	1.42

Table S13. Performance of the modelled~~in the modelling~~ aerosol chemical composition at the supersite on 12 Dec morning between 07:20–09:14. See Table S3 for further description.

Simulation name	Variable	FB	NMSE	FAC2	NMBF	NMAEF
$M_{MET}M_{PSD}$	SO_4^-	1.21	2.59	0.00	3.18	3.18
	OC	-0.41	0.20	1.00	-0.52	0.52
	NO_3^-	1.13	1.89	0.00	2.60	2.60
	NH_4^+	1.40	5.75	0.00	5.48	5.48
	BC	0.87	1.37	0.33	1.71	1.71
	$PM_{2.5}$	0.54	0.41	0.67	0.78	0.78
$O_{MET}O_{PSD}$	SO_4^-	1.84	21.50	0.00	22.21	22.21
	OC	0.72	0.58	0.50	1.06	1.06
	NO_3^-	0.87	1.03	0.17	1.57	1.57
	NH_4^+	1.63	7.46	0.00	7.62	7.62
	BC	0.11	0.22	0.67	0.20	0.46
	$PM_{2.5}$	0.88	1.04	0.50	1.52	1.52

S6 Sensitivity analysis

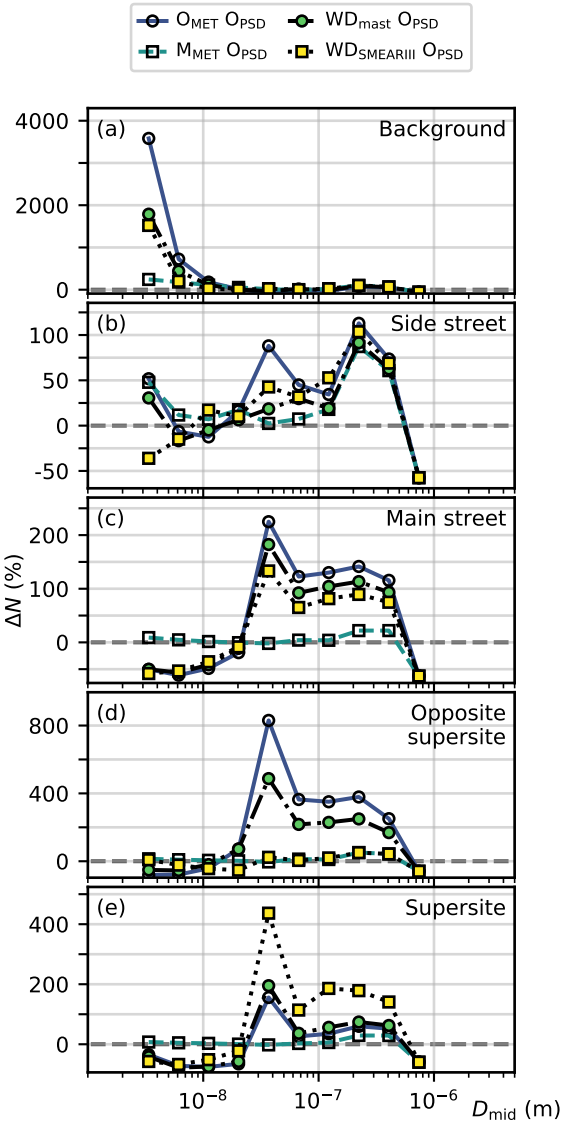

Figure S14. Relative difference in the aerosol number concentration ΔN (%) compared to $\mathrm{M_{MET}M_{PSD}}$ to as a function of aerosol particle diameter D_{mid} (nm) at $z = 1.5$ m on 9 Jun at 07:16–08:14. The figure shows the difference for $\mathrm{O_{MET}O_{PSD}}$ (solid line with empty circles), $\mathrm{M_{MET}O_{PSD}}$ (dashed line with empty squares), $\mathrm{O_{WD,mast}O_{PSD}}$ (dash-dot line with filled squares) and $\mathrm{O_{WD,SMEAR}O_{PSD}}$ (dotted line with filled squares).

References

Granier, C., Darras, S., Denier van der Gon, H., Doubalova, J., Elguindi, N., Galle, B., Gauss, M., Guevara, M., Jalkanen, J.-P., Kuenen, J., Liousse, C., Quack, B., Simpson, D., and Sindelarova, K.: The Copernicus Atmosphere Monitoring Service global and regional emissions (April 2019 version), https://doi.org/10.24380/d0bn-kx16, 2019.

Guenther, A., Karl, T., Harley, P., Wiedinmyer, C., Palmer, P. I., and Geron, C.: Estimates of global terrestrial isoprene emissions using MEGAN (Model of Emissions of Gases and Aerosols from Nature), Atmos. Chem. Phys., 6, 3181–3210, https://doi.org/10.5194/acp-6-3181-2006, 2006.

Karvosenoja, N.: Emission scenario model for regional air pollution, Tech. rep., Finnish Environment Institute, Helsinki, Finland, 2008.

Kristensson, A., Johansson, C., Westerholm, R., Swietlicki, E., Gidhagen, L., Wideqvist, U., and Vesely, V.: Real-world traffic emission factors of gases and particles measured in a road tunnel in Stockholm, Sweden, Atmos. Environ., 38, 657–673, https://doi.org/10.1016/j.atmosenv.2003.10.030, 2004.

Lana, A., Bell, T. G., Simó, R., Vallina, S. M., Ballabrera-Poy, J., Kettle, A. J., Dachs, J., Bopp, L., Saltzman, E. S., Stefels, J., Johnson, J. E., and Liss, P. S.: An updated climatology of surface dimethlysulfide concentrations and emission fluxes in the global ocean, Global Biogeochem. Cy., 25, https://doi.org/10.1029/2010GB003850, 2011.

Mårtensson, E. M., Nilsson, E. D., de Leeuw, G., Cohen, L. H., and Hansson, H.-C.: Laboratory simulations and parameterization of the primary marine aerosol production, J. Geophys. Res.-Atmos., 108, https://doi.org/10.1029/2002JD002263, 2003.

Paasonen, P., Kupiainen, K., Klimont, Z., Visschedijk, A., Denier van der Gon, H. A. C., and Amann, M.: Continental anthropogenic primary particle number emissions, Atmos. Chem. Phys., 16, 6823–6840, https://doi.org/10.5194/acp-16-6823-2016, 2016.

Ripamonti, G., Järvi, L., Mølgaard, B., Hussein, T., Nordbo, A., and Hämeri, K.: The effect of local sources on aerosol particle number size distribution, concentrations and fluxes in Helsinki, Finland, Tellus B Chem. Phys. Meteorol., 65, 19 786, https://doi.org/10.3402/tellusb.v65i0.19786, 2013.

Roldin, P., Ehn, M., Kurtén, T., Olenius, T., Rissanen, M. P., Sarnela, N., Elm, J., Rantala, P., Hao, L., Hyttinen, N., et al.: The role of highly oxygenated organic molecules in the Boreal aerosol-cloud-climate system, Nat. Commun., 10, 1–15, 2019.

Schaap, M., Timmermans, R. M., Roemer, M., Boersen, G., Builtjes, P., Sauter, F., Velders, G., and Beck, J.: The LOTOS-EUROS model: description, validation and latest developments, Int. J. Environ. Pollut., 32, 270–290, 2008.

Simpson, D., Andersson, C., Christensen, J. H., Engardt, M., Geels, C., Nyiri, A., Posch, M., Soares, J., Sofiev, M., Wind, P., and Langner, J.: Impacts of climate and emission changes on nitrogen deposition in Europe: a multi-model study, Atmos. Chem. Phys., 14, 6995–7017, https://doi.org/10.5194/acp-14-6995-2014, 2014.

Wang, F., Ketzel, M., Ellermann, T., Wåhlin, P., Jensen, S. S., Fang, D., and Massling, A.: Particle number, particle mass and NO_x emission factors at a highway and an urban street in Copenhagen, Atmos. Chemi. Phys., 10, 2745–2764, https://doi.org/10.5194/acp-10-2745-2010, 2010.